UNIVERSITY OF LONDON THESIS

Degree PhD Year 2007 Name of Author NATARAJAN, Sukina

Stability of Small Molecular Clusters Modelled with Stochastic and Deterministic Dynamics

Sukina Natarajan

Department of Physics and Astronomy
University College London

2007

Thesis submitted for the degree of Doctor of Philosophy

ProQuest LLC
789 East Eisenhower Parkway
P.O. Box 1346
Ann Arbor, MI 48106-1346

I confirm that the work presented in this thesis is my own. Where information has been derived from other sources, I confirm that this has been indicated in the thesis.

Sukina Natarajan

Abstract

This investigation concerns the transition pathway of the condensation phase transition. Under certain conditions condensation is initiated by nucleation events, which are driven by fluctuations or instabilities in the vapour phase. This involves the spontaneous formation of groups of particles, which we refer to as clusters. The clusters have a highly unstable nature and exist momentarily, before breaking up. This makes them difficult to study experimentally and model mathematically, in comparison to larger more stable systems.

The aim of this study is to explore the stability of these tiny molecular clusters that exist momentarily within their environment, in terms of the time taken for the cluster to lose particles (decay). To do this we employ a microscopic cluster model of n-nonane molecules in which the cluster is treated in isolation from the vapour particles that would normally surround it. The interactions between cluster particles are modelled using empirical potentials. The cluster's dynamics is modelled using deterministic molecular dynamics simulations. The simulations generate a time evolved trajectory of all the positions, velocities and forces of all the atoms in the cluster.

The process of cluster decay in n-nonane clusters is modelled using a Langevin interpretation of the decay mechanism. This treatment views cluster decay as a process of single particle escape from a confining potential of mean force, driven by a particle's interactions with the surrounding cluster particles. The motion of a cluster particle is modelled using a Langevin equation, which is parameterised using the MD generated data in order to extract the decay related parameters. The decay parameters are used to evaluate an Arrhenius type equation for the kinetic decay rate. This is used to calculate the mean timescale of cluster decay for n-nonane clusters, which we refer to as the mean cluster lifetime.

We compare the dynamically generated lifetimes calculated from the model to those predicted by experimental measurements, as well as classically derived lifetimes. We discover the dynamical model predicts lifetimes that compare well to experimental predictions. The

cluster decay model allows us to predict cluster decay timescales without decay events actually occurring. This makes it an essential tool for systems with long decay timescales, for which decay events can not be feasibly observed through MD simulations alone.

Finally, the last chapter presents recent work that has been conducted on ice cluster embryos. The ice embryos emerge during the freezing transition of supercooled water into ice I. Unlike the previous method of treating clusters in isolation from their surroundings, this study involves the treatment of ice clusters in coexistence with their environment. We utilise a molecular dynamics trajectory of supercooled water freezing into ice, which is used to identify and extract ice cluster embryos. It is evident from the MD simulations that at the initial stages of freezing the clusters are very amorphous and disordered. We investigate cluster properties such as the size distribution and molecular connectivity, and explore whether we are able to quantify the potential of mean force in order to estimate the mean lifetime of disordered ice cluster embryos.

Acknowledgements

This research was funded by the Natural Environmental Research Council (NERC). I would like to express my gratitude to the Aerosol Society (UK) for awarding me the C N Davies award, and providing me with financial support to attend various research conferences that were central to my work. I would also like to thank Dr M Matsumoto for providing me with the MD simulation trajectory that enabled me to conduct the calculations in Chapter 7.

I would like to thank my supervisor Dr Ian Ford for his amiable guidance and support throughout my PhD. I would also like to thank Dr Sarah Harris for her attentive help and insight into this field of study. Thank you to Andy Gormanly who was responsible for the computer cluster, and to Denise Ottley, for having an answer to every administrative question possible. Also, many, many thanks to Dr Charles Bird and Dr Che Gannarelli for their approachability with technical issues. Many thanks to Dr Dorothy Duffy for her insightful discussions, and for kindly reading the thesis, and many thanks to Wisdom Beyhum for doing the same.

I would especially like to thank my parents for believing in me, and my brother for his patience and motivation over the years. Finally, I would like to express my deepest gratitude to Dr Sascha Khakshouri for his support, and inspiration, throughout this time.

Contents

List of Symbols

Roman characters

$\mathbf{a}$	Particle acceleration
b	Bond length (page 60)
C_v	Specific heat capacity
D	Diffusion coefficient
e	Electric charge of an electron in Coulombs
E	Energy
E_c	Total cluster energy
E_x	Excess internal energy
$f(r)$	Mean radial force at position r
$\tilde{f}(t)$	Random fluctuating force
F	Free energy (Gibbs)
F_i	Free energy of formation of an i-cluster
$g(E)$	Density of energy states
$G(t)$	Velocity autocorrelation function (page 46)
H	Hamiltonian of the cluster and decayed particle
H_c	Hamiltonian of the cluster's bound particles only
H_{oc}	Hamiltonian of the cluster's decay particle interacting with the cluster particles
i	Number of system molecules/particles
i^*	Critical cluster size
I	Moment of inertia
J_i	Nucleation current
k	The Boltzmann constant
L	Latent heat of vapourisation
$\mathbf{L}$	Angular momentum

m	Mass
n_v^s	Monomer density of supersaturated vapour
n_l^e	Monomer density of liquid at equilibrium
n_i^e	Density of i-clusters at thermal equilibrium
n_1^e	Density of monomers at thermal equilibrium
p	Particle momentum
P	Pressure
$P(r)$	Probability density of particle position from the cluster centre of mass
$P(\eta)$	Probability density of time interval between successive carrier gas collisions
P_v^s	Supersaturated vapour pressure
P_v^e	Saturated vapour pressure (at equilibrium)
q	Electric partial charge of an atom/particle in Coulombs (page 102)
$\mathbf{r}$	Particle position (page 43)
r_e	Cluster escape radius
r_o	Far field position
R	Radius of a droplet/cluster
R_i	Radius of a cluster containing i molecules
S	Entropy (page 11)
S	Supersaturation (page 22)
T	Temperature
T_{rot}	Rotational kinetic energy
T_{trans}	Translational kinetic energy
U	Internal energy
$\mathbf{v}$	Particle velocity
$\dot{v}(t)$	Particle acceleration (page 45)
V	Volume
V_{ij}	Potential field between the i^{th} and j^{th} particles
$V^{bond}(\mathbf{r})$	Potential field for the bonded interactions
w	Angular velocity
$W(r,t)$	Probability density of finding a particle at position r, time t
ΔW_i	Work of droplet/cluster formation
ΔW^*	Work of critical cluster formation
$x^2(t)$	Mean square displacement
Z	Partition function

Greek characters

β_i Mean growth rate of an i-cluster

β_{i-1} Mean growth rate of an $(i-1)$-cluster

β_{i-1}^e Mean growth rate of an $(i-1)$-cluster at equilibrium (*ie* saturated vapour)

β_i' Growth rate coefficient of an i-cluster

δt Molecular Dynamics time step

γ Friction coefficient

Γ Random fluctuating force per unit mass (page 47)

ϵ Lennard-Jones potential well depth

η Coupling timescale between the cluster and Andersen thermostat (page 68)

θ Bond angle (page 60)

μ_l Chemical potential per molecule of bulk liquid

μ_s Chemical potential per molecule of surface

μ_l^e Chemical potential of per molecule of bulk liquid at equilibrium

μ_v Chemical potential per molecule of supersaturated vapour

ν_i Mean decay rate of an i-cluster

ν_{i+1} Mean decay rate of an $(i+1)-$cluster

ρ Density of the bulk liquid

σ Surface tension of the bulk liquid (page 22)

σ Lennard-Jones potential mean separation (page 43)

σ_E^2 Variance of energy fluctuations

τ_c Mean correlation time

τ_{class} Classically derived cluster decay timescale

τ_{expt} Experimentally determined cluster decay timescale

τ_{model} Langevin calculated cluster decay timescale

$\Phi(r)$ Potential of mean force at position r

$\Delta\Phi$ Potential of mean force depth

ω Bond torsion angle (page 60)

Chapter 1

The Phenomenon of Nucleation

1.1 The Motivation Behind Condensation

There is a rare consequence of particle interactions within solids, liquids and gases, whereby altering a system's ambient conditions induces a sudden and dramatic change in the system's properties, resulting in a transformation into a completely different state of matter. This process is known as a phase transition. The main problem concerning the physics of phase transitions is that given the present analytic and computational tools we are not able predict whether a transition will occur at certain conditions. This presents us with uncertainties concerning the behaviour and properties of systems that undergo phase transitions.

An important class of phase transition is the condensation of a vapour to a liquid. Condensation phase transitions encompass collective transformations in a wide range of natural and industrial processes. For instance, the formation of clouds in the atmosphere is driven by the condensation of cloud vapour into liquid droplets or aerosol particles. Clouds play an important role maintaining the earth's climate by scattering solar radiation from the upper part of the atmosphere and long wave radiation from the earth's surface. The formation of cloud aerosol particles is facilitated by the presence of cloud condensation nuclei (CCN), which act as seeds onto which the vapour can condense [1]. An increase in concentration of CCN increases the number of cloud aerosol particles, which increases the reflectivity of the cloud [2], and can also influence its lifetime. The relevance of condensation in industrial processes is also of central importance. For example, steam turbines that are used in power stations are subject to the deterioration of turbine blades, which is a major contributor to loss in power generation efficiency [3]. One of the main causes of

turbine deterioration is the condensation of water droplets onto the blades, which causes erosion [4].

1.2 Mechanisms of Condensation

A major objective in studies of phase transitions is to identify the rate at which a system evolves toward the new phase. A common approach to this problem is to focus on the underlying mechanisms that drive the transition, which occur over comparatively shorter timescales than the transition itself. To understand the mechanisms that drive condensation we must look beyond the macroscopic descriptions of matter, since the critical processes occur at the microscopic scale.

1.2.1 Microscopic description

On a molecular level, condensation is initiated by the formation of tiny molecular clusters from the vapour phase. The clusters are essentially density fluctuations that occur on the microscopic scale. The clusters spontaneously emerge from the vapour and exist for a short time before breaking up. The process of emerging groups of molecules or clusters is called nucleation. The clusters can either grow by colliding with surrounding vapour molecules that stick due to attractive interactions, or they can break up by losing fast moving molecules that have escaped the cluster's binding interactions. The latter process is cluster evaporation, which we refer to in this study as cluster decay. If the cluster maintains a certain stability, and survives for a relatively long timescale compared to the timescale of molecular collisions, then it is generally called quasi-stable. Very occasionally there may be a series of favourable density fluctuations and collision events that assist the cluster in growing to a critical size. At this point the energetic gain due to the molecular attractions start to balance the unfavourable entropy change associated with forming a high density region. This is the critical cluster size, which has an equal probability of growth or decay. Beyond the critical cluster size the new liquid phase is considered to form spontaneously. Generally speaking, clusters smaller than the critical cluster size are unstable with respect to the vapour phase, and have a tendency to break up rather than grow. This means that under certain conditions it can take a long time to reach the critical cluster size. In this situation the vapour is said to be metastable, which means it is stable in the dynamic sense, with respect to small fluctuations, but it has not reached full thermodynamic equilibrium.

Nucleation events that involve on type of particle are referred to as homogeneous nucleation whereas events that involve more than one type of particle are referred to as multicomponent homogeneous nucleation [23]. The presence of foreign particles or a surface can facilitate the process of nucleation as the cost of creating an interface in a coexisting system is reduced, which is called heterogeneous nucleation. Homogeneous nucleation was first recognised in 1897 by Wilson [5], and it has received much theoretical and experimental attention, and is the focus of this study.

1.2.2 Non-equilibrium thermodynamic description

If we compress a vapour (at constant temperature) it will start to condense. The pressure P plotted against volume V for such a process is illustrated in Figure 1.1, where the horizontal black line represents a region where the liquid and vapour coexist at thermodynamic equilibrium. The black dot on the $P-V$ diagram represents a saturated vapour at equilibrium. In reality, the vapour may become supersaturated, which means it is more dense than equilibrium conditions will allow. This is shown by the red line. The critical cluster size will be largest close to the black line and smallest far from the thick black line. Consequently, the lifetime of a metastable vapour will be longest close to the black dot, and shortest close to the red dot.

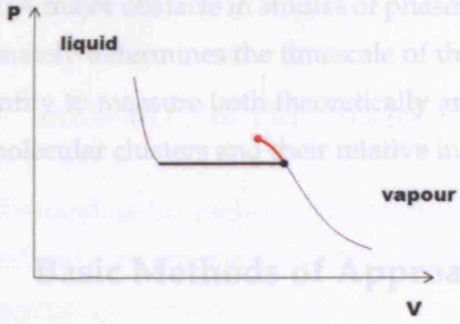

Figure 1.1: The pressure-volume variation (at constant temperature) illustrates the equilibrium thermodynamic description of the vapour-liquid transition. The red line represents the non-equilibrium situation in which the vapour is supersaturated (metastable).

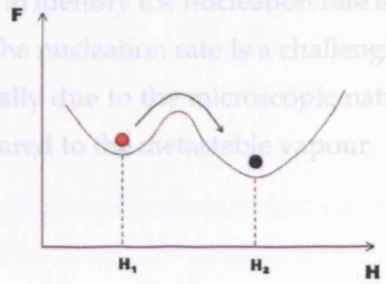

Figure 1.2: The free energy variation plotted against an arbitrary thermodynamic parameter H. The black and red particles assume global and local minima respectively. The red particle is stable with respect to small microscopic fluctuations but a sufficiently large fluctuation would drive it over the barrier into the global minimum. The black particle is in a stable thermodynamic equilibrium.

The energy available in the system to do work is the free energy, which can be defined as

$$F = U - TS \tag{1.1}$$

where U is the internal energy, S the entropy, and T the temperature. The difference in free energy between vapour and liquid is what favours the new phase to form, as a system will generally try to lower its free energy to reach a global minimum. For the system to be at thermodynamic equilibrium, it must be at a global minimum, as shown by Figure 1.2 (the black particle). If it is at a local minimum (red particle) then the system is metastable. There is a kinetic hindrance associated with the phase transition that prevents a vapour from spontaneously forming into a liquid, which is characterised by a free energy penalty or barrier that must be overcome for the transition to progress. Such transitions are generally known as first order phase transitions and they are usually associated with the transfer of energy referred to as the latent heat. The barrier is quantified by two competing processes; the free energy gain of forming cohesive clusters, and the unfavourable entropy or free energy cost of forming the cluster's interface in a coexisting system.

The main hindrance to condensation is quantified by the free energy barrier, which must be overcome for the transition to progress. The molecular clusters provide a means of climbing the free energy barrier and act like "stepping stones" through which the macroscopic transition can propagate. The process of nucleation must produce a critical sized cluster to overcome the free energy barrier. Reaching the very top of the barrier (the critical cluster size) is the least likely and slowest stage of the process, which is the bottle neck of the transition. The mean rate at which clusters of a critical size are formed is called the nucleation rate. A major obstacle in studies of phases transitions is to identify the nucleation rate as it ultimately determines the timescale of the transition. The nucleation rate is a challenging quantity to measure both theoretically and experimentally due to the microscopic nature of molecular clusters and their relative instability compared to the metastable vapour.

1.3 Basic Methods of Approach

A familiar thermodynamic approach used to study molecular systems is to regard them as being part of a larger macroscopic system. The zeroth law of thermodynamics states that a system in thermal equilibrium with its surroundings, which comprise a large system or heat bath, will have the same well defined temperature as the bath [6]. However, molecular clusters are not necessarily in thermal equilibrium with their surroundings, which means a precise definition of cluster temperature is difficult to establish. This introduces problems in the development of conventional thermodynamic relations of molecular clusters. We are faced with two central concerns: the microscopic and quasi-stable nature of clusters.

An alternative approach to thermodynamic studies of molecular clusters is through statistical mechanics. This discipline uses statistical techniques to derive macroscopic properties from the microscopic ingredients of a system. The connection between thermodynamics and statistical mechanics is established in the limit of a large number of particles N, in the system. The essence of statistical mechanics is the statistical ensemble: many identical copies of a system each with slightly different microscopic configurations but with identical macroscopic properties, such as temperature, volume and pressure. The ensemble allows macroscopic observables to be deduced from microscopic averaging of the system, which is clearly less successful for small systems, where averages contain large fluctuations. However, statistical mechanics can accommodate fluctuations and deviations from average behaviour, which gives it the power to deal with small systems and systems away from equilibrium. The main axiom of statistical mechanics is the ergodic theorem, which states that with sufficient time a system will sample all microscopic configurations of positions and momenta in phase space that are available to it. This suggests the use of the powerful method of molecular dynamics (MD), in which a computer simulation evolves a system according to Newton's laws of motion, such that average properties are deduced over molecular configurations in time. A concise theoretical understanding of the dynamics of molecular systems can be achieved through the combination of MD and statistical mechanics, which forms the basis of this work. These methods are discussed in more detail in Chapter 4.

1.4 Summary of this Study

Understanding the nature of fluctuations at the vapour-liquid boundary remains a theoretical and experimental challenge. This is a difficult problem to solve because it involves microscopic processes that are rarely occurring between observable states of matter. There remains an ongoing need to develop more suitable models that accurately describe the microscopic precursors to condensation.

This work aims to investigate the behaviour and properties of quasi-stable molecular clusters in condensation. We seek to better understand the cluster's evolution to the critical cluster size by calculating the mean cluster lifetime. We use a combination of statistical and dynamical methods, which collectively present a novel approach to investigate the physics of these unique and rarely occurring events.

To improve the computational efficiency of the task, the interactions between the cluster

and the surrounding vapour phase are represented using an average energy exchange mediated by a heat bath. This interpretation effectively treats the cluster in isolation from the vapour molecules that would normally surround it. The interactions between the cluster and vapour are averaged out over the timescale of interest. The cluster's dynamic properties are generated using molecular dynamic simulations which provide the time evolved positions, velocities and forces of the cluster's constituent molecules. The trajectory is used to parameterise a Langevin model of the cluster decay, which views the decay mechanism as a randomly driven process due to the interactions between cluster molecules. The combination of the molecular dynamics simulations and the Langevin treatment of cluster decay are used together to calculate mean cluster lifetimes, described using a type of Arrhenius equation.

The lifetimes predicted from the dynamic cluster model are validated with quantitative comparisons determined from experimental studies of condensation and classical nucleation theory with detailed balance in thermal equilibrium. The cluster models developed in this study provide a means to build up new theoretical approaches that provide better predictions of the rate of homogeneous nucleation.

1.5 Breakdown of Chapters

Chapter 2, reviews the most important principles and issues concerning condensation nucleation. It provides an outline of the experimental and theoretical methods developed in vapour-liquid homogeneous nucleation studies.

Chapter 3, contains a calculation of the experimentally determined cluster decay time and a derivation of the classical decay time under conditions of detailed balance in thermal equilibrium.

Chapter 4, introduces the foundations of the main mathematical and computational tools used in this study. It illustrates how MD and Langevin dynamics can be used together to interpret the process of cluster decay and quantify the mean cluster lifetime.

Chapter 5, describes in detail the issues relevant in conducting MD simulations in thermal equilibrium at constant temperature. It provides preliminary results of the molecular dynamics simulations, such as the calculation of the specific heat capacity from the mean cluster energy.

Chapter 6, describes the details of the Langevin interpretation of cluster decay, and approximations made in the absence of cluster decay. Mean cluster decay times are presented in

comparison to lifetimes predicted from experiments and classically derived lifetimes.

Chapter 7, is a study of ice cluster embryos in coexistence with the supercooled metastable liquid. We aim to apply the Langevin interpretation of cluster decay to ice clusters in order to estimate the mean ice embryo lifetimes.

Chapter 8, contains some concluding remarks about the cluster studies of *n*-nonane and ice clusters.

Chapter 2

Experimental and Theoretical Condensation Nucleation Studies

2.1 A Brief Overview of Nucleation Experiments

One of the main objectives of nucleation experiments is to determine the rate of nucleation. This is defined as the number of clusters, of a critical size, formed per second per unit volume. The rate of nucleation depends on two main variables, the temperature and supersaturation of the vapour. A supersaturated vapour is one that contains more vapour particles per unit volume than equilibrium conditions will allow. The amount by which a vapour is supersaturated is often expressed in terms of the saturation ratio, which is the ratio of vapour pressure to saturated vapour pressure at equilibrium. The saturation ratio is equal to 1 under conditions of equilibrium, and is greater than 1 for a supersaturated vapour.

Experimentally, the rate of nucleation is taken to be the rate of formation of observable droplets, assuming that droplets do not coalesce between nucleation and observation, or otherwise disappear by adsorbing onto the walls the of the experimental instruments. This is a reasonable assumption provided the growth of macroscopic droplets beyond the critical size occurs very quickly.

2.1.1 Experimental techniques and devices

There is a range of experimental techniques and devices used to measure nucleation rates. Different devices are suited to different substances, and function over different tempera-

tures and supersaturations, and can measure different ranges of nucleation rates. A brief review of the most popular techniques is provided by Arstila [7]. A schematic representation of the most popular devices and their corresponding range of nucleation rate measurable is illustrated in Figure 2.1.

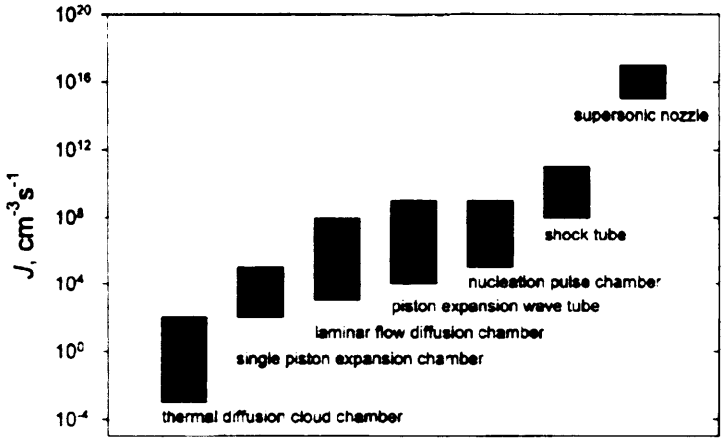

Figure 2.1: Schematic illustration of different experimental devices and their corresponding range of measurable nucleation rates, taken from Hyvärinen [8].

Early nucleation experiments often relied on measuring properties that vary with the nucleation rate such as the critical supersaturation needed to produce a particular nucleation rate, conducted at a fixed temperature [9]. In such studies, the vapour supersaturation is adjusted until droplet formation is observed. The size of the emerging droplets is measured using optical scattering techniques, and the population of droplet sizes is used to determine the nucleation rate.

More recent nucleation experiments measure the actual nucleation rate as a function of varying supersaturations and temperatures. This is a more direct measurement of nucleation rates than the previous technique. A popular example of such an experimental device is the thermal diffusive cloud chamber originally developed by Langsdorf [10]. The main chamber is filled with the vapour, and there are metallic plates at the top and bottom of the chamber. The lower plate is submerged in liquid and is maintained at a higher temperature than the upper plate. The temperature gradient between the top and bottom of the chamber drives an upward diffusion flow of vapour. The vapour will have a maximum supersaturation at some particular height of the chamber. The temperatures of the plates are adjusted so that the nucleation rate at a desired chamber height may be measured. The nucleating droplets are detected using a laser scattering technique, and the nucleation rate is simply measured by counting the number of droplets formed. The thermodynamic transport properties of the vapour are used to determine the supersaturation and temperature

at the height at which droplets are formed. The main advantage of the thermal diffusion cloud chamber is that it operates over a wide range of temperatures (eg. 233K-315K), and supersaturations (eg. $1 - 35$), and can measure a relatively wide range of nucleation rates (eg. 10^{-5}cm^{3}s - 10^0cm^{3}s), shown for the example of *n*-nonane [11].

Another familiar and popular device is the expansion cloud chamber developed by Wagner and Strey [12]. It works by the rapid cooling of vapour by adiabatic expansion, which leads to high supersaturations and induces a burst of nucleation. A small recompression is used to terminate the nucleation, which maintains the vapour in a supersaturated state and allows the nucleated droplets to grow to optically detectable sizes. Expansion cloud chambers are capable of producing significantly larger supersaturations and nucleation rates than diffusion cloud chambers. The expansion cloud chamber has been modified by Strey and Wagner [13] as the nucleation pulse method.

The laminar flow diffusion chamber [14] passes a mixture of vapour and carrier gas toward a cooling tube, where it becomes supersaturated, and nucleation occurs. The nucleating droplets are carried away with the flow so that growth of the particles does not deplete the supersaturated vapour within the nucleating region.

Turbulent mixing chambers [15], [16] use two or more flows of vapour with different compositions and temperatures. The flows are rapidly mixed in the chambers to produce the supersaturation required for nucleation. The local temperature and vapour pressure fluctuates rapidly over time, which can cause difficulties in interpreting the nucleation data.

2.2 A Theoretical Discussion of CNT

The main objective of theoretical studies is to predict the rate of nucleation, and for it to be in agreement with experimental data. In order to determine the nucleation rate, the net rate at which clusters grow into the critical cluster size must be quantified. The most prominent theory to emerge in theoretical homogeneous nucleation studies is the classical nucleation theory (CNT). This was first derived by Volmer and Weber [17], and Becker and Döring [18]. However, much of the basic theory was formalised prior to this by Gibbs, in the liquid drop model [19], [20]. The liquid drop model is one of the earliest and simplest thermodynamic descriptions of curved surfaces and small particles. In this section we shall build up a picture of CNT from the liquid drop model and illustrate how a set of simple rate equations can be used together with the Gibbs formalism to predict the growth and decay rates of a metastable system.

2.2.1 The liquid drop model

The liquid drop model was first developed to determine the thermodynamic properties of macroscopic bulk phase droplets. It assumes that the droplet is made up of the liquid bulk and is separated from the vapour by a well defined spherical boundary (*ie* the droplet's surface). A schematic of a droplet surrounded by vapour, and a droplet submerged in liquid is illustrated in Figure 2.2. The droplet in system A has very different interactions compared with the droplet in system B. The energetic difference between the two systems can be viewed as the energy required to form a droplet from the vapour phase. This is characterised by the free energy of formation, which can be interpreted as the "available energy to do work". We can write the free energy of formation F of a droplet made up of i molecules as the sum of a volume and surface term as shown by

$$F_i = i\,\mu_l\,(T,\,p) + \mu_s\,i^{\,2/3} \tag{2.1}$$

where $\mu_l\,(T,\,p)$ is the chemical potential per molecule of the bulk liquid, at a given temperature T, pressure p, and μ_s is the chemical potential per molecule of the surface. The first term in Equation (2.1) represents the free energy contribution due to the droplet's volume, which is proportional to the number of bulk liquid molecules that it contains. The second term represents the free energy cost of forming the droplet's surface, which is proportional to the cube root of the volume squared (in the Gibbs model).

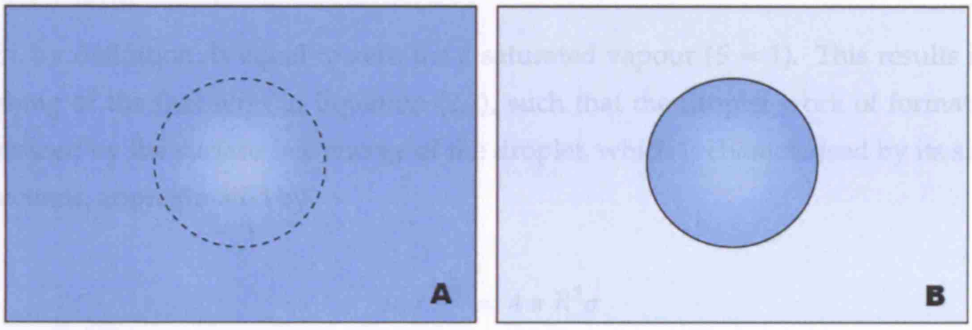

Figure 2.2: System A is a spherical droplet within a liquid. System B is a droplet of bulk phase liquid surrounded by the vapour phase. Both systems are at constant pressure. The droplet in system B is effectively isolated since its surroundings (*ie* the vapour) is considerably less dense. Clearly the isolated droplet will have different thermodynamic characteristics such as energy compared to the immersed droplet, since it is not surrounded by liquid. These differences are thought to be contained within the surface of the cluster, whilst the volume of the droplet is assumed to have the same characteristics as the bulk liquid.

The work of cluster formation

The change in free energy between the vapour phase and the droplet quantifies the reversible work of droplet formation, ΔW_i, which is given by

$$\Delta W_i = i(\mu_l^e - \mu_v) + \mu_s i^{2/3} \tag{2.2}$$

where μ_v is chemical potential (free energy) per molecule of the supersaturated vapour and μ_l^e is the chemical potential of the liquid phase at equilibrium. The first term in the brackets represents the free energy change in forming a liquid from a supersaturated vapour. As mentioned previously, the saturation ratio is defined as the supersaturated vapour pressure P_v^s divided by the saturated vapour pressure P_v^e. Under equilibrium conditions (which corresponds to a saturated vapour) the saturated vapour pressure can be taken to be the liquid pressure. To good approximation to an ideal gas, the ratio of pressures is equal to the ratio of monomer density in the supersaturated vapour n_v^s to the monomer density in the liquid at equilibrium n_l^e, as shown by

$$S = \frac{P_v^s}{P_l^e} \approx \frac{n_v^s}{n_l^e}. \tag{2.3}$$

We can write the change in chemical potential per molecule between the supersaturated vapour and the liquid at equilibrium as shown by

$$\mu_l^e - \mu_v = -kT\,lnS \tag{2.4}$$

which, by definition, is equal to zero for a saturated vapour ($S = 1$). This results in the vanishing of the first term in Equation (2.2), such that the droplet work of formation is determined by the surface free energy of the droplet, which is characterised by its surface interactions, approximated by

$$\mu_s i^{2/3} = 4\pi R^2 \sigma \tag{2.5}$$

where R is the radius of the droplet and σ is the surface tension of a planar bulk liquid. This treats the droplet as a bulk liquid with surface interactions described by a bulk planar surface tension, which is generally known as the capillarity approximation. The approximation works well for large particles like droplets, however, it carries major approximations if it is applied to small clusters that contain relatively few molecules, since

they do not have a well defined spherical surface that can be characterised using the surface tension of the bulk. The capillarity approximation is one of the main assumptions that is made by CNT in the treatment of molecular clusters.

The work of formation of a cluster containing i molecules (i-cluster) is illustrated in Figure 2.3. This is the change in free energy plotted against cluster size. As the cluster grows, and i increases, the volume term which is linear in i slowly begins to dominate over the surface term as more molecules are contained within the bulk. The work of formation has a maximum value at the critical cluster size i^*, which is shown in Figure 2.3. At this stage the cluster has gained a sufficient number of molecules with attractive interactions, which outweigh the unfavourable cost of the surface formation. The amount of reversible work needed to produce a critical cluster is quantified by ΔW^*. This defines the initial free energy barrier that a metastable system must surmount in passing from a local to a global minimum. Once a cluster reaches this critical size it has an equal probability of growth and decay, which in a sense means that it is the most stable cluster size, although it is the most unlikely cluster size. Beyond the critical cluster size the cluster grows very quickly into a droplet of new phase.

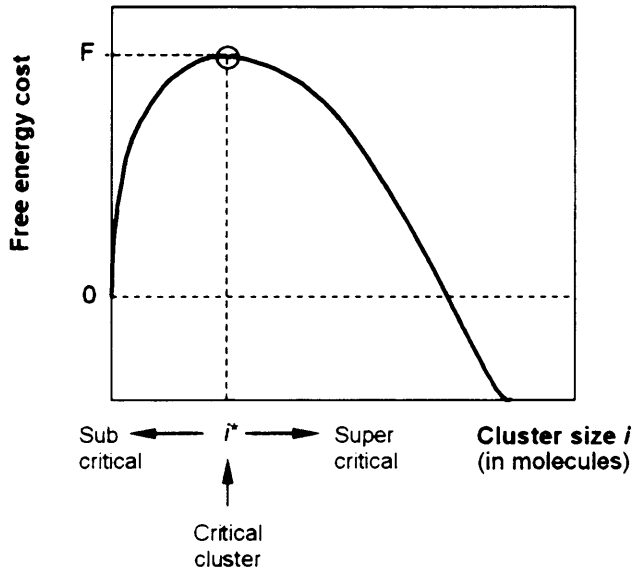

Figure 2.3: The free energy of cluster formation for a cluster of i molecules (cluster size). The critical cluster size i^* marks the maximum height of the barrier. It quantifies the amount of reversible work W^* that needs to be expended to form an i^* sized critical cluster from the same number of molecules within the bulk vapour phase. The barrier can be thought of as the free energy change necessary for the transition to progress freely, as climbing to the top of the barrier is the slowest step of the transition.

We know that the growth of clusters occurs through a series of conglomeration events. The clusters are considered to reach the critical size through a series of instantaneous, but

favourable violations of the laws of thermodynamics, which are essentially fluctuations. For a system in thermal equilibrium, the probability of a fluctuation is exponentially dependent on the reversible work needed to produce the fluctuation, which is well defined by Transition state theory [21]. An important approximation made by CNT is that it relates the probability of producing a fluctuation of given cluster size to the population of that cluster size given by

$$n_i^e = n_1^e \exp\left(-\frac{\Delta W_i}{kT}\right) \tag{2.6}$$

where n_i^e/n_1^e is the population density ratio of i-clusters to monomers in thermal equilibrium of a metastable supersaturated vapour, T is the temperature of the vapour, and k is the Boltzmann constant. It was argued by Volmer and Weber [17] that the nucleation rate should be proportional to the monomer density at equilibrium n_1^e, although their reasons for this assumption were not formally established.

2.2.2 The Becker-Döring equations and detailed balance in equilibrium

Intuitively, the process of nucleation can be viewed in the kinetic sense whereby an individual cluster grows and decays stochastically, and is occasionally driven into more stable cluster sizes. This process can be modelled using a simple set of rate equations that describe the growth and decay rates of the population dynamics of clusters. This principle forms the basis of the Becker-Döring equations [18], in which the population density of i-clusters (n_i) can vary over time via four principal mechanisms, assuming growth and decay occurs through the addition and subtraction of a monomer, as shown in Figure 2.4. The mean growth rate (monomer attachment) and decay rate (monomer detachment) for an i-cluster are given by β_i and ν_i respectively.

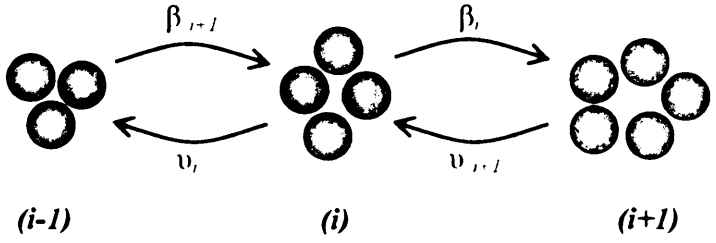

Figure 2.4: The four component pathways of the time variant population change for a given cluster size, assuming processes involving two or more clusters occur at negligible rates. The processes are assumed to be Markovian such that growth and decay are governed by the cluster's properties and not their histories.

favourable violations of the laws of thermodynamics, which are essentially fluctuations. For a system in thermal equilibrium, the probability of a fluctuation is exponentially dependent on the reversible work needed to produce the fluctuation, which is well defined by Transition state theory [21]. An important approximation made by CNT is that it relates the probability of producing a fluctuation of given cluster size to the population of that cluster size given by

$$n_i^e = n_1^e \exp\left(-\frac{\Delta W_i}{kT}\right) \tag{2.6}$$

where n_i^e/n_1^e is the population density ratio of i-clusters to monomers in thermal equilibrium of a metastable supersaturated vapour, T is the temperature of the vapour, and k is the Boltzmann constant. It was argued by Volmer and Weber [17] that the nucleation rate should be proportional to the monomer density at equilibrium n_1^e, although their reasons for this assumption were not formally established.

2.2.2 The Becker-Döring equations and detailed balance in equilibrium

Intuitively, the process of nucleation can be viewed in the kinetic sense whereby an individual cluster grows and decays stochastically, and is occasionally driven into more stable cluster sizes. This process can be modelled using a simple set of rate equations that describe the growth and decay rates of the population dynamics of clusters. This principle forms the basis of the Becker-Döring equations [18], in which the population density of i-clusters (n_i) can vary over time via four principal mechanisms, assuming growth and decay occurs through the addition and subtraction of a monomer, as shown in Figure 2.4. The mean growth rate (monomer attachment) and decay rate (monomer detachment) for an i-cluster are given by β_i and ν_i respectively.

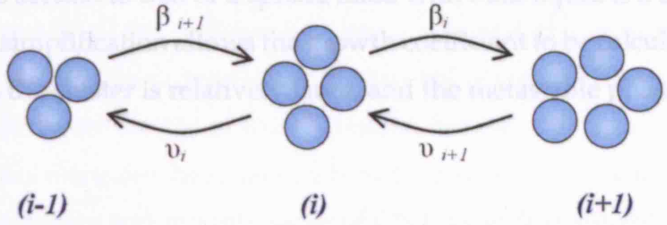

Figure 2.4: The four component pathways of the time variant population change for a given cluster size, assuming processes involving two or more clusters occur at negligible rates. The processes are assumed to be Markovian such that growth and decay are governed by the cluster's properties and not their histories.

The mean rate of change of population density of i-clusters is given by

$$\frac{d\,n_i}{d\,t} = \beta_{i-1}\,n_{i-1} + \nu_{i+1}\,n_{i+1} - \beta_i\,n_i - \nu_i\,n_i = J_{i-1} - J_i \tag{2.7}$$

where J_i describes the mean flow of cluster population between cluster sizes i and $(i+1)$, which is referred to as the nucleation current, as shown by

$$J_i = \beta_i\,n_i - \nu_{i+1}\,n_{i+1}. \tag{2.8}$$

Cluster growth

Assuming that cluster growth is driven by collisions with monomers, and that all collisions stick, the growth rate is proportional to the density of monomers n_1 in the vapour,

$$\beta_i = n_1\,\beta_i' \tag{2.9}$$

where collisions with dimers and larger clusters are assumed to be negligible. The growth rate coefficient β_i' is estimated from the collision rate between spherical clusters and a monomer in a saturated vapour [22] is given by

$$\beta_i' = \frac{4\,\pi\,R_i^2\,kT}{(2\,\pi\,m\,kT)^{1/2}} \tag{2.10}$$

where m is the mass of a molecule, R_i is the radius of an i-cluster, and T is the temperature of the vapour. The collision rate comprises the collision cross section of a sphere multiplied by a velocity. Obviously, this is a very simple view of the cluster growth mechanism with notable shortcomings. For instance, the approximation of the cluster's volume and collision cross section to that of a sphere filled with bulk liquid is a crude assumption. Nevertheless this simplification allows the growth coefficient to be calculated conveniently and exactly when the cluster is relatively large, and the metastable phase is an ideal gas.

Cluster decay

For a system in thermal equilibrium, the transition probability for a process and its reverse process are equal, which means the nucleation current is zero. If this is true for all pairs of

states in thermal equilibrium this is called detailed balance, which for the case of $J_{i-1} = 0$ leads to

$$\beta_{i-1}^{e} n_{i-1}^{e} = \nu_i n_i^{e} \tag{2.11}$$

where n_{i-1}^{e} and n_i^{e} represent the equilibrium population densities of $(i-1)$-clusters and i-clusters respectively, in a saturated vapour. To good approximation, the population densities are given by Equation (2.6), provided the timescale of interaction between the cluster and the vapour is much longer than the interactions within the cluster. We can presume this is true, since the vapour is much less dense than the cluster. The decay rate for an i-cluster is determined by rearranging Equation (2.11) to give

$$\nu_i = \beta_{i-1}^{e} \left(\frac{n_{i-1}^{e}}{n_i^{e}} \right) \tag{2.12}$$

where the growth rate β_{i-1}^{e} is determined as before using Equation (2.9) evaluated for a saturated vapour at equilibrium. Written in this form, the decay rate is governed by the cluster work of formation in the saturated vapour, which CNT approximates to the surface free energy of the cluster, calculated using the surface tension of a planar bulk liquid. The classical treatment of the decay rate under conditions of detailed balance in thermal equilibrium is discussed further in Chapter 3.

Nucleation Rate

In the steady state, the nucleation current is constant, such that $\frac{d n_i}{d t} = 0$ and J_i is constant for all i. Taking this steady state condition, Equation (2.7) can be solved for metastable vapour to give the steady state nucleation rate [23].

To conclude this section, we have seen that the cluster growth rates are estimated using a simple kinetic treatment of the collision between a sphere and a monomer in a saturated vapour. The decay rate is characterised by the reversible work done in forming a cluster, which is quantified by the height of the nucleation barrier. The growth rates and decay rates can be used to determine the steady state nucleation rate. In the next section we shall address the shortcomings and modifications of CNT, as well as developments in alternative theories and approaches.

2.3 The Failure of CNT and Alternative Theoretical Approaches

There is a concise review of comparisons made between experimentally measured nucleation rates and CNT predicted rates provided by Ford [24]. Comparisons of nucleation rates for water show that CNT successfully predicts the isothermal dependence of the nucleation rate on the supersaturation to within a couple of orders of magnitude at temperatures around 210K-260K [25], [26], [27]. However, the temperature dependence of the nucleation rate is systematically different from that predicted by CNT. Some early experimental nucleation data for *n*-nonane show deviations of several orders of magnitude from CNT [11], [28]. It is thought that the disparity between classical nucleation rates and experimentally measured rates is essentially due to the capillarity approximation. The free energy of cluster formation is proportional to the assumed surface tension, and this error is amplified due to the exponential dependence of the nucleation rate on free energy of cluster formation.

Despite its shortcomings, CNT still remains one of the most widely accepted formalisms used to describe homogeneous nucleation processes. Although it remains questionable whether CNT can be used as a rigorous means of calculating cluster properties, at the very least it serves as an order of magnitude tool when there are no substantial equivalent measures otherwise available.

2.3.1 Modifications of the capillarity approximation

The deviations between the experimental and CNT predicted nucleation rates have sparked the development of more sophisticated nucleation models. There is a useful review of a few prominently emerging alternatives to CNT, provided by Oxtoby [9]. One such example is the argument made by Lothe and Pound [29], [30] who argued the cluster free energy should take into account contributions from the rotational and translational degrees of freedom. This results in an increase in the nucleation rate by a factor of 10^{17}, which in most cases worsens the agreement between experiment and theory [9], [31]. Reiss [32] stated that the use of an experimental surface tension in the capillarity approximation already includes most of the effects of fluctuations in the centre of mass and rotation of a liquid like cluster, and that Lothe and Pound effectively "over counted" these effects.

An early extension to classical theory, suggested by Dillman and Meier [33], uses Fisher's droplet model [34] to determine the work of formation of a droplet of i molecules at constant pressure. The free energy of the cluster includes rotational, translational and config-

urational terms. In addition to this, the surface tension is modified to account for effects of curvature which is particularly important for small clusters.

Overall, the improved theories predict the rate of nucleation well for some substances under certain conditions, but fail in other cases. An intuitive and alternative approach to CNT involves molecular theories. This involves the explicit treatment of molecules using an interaction potential. There are two main molecular approaches to nucleation studies: density functional theory, and molecular simulations.

2.3.2 Molecular cluster studies

Molecular studies of nucleation avoid many limitations of classical and related theories. The system energy is modelled using presumed realistic interactions between molecules instead of bulk macroscopic properties of matter.

Density functional theory (DFT) is a powerful technique for the rigorous calculation of free energy barriers. It has the important advantage that it is not limited to the nucleation of liquids and ideal vapours. In the case of a supersaturated vapour, DFT treats the system as an inhomogeneous fluid with a density that varies in positional space. The theory focuses on the derivation of the free energy of cluster formation of the critical sized nucleus. DFT nucleation studies conducted by Oxtoby and Evans [35] developed new non-classical nucleation theories for homogeneous nucleation. The results show that DFT predicted nucleation rates are consistent with experimental data using cloud chambers. However, the extent of agreement between DFT and CNT strongly depends on the range of the attractive potential employed.

Molecular simulations provide a more realistic treatment of physical systems than CNT and its modifications. It involves solving equations of motion for each particle, which is a many body dynamical problem with high computational demands. For this reason it is almost impossible to obtain the average nucleation rate by direct simulation. However, it has been possible to observe nucleation events [36], and more recently entire phase transitions [37] but only using higher saturation ratios than can be achieved experimentally. To overcome the problem of high computational demands in nucleation studies, various indirect methods have been developed to model part of a nucleating system using molecular simulations. Recent studies of liquid argon clusters are modelled in thermal equilibrium, in isolation from the vapour [38]. The study uses a Langevin interpretation of cluster decay to calculate decay rates of molecular clusters [39].

The cluster definition

One of the most important considerations in molecular studies of clusters is how to define a cluster. Essentially the cluster definition should specify which particles are considered to be part of the cluster. A good review of recent progress concerning the use of cluster definitions is discussed in a paper by Senger [40].

One of the simplest means of defining a cluster in a physical sense, is to impose a geometrical constraint on molecular positions. An example of such a definition was used in a study by Reiss *et al.* [41], which restricted molecules to lie within the volume of a sphere about the centre of mass of the cluster. Another well known geometric cluster definition is the Stillinger cluster [42], which imposes a constraint of separation between cluster molecules so that each molecule must lie within a certain region centred around any other molecule within the cluster. This approach was used to model Lennard-Jones argon clusters in a study of cluster stability [38]. The main advantage of such geometric cluster definitions is that they are intuitive and straight forward to implement. However, their realism is questionable as they do not utilise dynamic information of the motion of particles. A geometric definition might include situations where particles pass close to each other without being captured. In this scenario, such "close encounters" between particles are considered to be clusters, even if they only exist momentarily, and do not possess a certain stability. One way of overcoming the simplification of the geometric definition is to use an energetic cluster definition. An early example of this approach was developed by Hill [43] who identified a cluster as a group of molecules that were confined to configurations which had a total energy that was negative. It was also required that the total energies of pairs of particles in a cluster should be negative, relative to their centre of mass, which defines an effective bond energy between particles.

In the case of liquid clusters there is a well defined difference in density between the cluster and the saturated vapour phase, which makes condensed phase clusters easy to distinguish from their surroundings. In the case of MD simulations of isolated liquid clusters, the cluster definition is only violated under instances of cluster decay, when particles leave the cluster. Under such circumstances it may be necessary to "repair" the cluster to its original state, which requires a suitable cluster definition. This treatment was used in the molecular dynamics study of liquid argon clusters [38] mentioned previously, which used geometric constraints to define the cluster. The mean lifetime of an isolated liquid argon cluster of 50 molecules at a temperature of 63K was deduced to be approximately 10.0ps. For certain systems with long decay timescales, the cluster invariably remains intact and

the cluster definition is rarely violated. For the rare instances when cluster decay does occur, periodic boundary conditions may be implemented to confine the evaporated particle to regions surrounding the cluster, so that it can recombine with the cluster given sufficient time.

2.4 Summary of Nucleation Studies

The most prominent theory to emerge from nucleation studies is CNT. It predicts the rate of nucleation using a simple set of birth and death rate equations. The rate coefficients are obtained from the treatment of the cluster in thermal equilibrium. This allows us to obtain the nucleation rate in terms of the population ratio of clusters in thermal equilibrium, which is dependant on the cluster work of formation. To calculate the cluster work of formation it is assumed that clusters comprise spherical droplets of a bulk phase liquid, with a surface tension of bulk phase flat film. This treatment is known as the capillarity approximation, which is the main assumption of CNT. The capillarity approximation is thought to be responsible for differences in experimentally measured and predicted CNT nucleation rates by several orders of magnitude. There have been numerous studies that have attempted to improve CNT by modifying the approximation of the cluster's surface work of formation to the surface tension of the bulk. The different versions of CNT have had varying degrees of success, mainly due to the difficulty in predicting the cluster work of formation rather than inaccuracies in approximate solution of the kinetic rate equations (Equation (2.7).

The next chapter discusses how experimentally measured cluster properties for the substance of *n*-nonane can be used to determine experimentally estimated cluster decay times to validate the dynamic calculations. It is also shown how a classical interpretation of cluster decay based on population balance in thermal equilibrium can be used to derive a classical cluster decay time, which is at present the only alternative means of predicting decay times.

Chapter 3

Properties of n-nonane Clusters

3.1 Experimental Nucleation Data of n-nonane

There has been a number of nucleation experiments conducted on organic substances such as alkanes, as they condense conveniently around room temperature. This makes the experimentation easy to perform, which can help improve the reliability of the data. A popular choice of vapour used in condensation nucleation studies is n-nonane, which has a boiling point of 300K, at atmospheric pressure. Typical nucleation studies of n-nonane involve condensation of the saturated vapour together with a carrier gas (typically helium or argon) performed over a range of temperatures and supersaturations.

An early study of n-nonane conducted by Adams *et al.* [44] involved the use of a single piston expansion cloud chamber. Typical nucleation rates of n-nonane were measured over the temperature range 215K-270K, as a function of supersaturation, which yielded rates between $10^2 - 10^5$ drops $cm^{-3}\,s^{-1}$. Nucleation rates greater than this for n-nonane were measured in a study by Wagner and Strey [12], [45] using a two piston expansion chamber over the temperature range 199K-241K, which yielded rates between $10^5 - 10^9$ drops $cm^{-3}\,s^{-1}$. A study of n-nonane using the upward thermal diffusion chamber [11] measured nucleation rates over temperatures 233K-315K to be $5 \times 10^{-5} - 5 \times 10^{0}$ drops $cm^{-3}\,s^{-1}$.

Overall, the nucleation rates of n-nonane measured by these studies compare poorly to nucleation rates predicted by CNT, with regard to the temperature dependencies of the rates [11]. One of the main objectives in the pursuit of newly developed nucleation theories is to achieve good reconciliation with experimentally measured quantities.

3.1.1 Nucleation theorems applied to *n*-nonane clusters

There are two nucleation theorems which use experimentally measured data to obtain properties of critical clusters. The first nucleation theorem was originally derived by Kashchiev in 1982 [46], [26], [47]. It relates the nucleation rate of droplets from the supersaturated vapour to the number of particles in the critical cluster. The first nucleation theorem is given by

$$\left(\frac{\partial \ln J}{\partial \ln S} \right)_T = 1 + i^* \tag{3.1}$$

which expresses the supersaturation S dependence of the experimentally measured nucleation rate J to the critical cluster size i^*. The second nucleation theorem was derived by Ford [22], [48] and relates the temperature T dependence (at constant supersaturation) of the measured nucleation rates to the critical cluster's internal energy

$$\left(\frac{\partial \ln J}{\partial T} \right)_S = \frac{1}{kT^2} [\, L - kT + E_x(i^*) \,]. \tag{3.2}$$

The quantity E_x defines the excess internal energy of the cluster, which can be interpreted as the energy difference between i molecules of the bulk liquid phase, and a cluster of i molecules. The excess energy is given by

$$E_x = E_c - i\,L \tag{3.3}$$

where E_c is the total energy of the cluster, and L is the latent heat of vaporisation per molecule of liquid.

The nucleation theorems provide a important means by which the properties of critical molecular clusters can be extracted from experimentally measured nucleation rates of droplets formed from the supersaturated vapour phase. The critical cluster size and excess energies for different organic substances have been extracted by Ford [22], [48] using experimental data measured by Hung *et al.* [11], Adams *et al.* [44], Wagner and Strey [25], and Rudek *et al.* [28]. Ford deduced that under the experimental conditions employed by Hung *et al.* and Rudek *et al.* the critical cluster sizes for *n*-nonane range from approximately 40 molecules to 70 molecules. We employ a range of cluster sizes, given in Table 3.1, that have been deduced to be critical by Ford [22] at the given temperatures and supersaturations, which will be simulated in the dynamical study. In the next two sections

we will outline two different methods of determining the cluster decay rate, which will provide a quantitative comparison to the dynamically generated results.

3.1.2 Experimentally derived lifetime of *n*-nonane clusters

Under the experimental conditions the cluster suffers collisions with the vapour and carrier gas that surround it. According to detailed balance, critical clusters have an equal probability of growth and decay, which means the average time between cluster growth events can be assumed to be equal to the average time between cluster decay events. We approximate the cluster decay rate to the cluster growth rate, assuming the mean growth rate of an i-cluster in a supersaturated vapour is equal to the collision rate, provided all collisions with the cluster stick. The collision rate is approximated using the collision cross section of a sphere with the vapour molecules, which is calculated using Equation (2.10), defined in Chapter 2. This is repeated here for convenience in terms of the growth rate of the cluster in a supersaturated vapour, as shown by

$$\beta_i = \left[\frac{4\,\pi\, R_i^2\, kT}{(2\,\pi\, m\, kT)^{1/2}} \right] n_1^s \tag{3.4}$$

where R_i is the radius of the i-cluster, T is the temperature of the vapour, m is the mass of a monomer, and n_1^s is the density of monomers in the supersaturated vapour. The term in the brackets is the collision cross section of the cluster multiplied by the mean velocity of monomers in the supersaturated vapour. The collision cross section of the cluster and mean monomer velocity are multiplied by the density of monomers in the vapour n_1^s, which gives the flow of monomers per unit area of the cluster's surface. To good approximation for an ideal gas, the density of monomers n_1^s in the supersaturated vapour is calculated by the saturation ratio, which is given by

$$S = \frac{P_v^s}{P_v^e} \approx \frac{n_1^s}{n_1^e} \tag{3.5}$$

where P_v^s is supersaturated vapour pressure, P_v^e is the saturated vapour pressure at equilibrium, and n_1^e is the density of monomers in the saturated vapour (at equilibrium). The saturated vapour pressure is a temperature dependent quantity [11], and is calculated for different temperatures as shown in Table 3.1. The cluster radius R_i is calculated from the temperature dependent bulk liquid density ρ_{liq} [11], which is calculated for the different temperatures as shown in Table 3.1.

i	T(K)	ρ_{liq}(Kgm^{-3})	R_i(Å)	R_{i-1}(Å)	P_v^e(Pa)	$n_1^e = \frac{P_v^e}{kT}$	σ(Nm^{-1})	S	n_1^s
40	233	765.051	13.88	13.76	2.28876	7.11×10^{20}	0.02888	29	2.06×10^{22}
50	250	751.699	15.04	14.95	13.6422	3.95×10^{21}	0.02688	20	7.90×10^{22}
67	300	712.268	16.88	16.79	654.889	1.58×10^{23}	0.02221	6	9.49×10^{23}

Table 3.1: Experimentally determined parameters obtained from Hung *et al.* [11], Rudek *et al.* [28], and Ford [22].

The collision growth rate is recast as the experimental cluster decay rate as shown by

$$\nu_i^{expt} = \left[\frac{4\pi(\frac{3mi}{\pi\rho})^{2/3}kT}{(2\pi mkT)^{1/2}}\right] n_1^s \tag{3.6}$$

which is evaluated for the selected cluster sizes using the supersaturation and temperatures at which the clusters were deduced to be critical by Ford [22], [48]. The experimentally determined cluster lifetimes are shown in Table 3.2 (page 34) along with the cluster sizes and the appropriate temperatures and supersaturations.

Although the kinetic treatment of cluster decay is a rather simplified interpretation of a complex process, it should provide a good estimate of the cluster decay time as it fundamentally relies on the experimentally measured quantities J and S, which have a limited uncertainty, and are reliably determined from the experiments. Overall, this approach presents a reasonably accurate estimation of cluster lifetimes, which should provide a useful comparison to the dynamically generated lifetimes, as well as those derived from classical theory, which is derived next.

3.2 Classically derived lifetimes of *n*-nonane clusters

As we have seen in Chapter 2, the population dynamics of molecular clusters can be modelled using the rate equations proposed by Becker and Döring [18], which describe the cluster's growth and decay. In the steady state the average number of growth events from an $(i-1)$-cluster to an i-cluster, minus the average number of decay events from an i-cluster to an $(i-1)$-cluster, per second, defines the nucleation current J_i. At thermal equilibrium, which corresponds to a saturated vapour, there is no net flow of nucleation current ($J_i = 0$) and the decay rate ν_i of i-clusters is directly proportional to the growth of rate of $(i-1)$-clusters β_{i-1}^e, through Equation (2.11) in Chapter 2, which is repeated here for convenience,

$$\beta_{i-1}^{e}\, n_{i-1}^{e} = \nu_i\, n_i^{e} \tag{3.7}$$

where n_i^e denotes the equilibrium population density in a saturated vapour. In CNT, the population of i-clusters in thermal equilibrium is related to the surface properties of the cluster, which are presumed to depend on the surface tension σ of the bulk liquid phase [17]. This is given in Equation (2.6), which is repeated here for convenience as

$$n_i^e \propto \exp\left[-\frac{4\pi R_i^2 \sigma}{kT}\right] \tag{3.8}$$

where R_i is the radius of an i-cluster, which is estimated as before, using the temperature dependent bulk liquid density [11]. These models are combined (*ie* Equations (3.7), (3.8), (2.10)), to provide an estimate for the classical cluster decay rate at thermal equilibrium, given by

$$\nu_i^{class} = \beta_{i-1}^{e} \exp\left[\frac{4\pi\left(R_i^2 - R_{i-1}^2\right)\sigma}{kT}\right] \tag{3.9}$$

where β_{i-1}^e is the growth rate of an $(i-1)$-cluster in a saturated vapour (assuming the cluster grows by collisions with monomers and that all collisions stick). The classical decay rate employs experimentally determined quantities similar to those used to extract the experimental decay rate, such as the saturated vapour pressure to determine the monomer density in equilibrium, and the bulk liquid density to determine the cluster radius, as shown for the i and $(i-1)$-clusters in Table 3.1. Furthermore, the classical decay rate uses the surface tension σ of a bulk planar interface [11], which is calculated for the different temperatures as shown in Table 3.1. An important difference between the classical decay rate (Equation (3.9)) and experimental decay rate (Equation (3.6)) is that the classical decay rate relies on the saturated monomer density in equilibrium n_1^e, whereas the experimental decay rate employs the supersaturated monomer density n_1^s. Both monomer densities are given in Table 3.1.

The classically derived lifetimes are calculated for each cluster size, as shown in Table 3.2. They appear to make a good comparison to the experimentally predicted lifetimes. The best comparison between the two results is for the largest cluster size, and the poorest comparison is for the smallest cluster size. This trend is consistent with the view that CNT best describes large clusters that resemble liquid droplets. The agreement between the experimental and classical results might seem surprising given the use of the surface

tension of a bulk planar interface to describe the surface interactions of the clusters. It is not expected that clusters containing as few as 40 molecules should behave like spherical droplets of bulk liquid. However, for reasons that are not entirely clear, this assumption appears to work (to first approximation).

Cluster Size i	**T (K)**	**S**	$\tau_{\mathbf{expt}}$ **(ns)**	$\tau_{\mathbf{class}}$ **(ns)**
40	233	29	44.0	34.0
50	250	20	8.80	9.20
67	300	6	0.53	0.47

Table 3.2: The experimental and classically determined cluster lifetimes are shown for the respective cluster size, temperature and supersaturation. The lifetimes are calculated using the mass of an n-nonane monomer of 128AMU, and the bulk liquid density and saturated vapour pressure, which are temperature dependent quantities as stated by Hung *et al.* [11]. The comparison between τ_{class} and τ_{expt} is poorest for the smallest cluster size.

In the dynamical cluster model, it will be important that we emulate the experimental conditions as closely as possible since the dynamic lifetimes will be quantitatively compared to the experimentally predicted lifetimes. In the next chapter we will outline the theoretical mechanisms used to model n-nonane clusters to extract the dynamical cluster decay times at the experimental conditions stated in Table 3.1.

Chapter 4

Theoretical Tools

This chapter introduces the foundations behind molecular dynamics and Langevin dynamics and shows how they can be used together to build up a theoretical framework in which the decay process of quasi-stable molecular clusters can be conveniently studied.

4.1 Principles of Statistical Mechanics in Molecular Dynamics

Thermodynamics is a phenomenological theory of matter that draws its concepts directly from experiments. This work involves the study of quasi-stable molecular clusters modelled in thermal equilibrium using equilibrium statistical mechanics as a tool for implementing thermodynamics.

Statistical mechanics is a well known technique that normally deals with the equilibrium statistics of large populations of particles N that are moving subject to a force. Consider a system of vapour particles at thermal equilibrium. The particles positions and momenta are subject to small changes over time. These variables are the microscopic properties of the system and can be used to determine the system's macroscopic average properties, such as temperature or pressure. Different sets of microscopic configurations are called microstates, and those that yield the same macroscopic average of a property are members of a statistical ensemble. The ensemble is a theoretical construct that comprises many identical copies of a system that are considered simultaneously, each having the same bulk macroscopic properties but different microscopic properties. The statistical ensemble is different to a real time evolving system, as it considers all microstates at the same instant of time.

Obviously, statistical averages are best represented in the limit of large N, and are not as meaningful for small systems, which are subject to large fluctuations. In large systems, there are a sufficient number of particles at any given instant, so that the average of a quantity over all particles is equal to the time average. The time average can be calculated from molecular dynamics simulations, by averaging over different molecular configurations. In a sense, an MD simulation generates a time evolving statistical ensemble, or microstates that vary over time. When dealing with small systems, such as molecular clusters, it is unsuitable to average over the system particles alone because there will be an error in the instantaneous mean. Instead, we must calculate time averages of molecular clusters rather than instantaneous ensemble averages. The approximation of the ensemble average to the time average forms the fundamental assumption of statistical mechanics known as the ergodic hypothesis.

4.1.1 Ergodicity and the microcanonical ensemble

The ergodic hypothesis states that a macroscopic system evolved over time will eventually explore all microscopic configurations of phase space that are available to it for a given energy surface, thereby sampling an equilibrium statistical ensemble. This means that a system at fixed energy will sample all configurations of phase space at that energy, given sufficient time. The time average and ensemble average are fundamentally different quantities: the time average samples the most likely microstates and the ensemble average samples all possible states. The ergodic hypothesis approximates these two averages to be equivalent in the long time limit. This enables the treatment of a small number of particles using equilibrium statistical mechanics.

The time average of a system property $f(p,q)$ observed over a time period τ is generally calculated by

$$\langle f(p,q)\rangle_\tau = \lim_{\tau\to\infty} \frac{1}{\tau}\int_0^\tau f\big(p(t),q(t)\big)\,dt \tag{4.1}$$

where p and q are position and momentum respectively. The ensemble average over all simultaneously observed configurations of phase space that have the same energy E, is calculated by

$$\langle f(p,q)\rangle_E = \int_{E=E_0} f(p,q)\;\; P(p,q)\; d^Np\;\; d^Nq. \tag{4.2}$$

which is a probability weighted average or expectation value, where N is the number of particles and $P(p,q)$ is the probability density distribution of the random variable $f(p,q)$, where Z is the partition function (the sum over all possible states), given by

$$Z = \int_{E=E_0} f(p,q)\ d^N p\ \ d^N q. \tag{4.3}$$

As mentioned previously, if Equations (4.1) and (4.2) are equivalent then the time average is equal to the ensemble average and the system is said to be ergodic.

For some situations it can be difficult to establish whether a system is ergodic or not, principally because it can be difficult to distinguish between configurations that are impossible and those that are just highly unlikely. For example, consider a system of vapour particles with an impenetrable dividing wall. The ensemble average for a property of the system will include all possible configurations on both sides of the wall. In reality, or in an MD simulation, these configurations would never occur regardless of how long we waited. This means that it is not a real ergodic system. In the case of an isolated cluster, if we performed molecular dynamics for a finite time we may not observe all possible microscopic configurations as some of them are very unlikely, such as the entire cluster in an evaporated state. However, if we waited for an infinite time we would eventually observe this state. The main assumption made in the MD simulations of isolated molecular clusters is that the system is ergodic.

The ergodic theorem has an important consequence for isolated systems at thermal equilibrium. An isolated system does not exchange energy with its surroundings, and thus its total energy remains fixed. It was postulated by Gibbs that this meant all microstates in this system are equivalent, and have the same probability of occurrence. Essentially, this means that there is only one invariant probability density for an ergodic system. A specific example of such a system is the microcanonical ensemble which has constant particle number N, volume V, and energy E. The probability weighting function for the microcanonical ensemble is proportional to a delta function over energy as shown by

$$\rho_{micro} = \delta\,(\,E(p,q) - E_0\,) \tag{4.4}$$

where ρ_{micro} is the weighting function, and p and q are the momenta and positions of the particles. Equation (4.4) confines the probability density to a constant energy value. The system temperature is free to fluctuate about a mean value and can be estimated at thermal equilibrium using the equipartition theorem given by

$$1/2\, m \langle v^2 \rangle = 3/2\, k\, T \tag{4.5}$$

which is an approximation to the average kinetic energy in 3-dimensions, where v is the particle velocity m the particle mass and T the temperature. Constant energy calculations are a desirable choice of treatment as they are relatively easy to perform. However, most experimental scenarios do not deal with isolated systems, but instead consider systems that are in thermal contact with the environment with which they can exchange energy or particle number. An important example of such a system is the canonical ensemble at constant particle number N, volume V and temperature T (NVT).

4.1.2 Temperature and the canonical ensemble

Thermodynamically, temperature is defined as the derivative of energy with respect to entropy at constant NVT [6]. However, it can also be defined in the kinetic sense as the average kinetic energy at thermal equilibrium through the equipartition theorem. This is a useful definition of temperature because it can be calculated conveniently from the particle velocities.

A drawback to the kinetic definition of temperature is that it poses a problem for small systems in contact with a heat bath, since they are subject to large fluctuations in kinetic energy over very short timescales, although over longer timescales the average kinetic energy remains fixed. This is a particular problem for molecular clusters as they have significant instantaneous deviations from mean behaviour. Although we can define the temperature of a cluster over a sufficiently long timescale, we can not treat temperature fluctuations in the same way as a true thermodynamic variable. This means it is unsuitable to define the temperature of small systems over short timescales using the kinetic energy. The characterisation of temperature fluctuations in small systems has been a source of much controversy, and remains a difficult and unresolved issue [49], [50], [51].

The canonical ensemble is allowed to exchange energy with its environment, such as a heat bath, and it has a well defined temperature. The probability that the system is in a given microstate is described by the probability density given by the Boltzmann distribution

$$P(E) = g(E)\, e^{-E/kT} \tag{4.6}$$

where $g(E)$ defines the number of available states per unit of energy known as the density

of states. The density of states increases with energy [52], as there will be more available microstates at higher energies. The density of states can be approximately recovered from the probability density distribution obtainable from the MD simulations (see Chapter 5). All accessible microstates in the canonical ensemble are weighted according to the Boltzmann factor $e^{-E/kT}$, which is a decreasing function of energy. The combination of these two terms gives the Boltzmann distribution its familiar peaked shape.

In the canonical ensemble, fluctuations in energy have a linear relation with the specific heat capacity C_V, defined as the derivative of energy with respect to temperature at constant volume [53]. This represents the energy needed to increase the temperature of a substance per unit mass by one degree Kelvin. The relation between energy fluctuations and specific heat capacity can be derived from the definition of the mean energy and energy variance. The thermodynamic definition of the mean has already been given by Equation (4.2) and is recast in terms of energy as shown by

$$\langle E(p,q) \rangle = \frac{1}{Z} \int E(p,q) \; e^{\frac{-E(p,q)}{kT}} \; d^N p \; d^N q \tag{4.7}$$

where Z is the canonical partition function given by

$$Z = \int e^{\frac{-E(p,q)}{kT}} \; d^N p \; d^N q. \tag{4.8}$$

The variance in energy fluctuations σ_E^2 is given by

$$\sigma_E^2 = \langle E^2 \rangle - \langle E \rangle^2 \tag{4.9}$$

where E the instantaneous energy, and $\langle E \rangle$ the mean energy. It can be shown from Equations (4.9) and (4.7) that there is a linear relation between specific heat capacity and the energy fluctuations, given by

$$\sigma_E^2 = k T^2 C_V. \tag{4.10}$$

This relation only holds true for systems in thermal equilibrium, and it is questionable whether we can assume this for molecular clusters, which are not in thermal equilibrium over timescales of energy fluctuations.

So far we have established that an isolated system has a well defined energy with a temperature that cannot be explicitly defined, and fluctuates about a mean value. In contrast,

a system that is immersed in a heat bath has a well defined temperature, but can not simultaneously have a well defined energy. The relation between energy and temperature illustrates the complementarity that exists between these two thermodynamic variables. Whether certain aspects of this relation are comparable to the complementarity relation that exists between position and momentum, given by Heisenberg's uncertainty principle, is yet to be clarified [54], [55].

4.2 Molecular Dynamics Mechanisms and Approximations

There are different molecular modelling techniques available each with distinct methods of generating conformational states. Molecular Dynamics (MD) mimics the movement of particles over time. Successive configurations of the system are generated by integrating Newton's equations of motion. The result is a trajectory that specifies how the positions and velocities of particles vary with time, including the instantaneous force acting on each particle. MD describes the dynamic behaviour of the system from which the time averaged properties can be calculated. It can predict the state of the system at any future time from its current state. This means that for a given starting configuration the system will produce the same end configuration, if repeated. This behaviour is called deterministic. In contrast, Monte Carlo simulations assign random changes to the system by modifying a few degrees of freedom at a time, so that particles are moved randomly rather than deterministically.

Fundamentally, the physical binding forces between particles are ultimately determined from the interactions between electrons. In MD, it is assumed that because the nuclei are much heavier than the electrons, their centre of mass is fixed relative to the motion of the electron. This separates the nuclei and electron motions, so that the energy of an atom in its ground state can be described by the nuclear coordinates. This is known as the Born-Oppenheimer approximation, which is the main assumption of molecular dynamics calculations [56].

4.2.1 Empirical force field model

An important part of MD is to define a suitable particle interaction that mimics the physical interactions within the system. The level of detail included in the interaction potential will depend on the quantities being calculated. *Ab initio* molecular dynamics involves the quantum mechanical treatment of electrons. This is computationally expensive to perform because of the large number of particles that need to be considered in cluster simulations.

A simpler approach is to use an empirical "force field" to describe the potential energy of a particle as a function of the nuclear position. This treatment does not include the motion of electrons explicitly, and for this reason is less computationally demanding than *ab initio* calculations. The molecular dynamics force field is a potential energy function that describes the interaction between particles. It allows for the potential energy of particles to be represented as a multidimensional surface with atomic or molecular positions as variables. The force described by the force field changes continuously with particle separation. This behaviour describes the coupled nature of the motion of the particles, and is commonly termed collective motion. To define a force field we must specify the functional form of the potential and any necessary parameters (like harmonic constants). The force field is fitted against physical properties determined experimentally and with *ab initio* calculations, which make it empirical in nature. A widely used empirical potential is the Lennard-Jones $12-6$ potential given by Equation (4.11), where ϵ and σ are the potential well depth, and length scale respectively, and r_{ij} is the separation between the i^{th} and j^{th} particles. For a system of liquid argon, the Lennard-Jones parameters have values of $\sigma = 3.4050$Å and $\epsilon = 0.9955\text{kJmol}^{-1}$ [57].

$$V_{ij} = 4\,\epsilon \left[\left(\frac{\sigma}{r_{ij}} \right)^{12} - \left(\frac{\sigma}{r_{ij}} \right)^{6} \right] \tag{4.11}$$

The Lennard-Jones potential is an example of an intermolecular non-bonded interaction that is defined between different particles or molecules. In contrast, intramolecular bonded interactions are defined between atoms within the same molecule, such as covalent "chemical" interactions. There are different types of particle motion that are associated with bonded and non-bonded interactions, which are illustrated in Figure 4.1. Typically, bonded particles undergo bond stretching and bond bending motions as well as bond rotating motions that occur between planes. The angle between two rotating planes is called the dihedral rotation angle. The non-bonded interactions describe pairwise interactions between atoms in different molecules, or within the same molecule provided they exclude bonded atoms [56]. This is because atoms bonded in the chemical sense should not participate in intermolecular interactions [58]. Most molecular force fields exclude a minimum of three nearest neighbours within the same molecule for the calculation of non-bonded interactions [59].

A key attribute of empirical force fields is the transferability of the potential functional and the parameters to describe interactions in similar types of molecules. This enables a set of

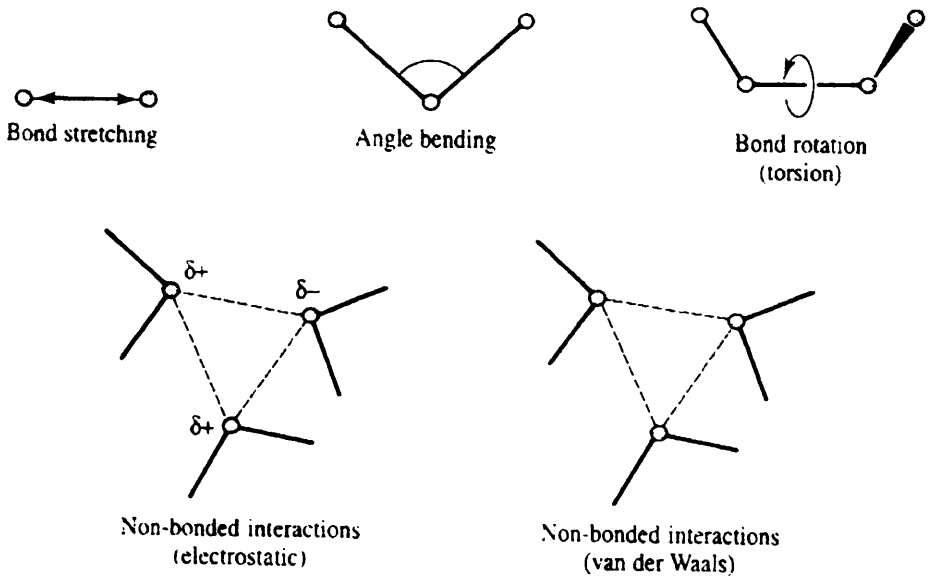

Figure 4.1: A schematic representation of the five basic interactions important for molecular systems: bond stretching, angle bending, torsional terms (due to bond rotations between molecular planes), as well as non-bonded electrostatic and Van der Waals interactions [56].

parameters that are tested on a relatively small number of cases to be applied to a much wider range of problems. For instance, the same set of potentials and parameters are used to model a series of liquid alkanes [59] in a study of the liquid properties.

4.2.2 Equations of motion and the Verlet algorithm

Under the influence of a continuous potential, the motion of particles are coupled together giving rise to a many body problem that can not be solved analytically. Instead, the equations of motion are approximated by a numerical integration based on a finite difference method. This approach breaks down the integration into many small stages each separated by a fixed time δt. The positions, velocities and accelerations can be approximated by a Taylor expansion to first order, provided δt is sufficiently small, and the force acting on the particle is slowly varying. This is the basis of most varieties of integration algorithm that are used to solve the equations of motion in MD. A popular velocity integration algorithm is the Verlet Leapfrog algorithm. Particle positions at time t are used to evaluate the force at t, which are then used to get the acceleration at t. The acceleration is used together with the velocity at the previous half time step $t - \frac{1}{2}\delta t$ to calculate the velocities at the next half time step $\mathbf{v}(t + \frac{1}{2}\delta t)$ as shown by

$$\mathbf{v}(t + \frac{1}{2}\delta t) = \mathbf{v}(t - \frac{1}{2}\delta t) + \delta t\,\mathbf{a}(t). \tag{4.12}$$

Hence the positions and forces are defined at time t, while the velocities are defined half a time step behind. The positions at the next full time step $\mathbf{r}(t + \delta t)$ are deduced from the velocities calculated in Equation (4.12) together with the positions at time t as shown by

$$\mathbf{r}(t + \delta t) = \mathbf{r}(t) + \delta t\,\mathbf{v}(t + \frac{1}{2}\delta t). \tag{4.13}$$

The subsequent velocities at time t are calculated using

$$\mathbf{v}(t) = \mathbf{v}(t + \frac{1}{2}\delta t) + \mathbf{v}(t - \frac{1}{2}\delta t). \tag{4.14}$$

In this sense, the velocities are considered to "leap" over the current integer time step to give values at the next half integer time step, which is why it is called the Leapfrog algorithm. This has the obvious disadvantage that the positions and velocities are out of sync, and are never calculated at the same time instant. This means that the kinetic energy which is determined from the velocities, can not be calculated at the same time as the potential energy, which is determined from positions. Despite this inconvenience, the Leapfrog algorithm conserves energy and angular momentum, and it is time reversible, which make it sensible choice of integration method for this study.

4.3 Principles of Stochastic and Langevin Dynamics

Another important modelling technique in this study is stochastic dynamics. Stochastic behaviour is not deterministic but random in the sense that the next state can not be fully predicted from the previous state. A stochastic process can be used to model the evolution of variables which are governed by a complex dynamic. The behaviour of such systems can not be predicted easily using deterministic molecular dynamics because of the considerable and arbitrary size of the numerical task. This forces us to represent the system's evolutionary behaviour to a seemingly unpredictable or random factor. Examples of stochastic processes can be physical, such as the turbulent motion of air flow [60], or non physical such as the price of stock in the stock market and exchange rate fluctuations [61].

A well known example of a simple physical stochastic process is Brownian motion. This describes the perpetual random motion of a macroscopic particle such as a pollen grain

when immersed in a fluid of liquid or gas particles. Brownian motion was first observed by Robert Brown with pollen grains in water. Brown, who was a botanist, concluded the behaviour of the pollen grain was due to "a general life force in organic matter". It was later deduced by Einstein [62], [63] that this behaviour of pollen grains arose from the continuous bombardments of the surrounding water molecules. If the system were treated exactly using molecular dynamics, we would need to solve the coupled equations of motion for all the particles in the system. This is a difficult task to accomplish, since we do not know the initial position of all the particles in the fluid. Instead, the force on the Brownian particle is approximated using an effective treatment of its interactions with the environment. The random impacts of the surrounding particles generally cause two types of effect. Firstly, they act as the random driving force responsible for the particle's incessant irregular motion. This force is characterised by a mean number of random collisions per unit time. The motion of the particle through its environment gives rise to a second force, which represents the drag experienced by the particle due to its motion through a fluid. Within the time taken for the Brownian particle to move a relatively short distance in the fluid, it will have suffered many collisions with the fluid particles. The motion of the Brownian particle occurs over a much longer timescale than the collisions as the particle is much larger than the surrounding fluid particles. The Brownian particle feels an average force due to the preferential collisions opposing its direction of motion. This is defined as the friction force which is proportional to the negative velocity, so that the faster the Brownian particle moves, the more resistance is felt [64]. The friction force is dissipative in nature, because if no other forces acted on the Brownian particle, its velocity would eventually reach zero as its momentum is transferred to the fluid.

A better understanding of the two forces can be achieved by viewing the system in terms of frames of reference. If we imagined the Brownian particle's centre of mass to be fixed, then the bombardments from the fluid are equally likely to occur from all directions, and the average force due to these collisions will be zero. In contrast if we imagine the centre of mass motion of the fluid to be fixed, then a moving particle will experience higher impact collisions against the direction of motion. In other words the preferential force felt by the moving particle opposes the direction of motion. The random force and the friction force have the same origin, which means that they must be related in a fundamental way. The relationship between the friction and random parts of the microscopic force is a special form of the Fluctuation Dissipation Theorem (FDT) [65].

In certain situations, a Brownian description of motion has been used for particles that

are a similar size to the surrounding fluid particles [6]. In this case, the immersed particle incurs collisions with the fluid over the timescale of its motion. This means that within the time taken for it to travel a short distance, there will have been only a few collisions with the fluid, which are likely to change the particle's velocity. Consequently, the immersed particle does not feel an average opposing force, at least over the timescale of collisions. However, over a sufficiently long timescale the immersed particle will have experienced so many collisions that oppose its direction of motion, that it feels an average force acting against it. The equation of motion for a light immersed particle undergoing Brownian motion is given by the Langevin Equation,

$$m\,\dot{v}(t) \;=\; -\,m\,\gamma\,v(t) \;+\; \tilde{f}(t). \tag{4.15}$$

The equation is an inhomogeneous, first order, stochastic differential equation, where v is the velocity in 1-dimension, and γ is the coefficient of friction with units s^{-1}. The total force acting on the immersed particle is decomposed into the fluctuating stochastic force $\tilde{f}(t)$, which is brought about by the particle's continual bombardment with its surroundings, and the force attributed to friction $-m\gamma\,v$, which is due to the particle's motion through the fluid.

The Langevin Equation has a different interpretation for massive Brownian particles and lighter immersed particles, since their relative motions operate over very different timescales. For large Brownian particles like pollen grains, the timescale of their motion is much longer than the timescale of collisions they experience with the fluid. This means that the friction and random forces are averaged over numerous collisions with the surrounding fluid. Under such circumstances the Langevin Equation represents a true equation of motion, in the sense that it is evolving in real time. However, for lighter immersed particles of similar or equal size to the fluid particles, the Langevin Equation is only valid over sufficiently long timescales, over which the friction and random forces are time averaged. This condition regards lighter particle dynamics as Brownian on some coarse timescale, where determinism is not apparent but the complex behaviour is.

The general solution for an inhomogeneous first order ordinary differential equation is of the form

$$v(t) \;=\; v(0)\;e^{-\gamma\,t} \;+\; \int_0^t e^{\gamma\,(t'-t)}\,\Gamma(t')\,dt' \tag{4.16}$$

where t' represents a dummy time variable, and Γ represents the randomly fluctuating

force per unit mass where $\Gamma = \frac{\tilde{f}}{m}$. The first part of the solution $v(0)$ depends on the initial conditions. The second part of the solution persists when the memory of the initial conditions is lost.

4.3.1 The autocorrelation function

An important part of dealing with random processes is the relationship between fluctuations of random variables. By definition, the deviations of a random variable from the mean will be zero on average, but the average of the square of the deviations will not. The measure of association between two random variables indicates how well the value of one variable can be predicted from the other. This is the measure of correlation between any two random variables, which is determined by the correlation function. In general, the correlation function is equal to the average of the product of two random variables. If the correlations are between two different random variables, considered at the same time, then it is called a mutual correlation function. If the correlations are between the same random variable but at different times then it is called the autocorrelation function. The autocorrelation function is an important quantity in dynamical systems because it characterises the time dependent behaviour of random fluctuations.

The velocity autocorrelation function

The velocity autocorrelation function $G(t)$ indicates the timescale over which correlations between particle velocities persist, as shown by

$$G(t) = \langle v(0)v(t) \rangle. \tag{4.17}$$

If we consider the autocorrelation function of a particle's velocity, there will be a maximum correlation equal to the mean square velocity $\langle v^2 \rangle$ at the initial time $t = 0$, since the two velocities are identical. As the time interval between velocities increases, the particle will be subject to random collisions from the fluid. This reduces the degree of correlation on average, and the correlation function decreases. After a sufficiently long time the two velocities are completely independent and the velocity autocorrelation function goes to zero.

The time taken for the correlation function to fall by $\frac{1}{e}$ defines the mean correlation time τ_c. In a sense this defines the period of time for which the system retains a memory of

its previous velocity. Assuming the correlation function decays exponentially, the mean correlation time is given by

$$\tau_c = \frac{1}{G(0)} \int_0^\infty G(t')dt' \tag{4.18}$$

which relates τ_c to the area under the velocity autocorrelation curve, which is calculated by multiplying the height of the correlation function at $t = 0$ (*ie* $(G(0))$) with the time taken for $G(t)$ to reach $\frac{1}{e}$ of its original value.

4.3.2 Mean square displacement

The distance travelled by an immersed particle in time t can be found by integrating its velocity

$$x(t) = \int_0^t v(\tau)d\tau. \tag{4.19}$$

The mean square displacement can be related to the velocity autocorrelation function $G(t)$, using Equation (4.19). This involves a non-trivial derivation [6], which leads to the relation

$$\langle\, x^2(t)\,\rangle = 2\int_0^t (t-\tau)\, G(\tau)\, d\tau. \tag{4.20}$$

Next, we will consider the mean square displacement for two limiting cases of timescale, which result in two very different types of particle motion.

Short time limit

For times much shorter than the correlation time $t \ll \tau_c$ the autocorrelation function will not have changed much from its initial value, so we can say $G(t) \approx G(0)$. This can be substituted into Equation (4.20), which gives

$$\langle\, x^2(t)\rangle = v^2(0)\, t^2 \tag{4.21}$$

where $\langle x^2(t)\rangle$ is proportional to t^2, which indicates the particle is moving freely. This is due to the fact that over short timescales the particle will not have experienced sufficient random collisions to have a significant effect on its motion.

Long time limit (diffusion)

The second case is for times much longer than the correlation time $t \gg \tau_c$. Over sufficiently long timescales, we can assume the autocorrelation function will have decreased to zero, so that $G(t) \approx 0$. This means that to good approximation we can evaluate Equation (4.20) with an upper limit of ∞, which gives

$$\langle x^2(t) \rangle = 2 \int_0^\infty G(\tau)\, t\, d\tau - 2 \int_0^\infty G(\tau)\, \tau\, d\tau \tag{4.22}$$

where the second term is independent of time t, which makes it negligible compared to the first term (since we are considering the long time limit). Therefore we can write the mean square displacement as,

$$\langle x^2(t) \rangle = 2\, t \int_0^\infty G(\tau)\, d\tau \tag{4.23}$$

which shows that $\langle x^2(t) \rangle$ is proportional to time t, which is characteristic of a diffusive process [6]. We can write the mean square displacement (in 1-dimension) as shown by

$$\langle x^2(t) \rangle = 2\, D\, t \tag{4.24}$$

where D is the diffusion coefficient defined as the area under the velocity correlation curve, given by

$$D = \int_0^\infty G(\tau)\, d\tau. \tag{4.25}$$

We recall that the area under the velocity correlation curve is related to the velocity autocorrelation time, which was defined by Equation (4.18). Therefore, we can write the diffusion coefficient in terms of the velocity autocorrelation time, as shown by

$$D = v^2(0)\, \tau_c. \tag{4.26}$$

Assuming the immersed particle is in thermal equilibrium with its surroundings, we can use the equipartition theorem (Equation (4.5)) in 1-dimension to write the particle velocities as $v^2 = kT/m$, which leads to a relation between the diffusion coefficient and the velocity correlation time, given by

$$D = \frac{kT}{m}\tau_c. \tag{4.27}$$

Equation (4.27) is generally known as the Einstein relation [66], where T is the temperature of the system, m is the mass of a molecule, and τ_c is the velocity autocorrelation time. It should be noted that the diffusion coefficient is not directly proportional to temperature, since τ_c is also a function of temperature.

4.3.3 The fluctuation dissipation theorem

The stochastic Langevin force Γ, defined in the context of Equation (4.16), is assumed to have an ensemble average equal to zero, for $v = 0$, as shown by

$$\langle\, \Gamma(t)\, \rangle = 0. \tag{4.28}$$

It is also assumed that the stochastic forces at time t_1 and some later time t_2 are approximately independent, which is valid if the timescale of collisions is much smaller than the timescale over which the force is observed, which is given by

$$\langle\, \Gamma(t)_1\, \Gamma(t_2)\rangle = \Gamma^2\, \delta\,(t_1 - t_2). \tag{4.29}$$

This assumption is important for systems with a light immersed particle, because it means that sufficient time has passed between consecutive collisions for the effect of a collision to have dissipated. A random force with this property is said to be δ-correlated, which is also called white noise, where Γ can be viewed as the "strength" of the noise. In contrast, a random force that is not δ-correlated is called coloured noise.

When the assumptions described by Equations (4.28) and (4.29) are applied to Equation (4.16) in the long time limit, under conditions of thermal equilibrium [64], we get the relation

$$\gamma = \frac{m}{2\,k\,T}\ \Gamma^2. \tag{4.30}$$

This illustrates the connection between the frictional force, which is related to γ and the random force, which is described by Γ. This important result is a fluctuation dissipation theorem (FDT) [66], and it relates in a fundamental way the random fluctuations in the system to the dissipative force characterised by friction.

4.3.4 The frictional force

Typically, frictional forces occur when a body moves through a static fluid, and to first approximation the opposing force it experiences is proportional to its velocity. The force is a direct consequence of the moving body's collisions with the surrounding fluid particles. The mechanism of the friction force can be understood in terms of molecular motions. As a molecule moves in a particular direction it undergoes a change in velocity over a given time period. If we consider the particle to have a velocity $v(t)$ and a future velocity $v(t + \tau)$, then the velocity change over the time interval τ is the molecular acceleration at time t. If τ is very large, then it is likely the particle will have experienced so many collisions with its neighbours that its acceleration is no longer related to its initial velocity $v(t)$. In contrast, if τ is small then the particle may not have travelled far enough to experience sufficient collisions with its neighbours for it to feel the preferential force opposing its velocity. Instead, its acceleration will be deterministic in nature. In between these two limiting cases there is a time interval for which the particle acceleration will be proportional to its velocity at time t. This timescale defines the duration over which frictional forces act within the system.

When a cluster molecule suffers a collision with a neighbour its energy changes in response to that collision. This brings about fluctuations in the kinetic energy, and consequently the molecule's velocity. The time taken for the energy to dissipate defines the time for which there is a correlation between the initial and final velocities of the molecule, which can be viewed as the molecule's "memory".

As mentioned previously, the frictional force is proportional to the particle velocity. This means that the velocity correlation time must also be related to the frictional force. This relation can be derived from the solution to the Langevin equation [6], given by Equation (4.16), and from the definition of the velocity autocorrelation function for a time interval τ, as shown by Equation (4.31). The first term on the right of Equation (4.31) describes the initial state of the system which goes to zero for long timescales. The second term describes the correlation between the initial velocity $v(0)$ and the acceleration $\Gamma(t')$, at a much later time, which is equal to zero. The remaining third term describes the equilibrium steady state behaviour independent of the initial conditions.

$$\begin{aligned}\langle\, v(t)\, v(t+\tau)\,\rangle \;&= v^2(0)\; e^{-\gamma\,(2t+\tau)} + \\ &e^{-\gamma\,(2t+\tau)} \int_0^t e^{\gamma\, t'}\, v(0)\, \langle\, \Gamma(t')\,\rangle\, dt' + \\ &e^{-\gamma\,(2t+\tau)} \int_0^t dt' \int_0^{t+\tau} e^{\gamma\,(t'+t'')}\, \langle\, \Gamma((t')\,\Gamma(t'')\,\rangle\, dt''\end{aligned} \tag{4.31}$$

Substituting Equations (4.28) and (4.29) into this expression, forces the two time variables t' and t'' to be equivalent, so that the velocity autocorrelation function can be written as

$$G(\tau) \;=\; \langle\, v^2(0)\,\rangle\, e^{-\gamma\,\tau} \tag{4.32}$$

where $\langle\, v^2(0)\,\rangle \;=\; \frac{\Gamma^2}{2\gamma}$, which is deduced from Equation (4.30) and the equipartition theorem. This result is substituted into Equation (4.18) and integrated, which gives the velocity autocorrelation time in relation to the friction coefficient as

$$\tau_c \;=\; \gamma^{-1}. \tag{4.33}$$

We recall that in the long time limit, τ_c is related to the diffusion coefficient D, which was previously defined by Equation (4.27). This means the frictional forces in the system are also related to diffusion.

4.3.5 The Fokker-Planck Equation

The velocity of the Langevin particle is dependent on the random force, which means it will vary stochastically. Since velocity is a continually changing variable, the probability associated with finding the system at a particular velocity interval ($v \;\rightarrow\; v + \delta\, v$) is defined by the probability density distribution of particle velocities $W(v)$. It is standard manipulation to convert a Langevin equation of motion (in 1-dimension) into a time evolution of the probability density [66], as shown by

$$\frac{\partial\, W}{\partial\, t} \;=\; \gamma\, \frac{\partial\,(vW)}{\partial\, v} \;+\; \gamma\, \frac{k\,T}{m}\, \frac{\partial^2\, W}{\partial v^2} \tag{4.34}$$

where v is a 1-dimensional velocity. This is also known as a Smoluchowski Equation, which is the equation of motion for probability density in 1-dimension [66].

4.4 Langevin Dynamics Applied to Cluster Decay

In this section we use the Langevin picture of particle motion through a fluid to describe the decay mechanism of molecular clusters. The Langevin treatment of a cluster views the decay mechanism as single particle escape from a constraining potential, driven by a random force due to all the other molecules in the cluster (and the carrier gas if present). This means that cluster decay is viewed from the perspective of an individual molecule within the cluster, where the constraining potential is a potential of mean force. Each molecule in the cluster is considered to move in a 3-dimensional potential well due to its average interactions with all the other cluster molecules that are randomly colliding with it. A similar approach was used by Nowakowski and Ruckenstein [67], [68], which modelled cluster decay as a diffusive process along an energy reaction co-ordinate. However, this approach failed to take into account the radial position of particles within the cluster, and thus was not a realistic view of cluster decay, as a fluctuation to positive energy will only lead to decay if the particle is near the cluster's surface.

More recently, a variation of this approach was adopted by Ford and Harris [39], which considered the motion of Lennard-Jones particles in real space along a radial reaction co-ordinate. The radial motion of an individual molecule relative to the cluster's centre of mass was modelled using a Langevin equation for noise-driven dissipative motion in a potential well, given by

$$m\dot{v} = f(r) - m\gamma\, v + \tilde{f}(t) \tag{4.35}$$

This equation is similar to Equation (4.15) except it includes the mean force $f(r)$ on the particle due to its average potential interactions with the surrounding particles. The mean force is the average potential interactions felt by a particle due to its neighbours. It is very different to the collision induced frictional force and the random force, which are principally kinetic in nature. The particle forces are treated in 1-dimension along the radial co-ordinate relative to the cluster's centre of mass, assuming the cluster is spherically symmetric. This reduction in the degrees of freedom implicitly assumes a certain symmetry of the dynamics, and that the inclusion of higher dimensions would yield the same result. This is a reasonable assumption since a single-particle dynamical model with a spherically symmetric forcefield will invariably produce a spherically symmetric mean radial force.

It seems sensible that the likelihood of particle escape is related to its position in the cluster, as well as its energy. In addition to this, if the cluster is surrounded by a carrier gas this

will increase thermal fluctuations within the cluster and assist the particle's escape. A sensible guess for the equilibrium probability density distribution $P(r)$ for a particle at radial position r from the cluster's centre of mass would be the Boltzmann distribution, given by

$$P(r) \propto e^{-\Phi(r)/kT} \tag{4.36}$$

where Φ defines the potential of mean force, which is related to the mean radial force by

$$\Phi(r) \equiv \int_0^r d\Phi(R) = -\int_0^r f(R)\, dR \tag{4.37}$$

If we evaluate the integral in Equation (4.37) between $r = 0$ (the cluster's centre of mass) and r_e, which is the cluster escape radius defined as the radius at which Φ first reaches a plateau, we obtain the change in potential of mean force $\Delta\Phi$, which we refer to as the cluster potential of mean force depth. The larger the potential depth, the less likely it will be for a particle to escape as large thermal fluctuations will be needed to assist it out of the confining potential. The relation between the particle escape rate and confining potential depth is illustrated schematically in Figure 4.2. The relation is mathematically represented in terms of the Langevin cluster decay rate, which is derived from the equation of motion of probability density in 3-dimensions (*ie* the Fokker-Planck Equation). The derivation of the Langevin cluster decay rate is outlined next, and it is largely adapted from Tang and Ford [69], and Harris and Ford [39].

The Langevin description of particle motion can be simplified by taking the small mass, or high friction limit, which treats the decay particle as comparable to those comprising the surrounding fluid. The Fokker-Planck equation in 3-dimensions is given by

$$\frac{\partial W}{\partial t} = \frac{1}{m\gamma}\left[-\nabla \cdot (\mathbf{f} W) + kT\,\nabla^2 W\right] \tag{4.38}$$

where $\mathbf{f} = -\nabla\Phi(x, y, z)$ and $W(r, t)$ is the probability density of finding a particle at position r and time t. This represents the full 3-dimensional Fokker-Planck equation, as opposed to the 1-dimensional one stated in Equation (4.34). The model can be simplified to a form more suitable for a molecular cluster by transforming the problem into spherical polar coordinates, relative to the cluster's centre of mass (assuming spherical symmetry). In this scenario only the radial properties are needed, and the mean force becomes the mean radial force $f = \frac{\partial\Phi}{\partial r}$ as shown by

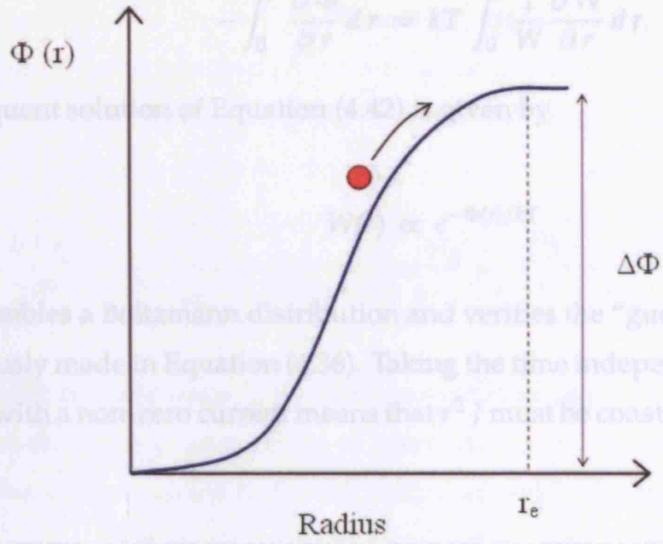

Figure 4.2: A schematic representation of a particle in a cluster confined by a potential of mean force $\Phi(r)$. The potential of mean force is centred about the cluster centre of mass position at $r = 0$. The particle can escape by reaching a radial position of r_e, driven by a phenomenological stochastic force. The cluster escape radius r_e has an arbitrary value that can be estimated for a decay event to be the radius at which the potential of mean force first reaches a plateau.

$$\frac{\partial W}{\partial t} = \frac{1}{m\gamma}[-\frac{1}{r^2}\frac{\partial}{\partial r}(r^2 f W) + \frac{kT}{r^2}\frac{\partial}{\partial r}(r^2 \frac{\partial W}{\partial r})]. \tag{4.39}$$

The rate of change of the probability density can be interpreted as the divergence of the probability current moving outward from the cluster's centre of mass (in a radial direction), as shown by

$$\frac{\partial W}{\partial t} = -\nabla \cdot \mathbf{J}(r) = -\frac{1}{r^2}\frac{\partial}{\partial r}(r^2 J) \tag{4.40}$$

where equating and rearranging Equations (4.39) and (4.40) gives the probability current $\mathbf{J}$ as shown by

$$J = \frac{1}{m\gamma}[f W - kT\frac{\partial W}{\partial r}] \tag{4.41}$$

where J is the radial component of $\mathbf{J}$. The characteristic boundary condition for the probability density at the edge of the cluster, which we regard as the cluster's escape radius r_e is $W(r_e) = 0$. We can implement this boundary condition by writing the steady state solution as $J = 0$, upon which integrating gives

$$-\int_0^r \frac{\partial \Phi}{\partial r}\, dr = kT \int_0^r \frac{1}{W}\frac{\partial W}{\partial r}\, dr. \tag{4.42}$$

The subsequent solution of Equation (4.42) is given by

$$W(r) \propto e^{-\Phi(r)/kT} \tag{4.43}$$

which resembles a Boltzmann distribution and verifies the "guess" of the probability density previously made in Equation (4.36). Taking the time independent situation from Equation (4.40) with a non-zero current means that $r^2 J$ must be constant with respect to r, which gives

$$\frac{\partial W}{\partial t} = \frac{1}{r^2}\frac{\partial}{\partial r}(r^2 J) = 0. \tag{4.44}$$

This is a rough approximation, since it implies that there is no probability of escape, which means the cluster never decays. In actual fact, this is not true and it is assumed there is a small steady drain of probability or "leakage" such that $\frac{\partial W}{\partial t} < 0$. The probability current J can be rewritten in the form

$$J(r) \exp\left[\frac{\Phi(r)}{kT}\right] = -\frac{kT}{\gamma m}\frac{d}{dr}\left(W(r)\exp\left(\frac{\Phi(r)}{kT}\right)\right) \tag{4.45}$$

where the integration of both sides over all radii, from 0 to the escape radius r_e, given by the boundary condition $W(r_e) = 0$, leads to the expression of the probability current at the escape radius as shown by

$$J(r_e) = \frac{kT}{\gamma m} W(0)\left(r_e^2 \int_0^{r_e} \frac{1}{r^2}\exp\left(\frac{\Phi(r) - \Phi(0)}{kT}\right) dr\right)^{-1}. \tag{4.46}$$

The probability density at the centre of mass $W(0)$, can be evaluated by normalising the steady state solution over all space, so that

$$W(0) = \exp\left[-\frac{\Phi(0)}{kT}\right]\left(4\pi \int_0^{r_e} r^2 \exp\left(\frac{\Phi(r)}{kT}\right) dr\right)^{-1}. \tag{4.47}$$

Since $J(r_e)$ represents the probability current of a single particle at the edge of the cluster (assumed to be spherical), the decay rate of an i-cluster will be proportional to the number of particles i, and is given by

$$\nu_i^{kin} = 4\,\pi\,r_e^2\,i\,J(r_e). \tag{4.48}$$

The complete form of the kinetic decay rate is given by

$$\nu_i^{kin} = \frac{i\,k\,T\,r_e^2}{\gamma\,m}\,\frac{\exp\left(-\frac{\Delta\Phi}{kT}\right)}{\left[\int_0^{r_e}\exp\left(-\frac{\Phi(r)-\Phi(0)}{kT}\right)dr\right]\left[r_e^2\int_0^{r_e}\frac{1}{r^2}\exp\left(\frac{-\Phi(r)-\Phi(0)}{kT}\right)dr\right]} \tag{4.49}$$

where m is the particle mass, $\Delta\Phi_i$ is the potential of mean force depth for an i-cluster, r is the radius from the cluster centre of mass, and r_e is the escape radius, which may be estimated for a decay event to be the radius at which the potential of mean force first reaches a plateau. This result has been provided by Tang and Ford [69], and represents a complete 3-dimensional description of the variables. The decay rate shown by Equation (4.49) differs from the decay rate derived by Ford and Harris [39] by a factor of r^2/r_e^2 inside the second integral. The decay rate of an argon cluster of 50 molecules at 49 K, calculated using Equation (4.49) is approximately 1.5 times smaller than that predicted by Harris and Ford.

In essence, Equation (4.49) is a form of Arrhenius Equation, since it is defines the frequency of decay in terms of a temperature dependent exponential quantity. The important result here is that the kinetic decay rate is dependant upon the potential of mean force depth $\Delta\Phi$ and the frequency of particle collisions represented by γ. The practical implications of Equation (4.49) are important for cluster systems which have lengthy decay timescales and are quasi-stable at a given temperature and supersaturation. In these systems, the observation of dynamically generated cluster decay configurations are typically very rare, and obtaining sufficient decay statistics is a formidable if not impractical task. The kinetic decay equation shown here provides a crucial means of predicting cluster lifetimes. It can be used in the absence cluster decay configurations with certain approximations (discussed in Chapter 6), which makes it a highly efficient and desirable tool for this type of study.

4.5 Summary of Methods Applied to Cluster Dynamics

Molecular dynamics models of clusters provide a realistic treatment of the system dynamics. This study pursues an approach of treating clusters in isolation from the vapour in thermal equilibrium, using molecular dynamics simulations performed at constant tem-

perature. We focus on the calculating the decay timescale of clusters of complex molecules, using a Langevin interpretation of the decay mechanism. This bypasses the need to calculate the cluster work of formation and instead focuses attention on the potential of mean force of the cluster. The potential of mean force describes the average force felt by a particle at a particular radius from the centre of mass, which is related to the free energy required to remove a particle from the cluster to infinity. The cluster work of formation is the free energy required to form an i-cluster from i particles of vapour. The potential of mean force is easier to determine than the cluster work of formation as it is calculated from the molecular dynamics generated forces. Another important factor in determining the cluster decay rate is the frequency of particle collisions. This is characterised by the friction coefficient, which can be determined from the particle motion. In the next chapter we will discuss details of the dynamic cluster model, and test the MD tools employed.

Chapter 5

The Molecular Dynamics Model of *n*-nonane Clusters

The MD model of *n*-nonane clusters is based on the treatment of the clusters in isolation from the supersaturated vapour under the experimental conditions. This eliminates the interactions a cluster would normally experience with the surrounding vapour molecules. The approach of removing the cluster from its normal surroundings is often used in MD simulations of molecular clusters [38], [70] to improve the computational efficiency of the task. The approach used by this study is an effective treatment of molecular clusters, even though it is not the most direct treatment of the problem. Since the cluster is isolated, it is not allowed to grow by collision but it can still lose fast moving molecules by evaporation, so decay events can still occur. This constraint is illustrated in Figure 5.1, which implies that the evolutionary dynamics of the cluster, induced by collisions with vapour molecules will not be investigated. Instead, we focus on the interactions within the cluster itself that occur between cluster molecules, and observe how these interactions affect the cluster decay dynamics.

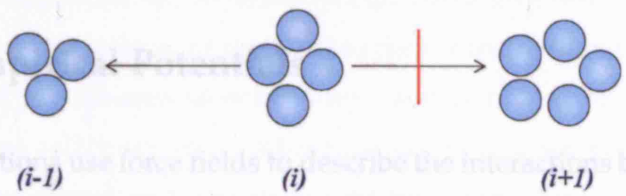

Figure 5.1: A schematic showing the isolating treatment of the cluster during the MD simulations. Growth by collision is not allowed but the cluster can still lose molecules by evaporation, so decay can occur.

5.1 Timescales of Interest

Under the experimental conditions, the cluster suffers collisions with the vapour molecules and the carrier gas molecules that surround it. The carrier gas collisions occur over a much shorter timescale than the vapour collisions, since the carrier gas molecules are much lighter than the vapour molecules and the concentration of the carrier gas is higher than the vapour. The timescale of collisions between the carrier gas and cluster can be estimated approximately from the kinetic theory for a collision cross section of a sphere. We calculate the typical collision time between a helium carrier gas and a cluster by evaluating the collision growth rate according to Equation (3.6) for a helium atom at the prevailing experimental conditions. We use a carrier gas pressure of 40kPa [11] and temperature of 233K for helium to determine the number of helium atoms, assuming it to be an ideal gas. The average collision time between the helium carrier gas and a 40-cluster is estimated to be 10ps. This is a significantly shorter timescale than the vapour collisions with the cluster, which was calculated to be 44.0ns for a 40-cluster at a temperature of 233K, with a supersaturation of 29, a saturated vapour pressure of 2.2889Pa, and a liquid bulk density of 765.1 Kg m^{-3} [11] (as stated in Chapter 3). The two collision timescales have a quantitative difference of about 3 orders of magnitude, so it is reasonable to assume there will be a substantially large number of carrier gas collisions in between vapour collisions with the cluster. Under these circumstances, to good approximation, the mean kinetic energy of a cluster molecule inside the cluster remains equal to that of the carrier gas. Provided there are a sufficiently large number of thermalising carrier gas collisions with the cluster, it is reasonable to assume that the cluster grows, and by implication decays, when it is at thermal equilibrium with the carrier gas. This suggests the use of constant temperature dynamics in the MD simulations, which can be implemented by immersing the cluster in a heat bath at a constant temperature T, to maintain the cluster in thermal equilibrium with its surroundings.

5.2 Liquid Empirical Potentials

Classical MD simulations use force fields to describe the interactions between the particles of a system. Typically, force fields describe the behaviour of particles comprising the bulk phase. Defining a force field for molecular clusters is not an easy task as it should describe both the surface and bulk interactions within the cluster. It is not clear how the potentials must be adjusted to correctly represent interactions of molecular clusters, a task which is

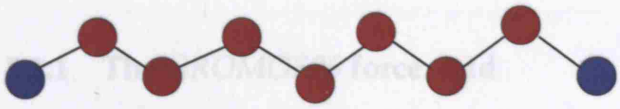

Figure 5.2: A schematic representation of the united atom model of a n-nonane molecule. The blue particles represent CH_3 groups and the red particles represent CH_2 groups. The united atom model has fewer degrees of freedom, which reduces the number of pairwise calculations that are needed to evaluate the potential energy.

beyond the scope of this study. Instead, we use empirical potentials of the bulk liquid to describe the interactions within the cluster. Although this is not an ideal approximation, it provides a practical means by which we can perform MD simulations of clusters. The simulations will ultimately test the suitability of liquid empirical potentials at describing the interactions within small molecular clusters.

The number of non-bonded interactions within a molecule scale with the square of the number of interaction sites present. In the case of n-nonane, each molecule has 9 carbon atoms and 20 hydrogens, which means there are approximately $\frac{29\times28}{2}$ pairwise calculations to perform to determine the molecular potential energy. Clearly there is a computational advantage if the number of interactions sites can be reduced. The simplest way to do this is to subsume the hydrogen atoms into the carbon atoms, so that a CH_3 group can be modelled as one particle called a united atom. Using a similar approach with the remaining CH_2 groups, n-nonane is reduced to a 9 particle united atom representation as shown in Figure 5.2.

By employing the united atom approach we aim to improve simulation efficiency by averaging out explicit degrees of freedom; however it is important that the united atom model still describes the dynamics of the cluster correctly. Obviously, the reduced system dynamics has certain limitations. For instance, polar molecules have large asymmetries in charge distribution [56], which can not be modelled as a single unit with spherically symmetric interactions. This is not an issue for n-nonane, since it is a charge neutral molecule. Another obvious consequence of the reduced dynamics approach is the necessary modification of the Van der Waals interactions for the united atom. Invariably, these interactions are centred on the largest atom's nucleus, as opposed to the centre of mass position of the united atom, which can lead to problems associated with energetic conformations. In the case of n-nonane this makes a relatively small difference since the hydrogens are comparatively lighter than the carbon atoms, and we can assume the centre of mass of the united atom is the same as the centre of mass of the carbon.

Overall, it is reasonable to assume that the spherical united atom model centred on the carbon nucleus is a fair approximation of the interactions sites of n-nonane, and similarly

for most hydrocarbons.

5.2.1 The *GROMOS96* force field

The intramolecular and intermolecular interactions of *n*-nonane clusters are modelled using the *GROMOS96* suite of united atom potentials [71]. The potentials are directly parameterised to reproduce the enthalpy of vaporisation, and the vapour pressure of liquid alkanes at 298K [59], [72]. The potentials comprise of bonded and non-bonded interactions, which result in the molecules having flexible bonds and a flexible structure. The united atom potential treats the hydrogen atoms implicitly, which is a reasonable approximation since *n*-nonane is overall non-polar, and the hydrogen atoms are assumed to have a negligible effect on the molecule's overall dynamics.

The bonded interactions are described by a combination of harmonic and an-harmonic potentials, as shown by

$$\begin{aligned} V^{bond}(\mathbf{r}) = & \sum_{n=1}^{N_b} \frac{1}{4} K_{b_n}[b_n^2 - b_{n_0}^2]^2 + \\ & \sum_{n=1}^{N_\theta} \frac{1}{2} K_{\theta_n}[cos\theta_n - cos\theta_{n_0}]^2 + \\ & \sum_{n=1}^{N_\iota} K_{\iota_n}[1 + cos(\delta_n)\, cos(m_n \psi_n)] \end{aligned} \tag{5.1}$$

where $\mathbf{r}$ is the $3N$-dimensional position vector of N atoms in the system. Generally, K defines the force constant, b defines the instantaneous bond length, θ the instantaneous bond angle, and ψ defines the torsion angle between two planes (see Figure 4.1). For the torsional interaction, δ_n is the equilibrium rotation angle between two planes and and m_n is the "strength" of the coupling. The superscript 0 refers to the equilibrium value of the respective quantity. The first summation describes the bond stretching motion between two covalently bonded atoms, and hence requires the specification of two atomic positions. The second summation describes the bond angle bending motion, which requires the specification of three atom positions. The third summation describes the interaction arising from the torsional forces that act on an atom as a result of bond rotations (see Figure 4.1), which requires the specification of four atom positions.

The non-bonded interactions usually comprise short range Van der Waals interactions, as well as long range electrostatic interactions for charged atoms. Since *n*-nonane is a non-

Bonded Interaction	Force Constant	Equilibrium Value
$CH_n - CH_n$	$K_{b_n} = 7.15 \times 10^6\,\mathrm{kJmol^{-1}}$	$b_{0_n} = 1.53\,\text{Å}$
$CH_n - CH_n - CH_n$	$K_{\theta_0} = 530\,\mathrm{kJmol^{-1}}$	$\theta_{0_n} = 109.5^o$
$CH_n - CH_n - CH_n - CH_n$	$K_{\Psi_n} = 5.92\,\mathrm{kJmol^{-1}}$	$cos(\delta_n) = +1.0$
		$m_n = 3$

Non-Bonded Interaction	ϵ (kJmol^{-1})	σ (Å)
$CH_2 \quad (-CH_2)$	0.4899	3.990
$CH_3 \quad (-CH_2)$	0.7327	3.905
$CH_3 \quad (-CH_3)$	0.7327	3.875

Table 5.1: The bonded and non-bonded parameters of n-nonane that are used in the MD simulations. The parameters are taken from the *GROMOS96* force field [59], [72].

polar molecule it does not have permanent dipole charges, so the electrostatic interactions can be neglected. The Van der Waals potential is modelled using a Lennard-Jones interaction, which has already been stated by Equation (4.11) in Chapter 4. This is an effective short ranged pair potential that describes the interaction between two uncharged atoms. It is strongly repelling for very small radii but weakly attractive for large radii. The *GROMOS96* parameters for the bonded and non-bonded interactions in n-nonane, that are used in the simulations are defined in Table 5.1.

5.3 Thermostatting Clusters

In order to achieve thermal equilibrium in MD it is essential that there be a suitable means of controlling the temperature of the system correctly. For clusters with just a few molecules this can be a difficult problem and consequently the issue of fixed temperature cluster dynamics is often avoided in MD, in favour of treating clusters in isolation, without a surrounding heat bath. This fixes the total energy of the cluster, which means that its thermodynamic temperature cannot be completely defined. The thermodynamic temperature is defined as the derivative of the system energy with respect to entropy $T = \partial E/\partial S$, which is different to the kinetic temperature, which is defined as the average kinetic energy of the system, given by the equipartition theorem $1/2m\langle v^2 \rangle = 3/2\,kT$. A molecular cluster that is isolated from its environment does not interact with its surroundings, but

its kinetic energy can vary about a mean value. Provided the mean kinetic energy has converged, we can characterise the thermal state using the kinetic temperature, obtained using the equipartition theorem. It is also possible to fit the distribution of velocities of a cluster molecule to a Maxwell-Boltzmann distribution, and use it to obtain an estimate for the cluster temperature, which provides a quantitative comparison to the kinetic temperature. Fixing the cluster's energy is not the most realistic approximation because the cluster normally interacts with a carrier gas (and the supersaturated vapour) under experimental conditions. It is preferable to impose canonical energy fluctuations on clusters with relatively long lifetimes (*ie* longer than the thermal equilibration time). This is achieved by maintaining the cluster in thermal contact with a larger system such as a heat bath. The correct thermalisation of the cluster is crucial, as the decay rate will be sensitively dependent upon the average kinetic energy per molecule.

5.3.1 The Berendsen thermostat

In MD, thermal equilibrium is achieved by using a thermostat to maintain the system at a fixed temperature. This means the simulated microscopic configurations are at the same temperature, and make up a canonical ensemble. There are various thermostats that are used to control the simulation temperature in MD. The method of temperature control employed should populate energetic modes according to the equipartition theorem. A familiar method used to control temperature is the Berendsen thermostat [73], which uses a simple approach of velocity scaling. It responds to kinetic energy fluctuations with a global rescaling of all velocities. Each particle velocity is multiplied by the same factor, to achieve the correct system temperature. Since each particle velocity is multiplied by the same scalar factor this is equivalent to scaling the system's total momentum by the same factor. The Berendsen thermostat is expected to conserve angular momentum [73], however, the global rescaling of the system velocities creates unphysical correlations between each particle and the rest of the system. For a large number of particles this is a fair approximation because the magnitude of rescaling is small since it is equally shared among all of the particles. However, for a small number of particles, the magnitude of rescaling for each particle is much larger, creating unrealistic correlations between particles in microscopic systems. This could lead to an incorrect equipartition of energy. If equipartition is not established properly in microscopic systems, a thermostat that populates translations and rotations about the centre of mass may cause the system to translate or spin nonphysically.

We employ constant temperature dynamics for a 40-cluster and 50-cluster using the Berend-

sen thermostat for a time period of 5ns. We use a coupling time parameter of 0.01ps, which is approximately three orders of magnitude greater than the coupling time between the cluster and a helium heat bath, as deduced at the start of the chapter, which accelerates the thermalisation between the cluster and the surrounding heat bath. To ensure that the Berendsen thermostat correctly conserves the cluster angular momentum we calculate the angular momentum of the cluster at each snapshot. The angular momentum for a system of particles about the centre of mass is given by

$$\mathbf{L} = \sum_{i}^{N} m_i \, \mathbf{r_i} \times \mathbf{v_i} \tag{5.2}$$

where m is the mass of the i^{th} particle in the cluster, r_i is its radial position relative to the centre of mass, and v_i is its linear velocity relative to the centre of mass [74]. The angular momentum can be expressed in terms of the angular velocity ω and the moment of inertia I as shown by

$$\mathbf{L} = I\,\omega \tag{5.3}$$

where $\omega = vr$ and I is given by

$$I = \sum_{i}^{N} m_i \, \mathbf{r_i}^2. \tag{5.4}$$

The angular momentum is related to the rotational kinetic energy given by

$$T_{rot} = \sum_{i}^{N} \frac{L_i^2}{2\,I_i} \tag{5.5}$$

which is analogous to the translational kinetic energy $T_{trans} = \sum \frac{p_i^2}{2m_i}$. The angular momentum of the cluster is calculated from Equation (5.2) using the positions and velocities from the MD trajectory. The magnitude of angular momentum L is plotted against snapshots in time for the 40 and 50 clusters, as shown in Figures 5.3 and 5.4 respectively. For both cluster sizes, the Berendsen thermostat causes a sharp increase in magnitude of the angular momentum. This could be due to the fact that the majority of the cluster's kinetic energy is contained in the centre of mass translation and rotation, leaving the vibrational degrees of freedom unpopulated. Other groups have reported similar difficulties concerning poorly conserved angular momentum of small clusters [75]. The Berendsen treatment of locally

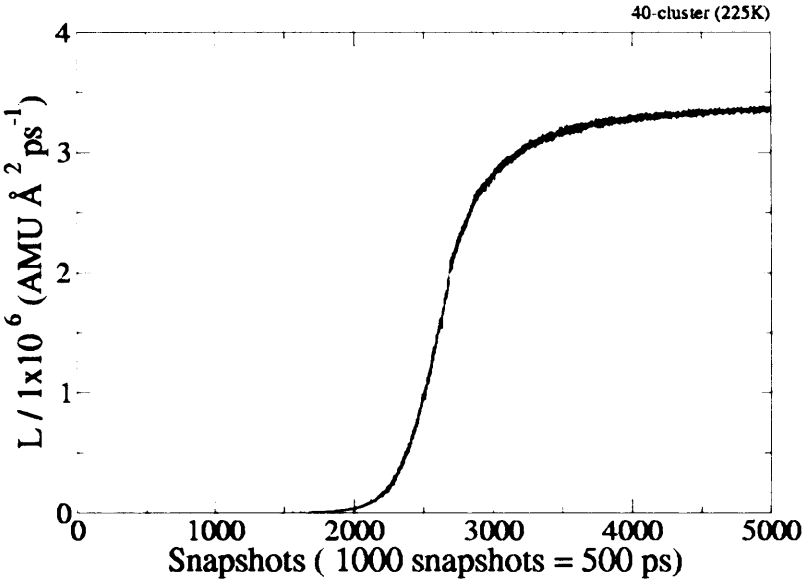

Figure 5.3: The angular momentum of a 40-cluster simulated at 225K for approximately 2.5ns with coupling time parameter 0.01ps. During this time the cluster suffers around 250000 thermalising collisions with the heat bath. The angular momentum is calculated from the united atom masses, positions, and velocities.

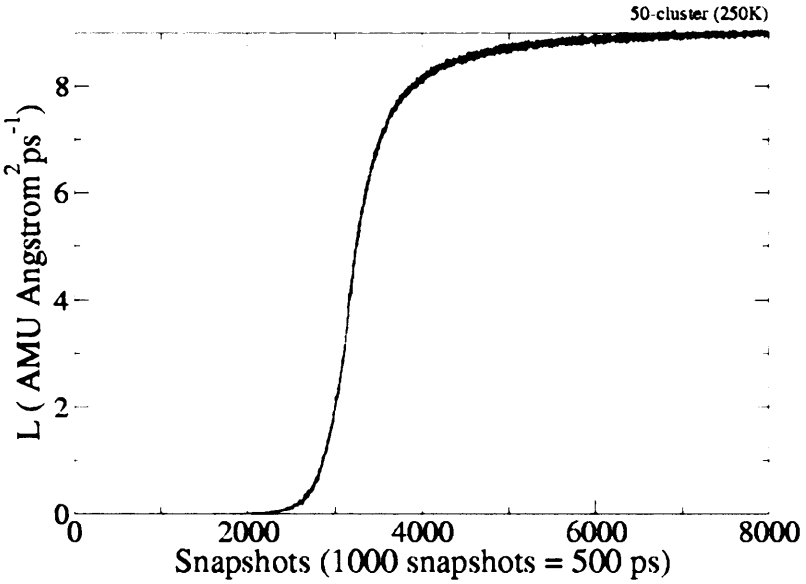

Figure 5.4: The angular momentum of a 50-cluster at 250K over approximately 4ns with coupling parameter 0.01ps. There are about 400000 collisions between the cluster and its surroundings during this time. The angular momentum is calculated from the united atom masses, positions, and velocities.

occurring kinetic energy fluctuations through a global velocity scaling of all particles is an unrealistic representation of the fluctuations in a microscopic system. For the case of the bulk, the Berendsen method may be sufficient, but for microscopic quasi-stable clusters, it carries serious consequences as it clearly does not conserve the cluster's angular momentum correctly.

5.3.2 The Andersen thermostat

An alternative approximation of the energy exchange between the cluster and carrier gas can be achieved using random collisions. This approach is implemented through the Andersen stochastic thermostat [76], [77], which mimics the effect of carrier gas collisions with the cluster using effective random collisions characterised by a random momentum transfer. The carrier gas collisions are treated implicitly, rather than explicitly. A recent MD study conducted by Tang and Ford [69] investigates the effect of explicitly modelled carrier gas collisions with argon clusters. However, this approach involves a large number of interacting particles, which can be a computationally demanding task to generate. The Andersen thermostat assumes that all atoms in the system are equally likely to suffer a collision, and that successive collisions are uncorrelated. This means that the probability distribution of time intervals between two successive collisions is of the form

$$P(\eta) = \eta \, exp\,[-\eta\,\tau] \tag{5.6}$$

where η is the collision frequency of the cluster atom with the carrier gas, which is equal to one over the mean atom lifetime, $1/\langle\,\tau\,\rangle$. The probability of uninterrupted motion of a cluster atom diminishes exponentially with τ, since it is unlikely for a cluster atom to survive for a long time without experiencing a random collision. The Andersen thermostat works by randomly selecting a cluster atom which is to suffer a carrier gas collision at some randomly sampled time. The atom is assigned a random velocity sampled from a Gaussian distribution at the temperature of the carrier gas (*ie* the average kinetic energy of the carrier gas).

The random nature of the Andersen thermostat means that the probability of incurring a collision is equally likely from all directions. Therefore the Andersen thermostat should conserve the angular momentum of the cluster, regardless of the system size, and the duration of simulation. To check that this is true, we calculate the angular momentum magnitude of a 40-cluster simulated at 225K using Andersen thermostat, maintained at NVT,

with a coupling time of 10ps. The magnitude of the angular momentum is plotted against time in snapshots as shown in Figure 5.5.

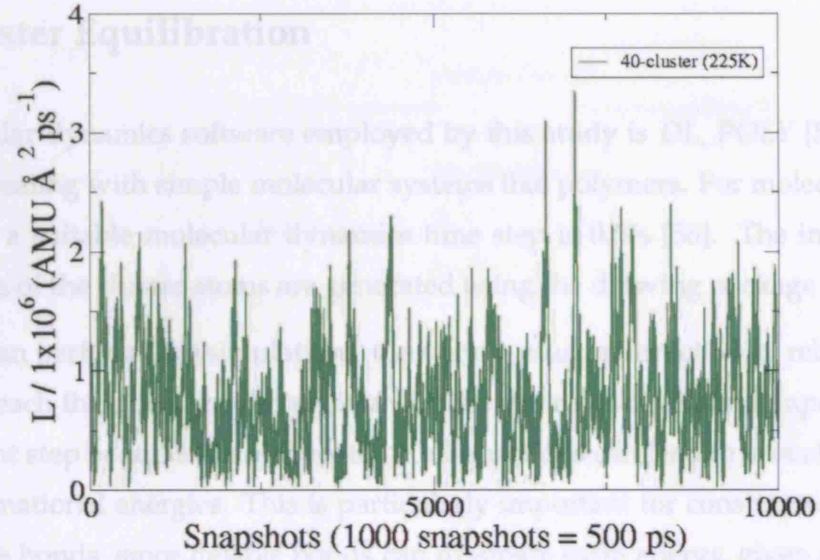

Figure 5.5: The angular momentum magnitude for a 40-cluster simulated at 225K for 5ns. During this time the cluster suffers approximately 500 thermalising collisions with the "effective" carrier gas modelled using the Andersen thermostat.

The plot indicates that the Andersen thermostat appears to control the angular momentum of the cluster correctly, and does not lead to unphysical spinning clusters. The average angular momentum magnitude in Figure 5.5 is $7.633 \times 10^5 \text{AMU}\text{Å}^2\text{ps}^{-1}$. We can check whether this is a quantitatively reasonable value by calculating the rotational kinetic energy of the system. According to equipartition theorem, a system in thermal equilibrium will have on average 1/2kT of energy for each degree of freedom. For a 40-cluster at 225K, this corresponds to an average rotational kinetic energy of 4.660×10^{-21}J. In contrast, the rotational kinetic energy can be calculated from Equation (5.5). To do this we calculate the moment of inertia about the cluster centre of mass using the united atom masses and positions, which is thus determined to have an average value over all snapshots of $8.267 \times 10^8 \text{AMU}\text{Å}^2\text{ps}^{-1}$. This is used in Equation (5.5), along with the average angular momentum magnitude squared to give an average rotational kinetic energy of 5.884×10^{-21}J. This value compares very well to the average rotational kinetic energy predicted by the equipartition theorem. Therefore, it is reasonable to assume the system is in approximate thermal equilibrium.

Overall, the Andersen thermostat provides a realistic and physical means of modelling

the experimental conditions that the cluster is exposed to. We have determined that the Andersen thermostat maintains the cluster angular momentum properly, with an average rotational kinetic energy of approximately 3/2kT.

5.4 Cluster Equilibration

The molecular dynamics software employed by this study is *DL_POLY* [58], which specialises in dealing with simple molecular systems like polymers. For molecules with flexible bonds, a suitable molecular dynamics time step is 0.5fs [56]. The initial positional co-ordinates of the cluster atoms are generated using the drawing package *XLeap*[1].

Before we can perform MD simulations, the system must be structurally relaxed so that all the atoms reach their equilibrium positions at the desired simulation temperature. This is an important step because unequilibrated configurations can lead to unrealistic structures and conformational energies. This is particularly important for constrained bonds rather than flexible bonds, since flexible bonds can dissipate extra energy, given sufficient time. A convenient approach to relaxing flexible *n*-nonane molecules is to gently elevate the temperature using molecular dynamics until the desired temperature is achieved. This is illustrated for a 5-cluster in Figure 5.6, in which the cluster temperature is increased by 50K (starting from 0K) every 125ps until the desired temperature is achieved (200K). The cluster is then simulated at the desired temperature for a sufficient amount of time to equilibrate its energy, as shown in Figure 5.7.

5.5 Molecular Dynamics Simulations of *n*-nonane Clusters

MD simulations are performed at *NVT* for *n*-nonane cluster sizes of 40, 50 and 67 at constant temperatures maintained using the Andersen thermostat. The simulated temperatures correspond to the experimental temperatures at which the clusters were deduced to be critical by Ford [22]. The simulations generate approximately 5ns of real time dynamics. We employ simple cubic periodic boundary conditions with a cubic cell parameter of 80Å, and a Van der Waals cut off radius of 30Å. The approximate time taken to conduct the MD calculations in real time, along with the computational specifications of the machine, are outlined in Appendix A.

[1] *Xleap* is part of the *AMBER* molecular dynamics modelling suite.

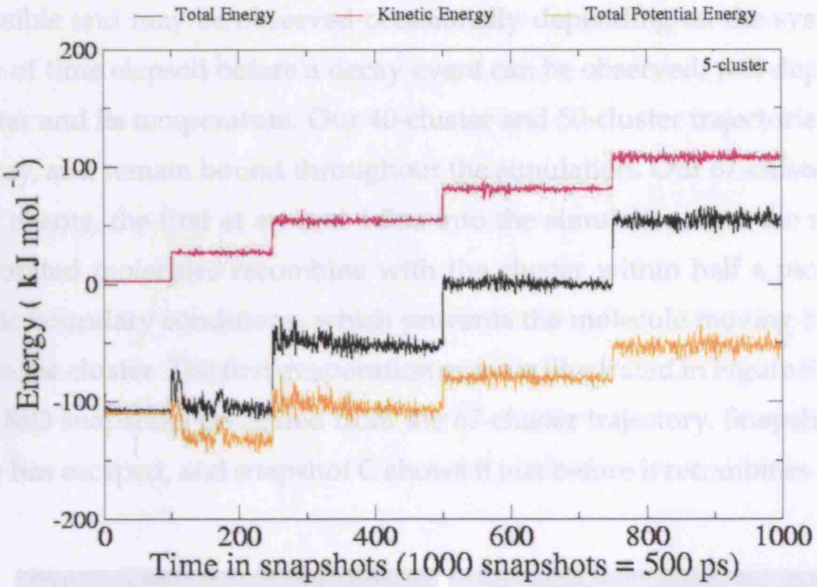

Figure 5.6: The temperature of the cluster is increased at intervals of 125ps, until the desired cluster temperature (200K) is achieved using a coupling parameter of 0.1ps. The total energy and potential energy are also plotted to show the relative change in energy contributions.

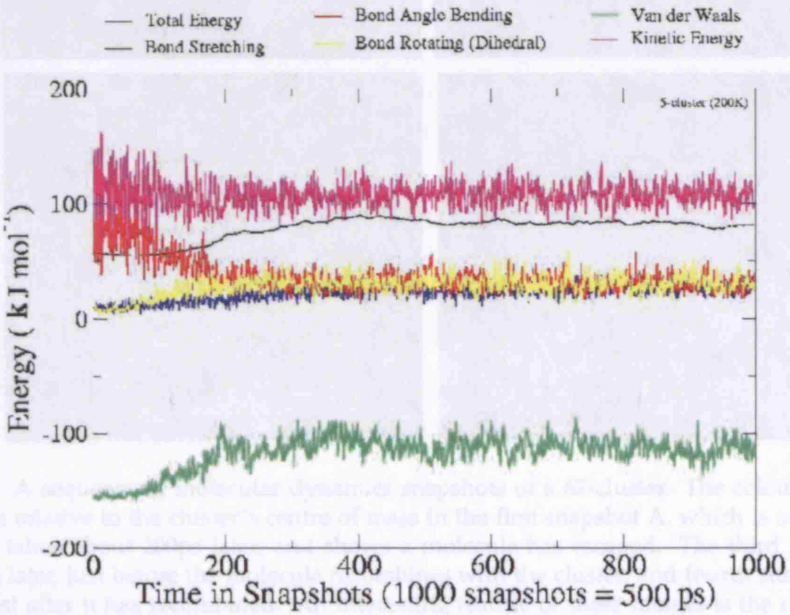

Figure 5.7: Equilibration of the 5-cluster after the temperature elevation to 200K, using a coupling parameter of 10ps. The different energy contributions are plotted against time in snapshots.

During the simulation the cluster is in thermal equilibrium with the effective carrier gas, but dynamically, it remains unstable with respect to decay. This means that decay events are permissible and may be observed occasionally depending on the system conditions. The length of time elapsed before a decay event can be observed, will depend on the size of the cluster and its temperature. Our 40-cluster and 50-cluster trajectories do not exhibit cluster decay, and remain bound throughout the simulation. Our 67-cluster trajectory has two decay events, the first at around 1.5ns into the simulation, and the second at 2.5ns. Both evaporated molecules recombine with the cluster within half a picosecond due to the periodic boundary conditions, which prevents the molecule moving beyond a certain region from the cluster. The first evaporation event is illustrated in Figure 5.8, which shows a series of MD snapshots generated from the 67-cluster trajectory. Snapshot B shows that a molecule has escaped, and snapshot C shows it just before it recombines with the cluster again.

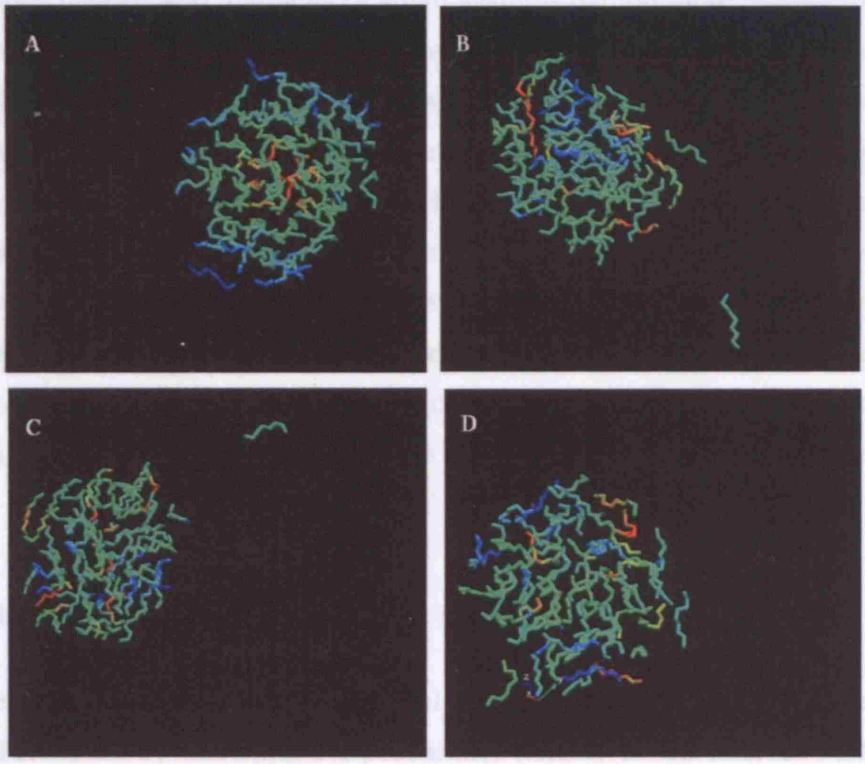

Figure 5.8: A sequence of molecular dynamics snapshots of a 67-cluster. The colour scheme represents radial position relative to the cluster's centre of mass in the first snapshot A, which is at 1.2ns. The second snapshot B is taken about 200ps later, and shows a molecule has escaped. The third snapshot C is taken another 200ps later, just before the molecule recombines with the cluster, and fourth snapshot D is a further 200ps later, just after it has recombined. An interesting feature of these images is the radial distribution of molecules within the cluster. As we might expect for a liquid cluster, the molecules appear to be disordered, which illustrates the cluster's unstructured fluid nature at 300K.

The colour scheme represents radial position relative to the centre of mass in snapshot A.

Clearly there are fewer molecules close to the cluster's centre of mass (red), and at the periphery (blue), than molecules within the cluster's main volume (green). This suggests that the sampling of forces for these regions may be relatively poor due to comparatively fewer statistics. At later stages of the simulation, the molecules explore different positions within the cluster, and become "mixed".

5.5.1 Temperature fluctuations

The cluster temperature is determined from the average kinetic energy, which is calculated from the particle velocities. The temperature of the cluster is plotted against simulation time in snapshots, as shown in Figure 5.9. The plot shows the temperature of a 40, 50, and 67-cluster. For all three cluster sizes, the temperature appears to fluctuate about a mean value, which is expected for small systems because the temperature is calculated from the average kinetic energy, and averages of small systems exhibit large fluctuations. In contrast, for large systems where $N \sim 10^{23}$, we expect the kinetic energy to remain relatively constant and the fluctuations to be small. This is because, in large thermodynamic systems, at any given instant, the large number of particles ensures that any variation of a system property from the mean will be negligible. Hence, for large systems, to good approximation, the temperature can be expressed in terms of the average kinetic energy. For small clusters, however, it is not sensible to define the temperature in the same way using the average kinetic energy because the instantaneous temperature is not fixed. The significant deviation in kinetic energy from the mean is obviously due to the cluster's small size, and this poses a problem over the validity of the kinetic definition of temperature over short timescales.

5.5.2 Particle velocities

We can determine whether a cluster's thermal fluctuations are correctly represented by the Andersen thermostat by deducing the probability density distribution of velocities. Following the discussions in Chapter 4, we expect the velocity to be distributed according to a Maxwell-Boltzmann distribution, provided the sum of independent velocity measurements has a finite variance. The Maxwell-Boltzmann probability density of velocities is given by

$$P(v) = A\, v^2 \exp\left[\frac{m\, v^2}{2\, k\, T}\right] \tag{5.7}$$

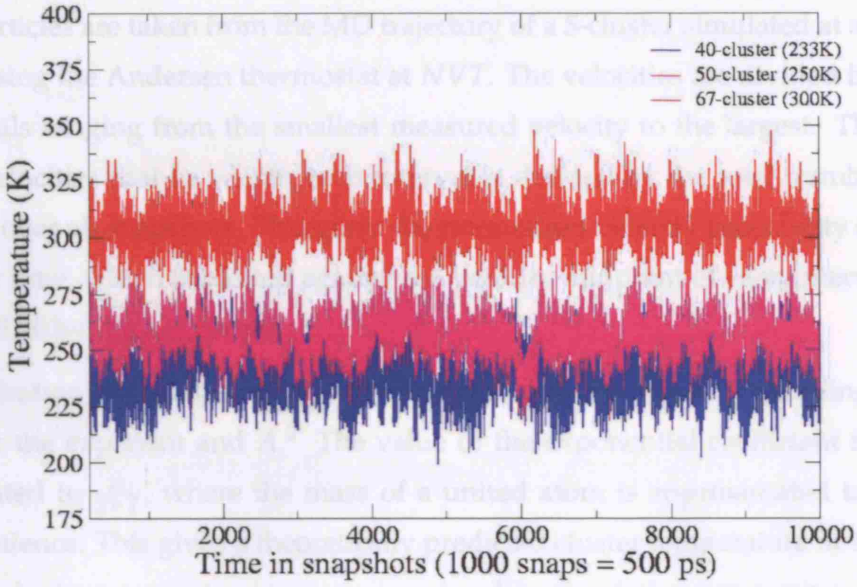

Figure 5.9: The temperatures for the 40, 50, and 67-clusters determined from the kinetic energy, plotted over 5ns (using the Andersen thermostat).

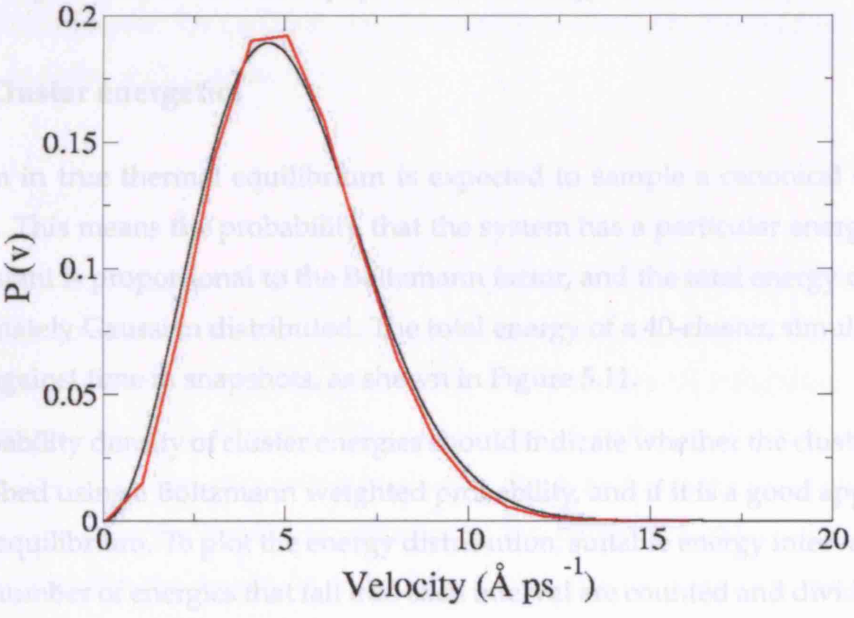

Figure 5.10: The red curve shows the normalised distribution of particle velocities obtained from the 5-cluster simulation at 175K. The black curve shows the predicted velocities from a Maxwell-Boltzmann distribution, which estimates the temperature to be 174.726K.

where v is the magnitude of the particle velocity, m is particle mass (united atom mass), T is the temperature of the cluster, and A is normalisation constant. The velocities of the cluster particles are taken from the MD trajectory of a 5-cluster simulated at a temperature of 175K using the Andersen thermostat at NVT. The velocities are divided into appropriate intervals ranging from the smallest measured velocity to the largest. The number of particle velocities that lie within each interval is divided by the total number of particle velocities over all snapshots. This gives the normalised velocity probability density, averaged over time, which is plotted against the velocity midpoint of each interval, as shown in Figure 5.10 by the red curve.

The distribution of Equation (5.7) is fitted to the simulated data by choosing appropriate values for the exponent and A.[2] The value of the exponential coefficient from the fit is then equated to $\frac{m}{2kT}$, where the mass of a united atom is approximated to that of CH_2 for convenience. This gives a theoretically predicted cluster temperature of 174.726K. The predicted cluster temperature compares very well to simulation temperature calculated by *DL_POLY* to be 175K, which is determined using the average kinetic energy of the cluster. The agreement between the two temperatures illustrates that the Maxwell-Boltzmann distribution is the correct representation of velocities for a cluster simulated at constant temperature at thermal equilibrium. It also supports the assumption that the Andersen thermostat produces the correct equipartition of energy for the cluster.

5.5.3 Cluster energetics

A system in true thermal equilibrium is expected to sample a canonical distribution of energies. This means the probability that the system has a particular energy state, at any given instant is proportional to the Boltzmann factor, and the total energy of the cluster is approximately Gaussian distributed. The total energy of a 40-cluster, simulated at 233K is plotted against time in snapshots, as shown in Figure 5.11.

The probability density of cluster energies should indicate whether the cluster energies can be described using a Boltzmann weighted probability, and if it is a good approximation to thermal equilibrium. To plot the energy distribution, suitable energy intervals are defined, and the number of energies that fall into each interval are counted and divided by the total number of cluster configurations (snapshots). The normalised population of each bin is the energy probability density, which is plotted against the midpoint value of each energy interval, as shown in Figure 5.12. The number of microscopic configurations of the cluster

[2]The theoretical fit is made in *Mathematica* using the *NonLinearFit* function [78]

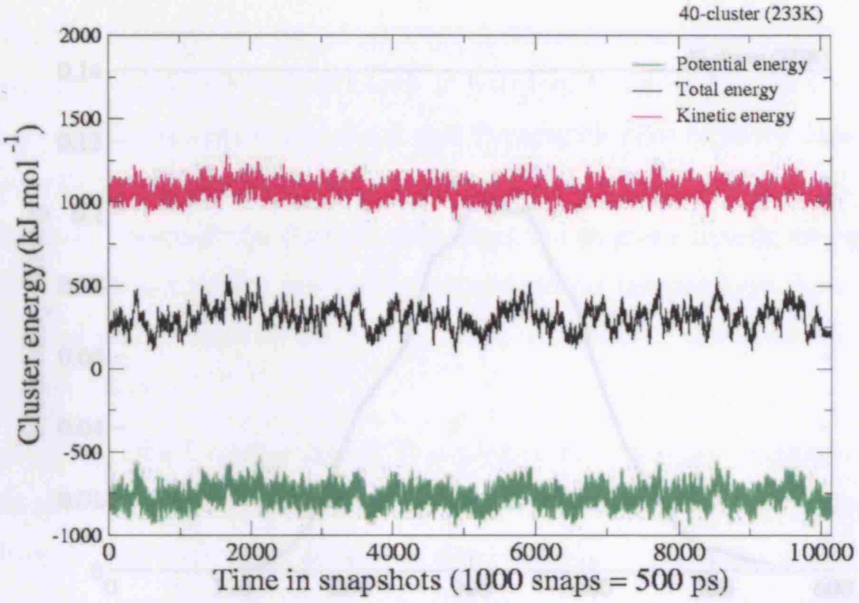

Figure 5.11: Total energy plotted against simulation time for a 40-cluster at 233K. The plot also shows the kinetic energy and potential energy contributions.

with a particular energy E defines the density of states $g(E)$. The density of states was originally defined in Chapter 4 by Equation (4.6), and can be loosely interpreted as the entropy of the cluster. We can evaluate the density of states approximately, by rearranging Equation (4.6) for $g(E)$ as shown by

$$g(E) = P(E)\, e^{E/kT}. \tag{5.8}$$

This requires knowledge of the partition function that is contained in $P(E)$. As we know the partition function is the sum over all possible energetic states of the system. We can evaluate the partition function approximately with a numerical integration over the probability energy density in Figure (5.12). This is used together with the cluster energies in Equation (5.8) to give an approximate value for the density of states shown in Figure 5.13. This plot illustrates the log-linear variation of the density of states with cluster energy. This illustrates that the density of states is an exponentially increasing function of energy [52]. The behaviour of the density of energy states in Figure 5.13 supports the view that the simulated n-nonane clusters are in approximate thermal equilibrium with the effective heat bath.

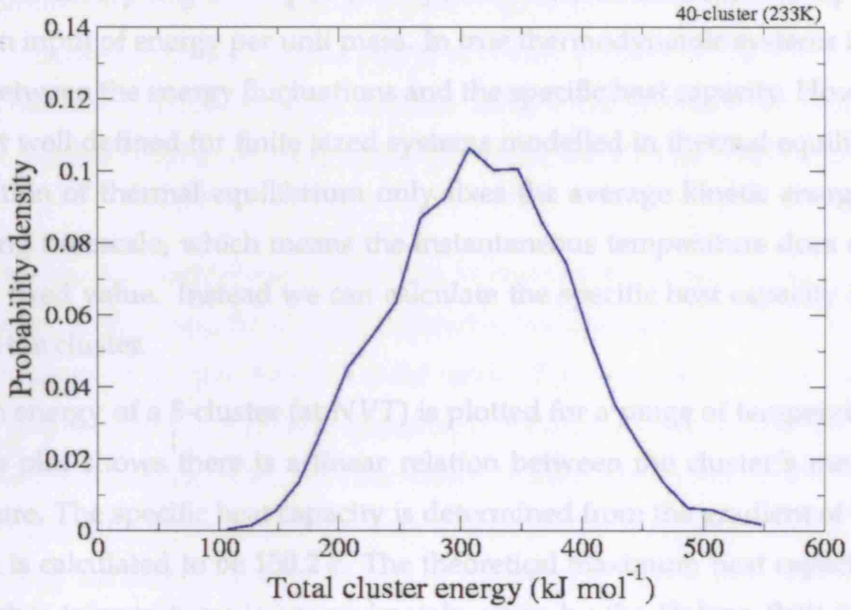

Figure 5.12: The probability density distribution of energies obtained from a 40-cluster simulation maintained at a constant temperature of 233K. We can use the distribution of energies to calculate the density of states, shown in Figure ??.

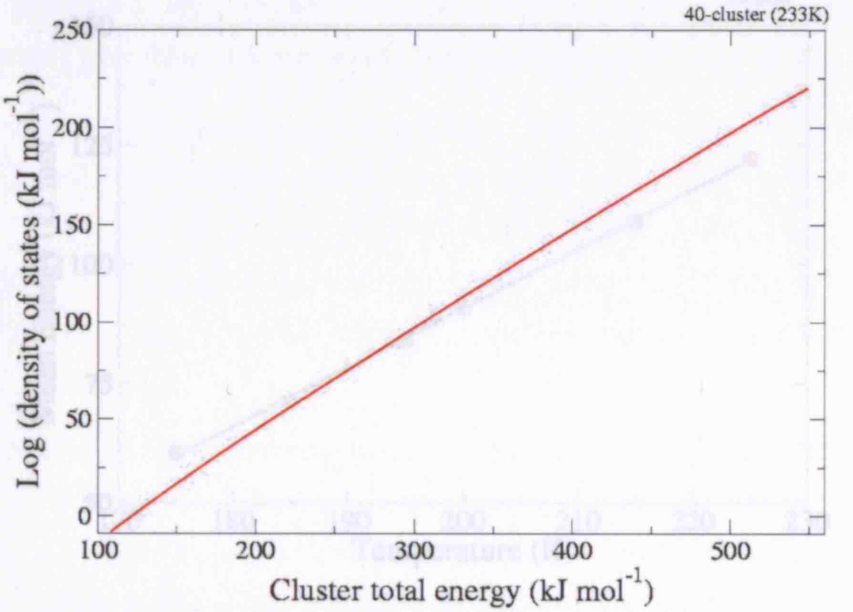

Figure 5.13: The logarithm of the density of states plotted against the total energy of a 40-cluster, simulated at a constant temperature of 233K.

Specific heat capacity

The specific heat capacity of a liquid (or any substance) is a measure of temperature change for a given input of energy per unit mass. In true thermodynamic systems there is a linear relation between the energy fluctuations and the specific heat capacity. However, this relation is not well defined for finite sized systems modelled in thermal equilibrium because the condition of thermal equilibrium only fixes the average kinetic energy over a sufficiently long timescale, which means the instantaneous temperature does not necessarily assume a fixed value. Instead we can calculate the specific heat capacity from the mean energy of the cluster.

The mean energy of a 5-cluster (at NVT) is plotted for a range of temperatures, in Figure 5.14. The plot shows there is a linear relation between the cluster's mean energy and temperature. The specific heat capacity is determined from the gradient of the line of best fit, which is calculated to be 150.2 k. The theoretical maximum heat capacity for an ideal gas at higher temperatures is approximately given by the Dulong-Petit limit 3 $N k$ [79], which yields a value of 135 k for a 5-cluster. Although the calculated specific heat capacity is slightly higher than this value, they are approximately consistent, which gives further evidence that the system is in thermal equilibrium.

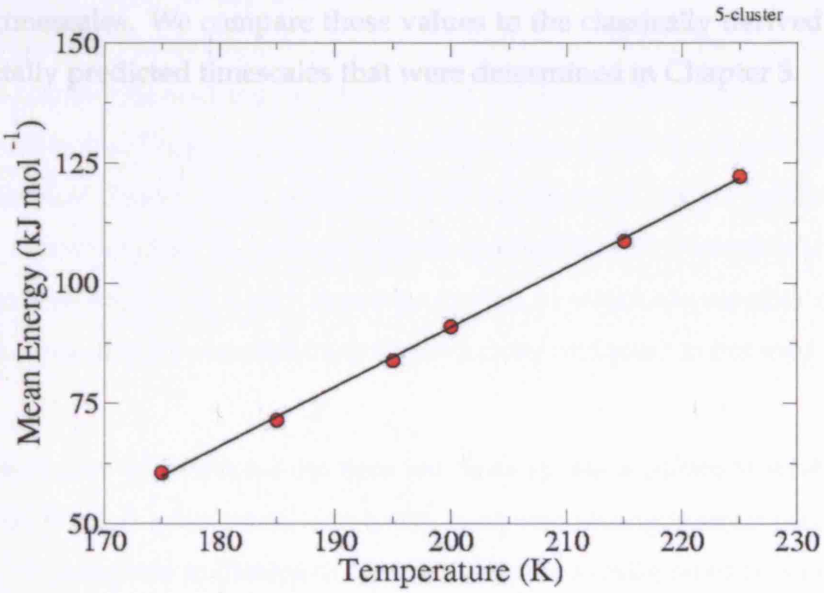

Figure 5.14: The mean energy of a 5-cluster maintained at constant temperature using the Andersen thermostat, plotted against increasing temperatures of 175K, 185K, 195K, 200K, 205K, 215K, 225K. The simulations are run for approximately 5ns.

5.6 Discussion and Conclusions

In this chapter we have put together a molecular dynamics model of n-nonane clusters treated in isolation from the vapour that is normally present in the experiments. The interactions between cluster atoms are defined using liquid empirical potentials. A reduced dynamic model of cluster atoms is employed to increase computational efficiency of the task.

We employ constant temperature dynamics to emulate the experimental conditions. This is achieved by submerging the clusters in an effective heat bath of thermalising helium particles to maintain its temperature at a fixed value. The heat bath delivers effective random collisions to the cluster, which is implemented through the Andersen stochastic thermostat. We have demonstrated that the Berendsen thermostat is unsuitable at controlling the angular momentum of molecular clusters correctly. The temperature of the cluster is approximated by the average kinetic energy of the effective heat bath, and for small systems the kinetic energy fluctuates about a mean value. This makes it difficult to establish a precise definition of temperature over short timescales for molecular clusters. However, over the timescale of the simulations we have shown that the Andersen thermostat maintains the clusters at thermal equilibrium.

In the next section we discuss the Langevin treatment of cluster decay and estimate cluster decay timescales. We compare these values to the classically derived timescales, and experimentally predicted timescales that were determined in Chapter 3.

Chapter 6

Langevin Model of *n*-nonane Cluster Decay

A direct way of measuring cluster decay timescales from molecular dynamics simulations is to simply observe the trajectory and count the number of evaporation events that occur, and deduce the mean cluster lifetime. This is a simple and straightforward means of estimating cluster lifetimes, which provides a competent test for the dynamically predicted lifetimes. This approach was used by Ford and Harris in a study of argon clusters [39]. The frequency of argon decay events was sufficiently substantial to provide good decay statistics. Ford and Harris reported that the mean argon cluster lifetime deduced from observing the trajectories was approximately 10ps at a kinetic temperature of 60K and cluster size of 50 molecules. This result was in good agreement with the cluster lifetime predicted by the dynamical cluster decay model used in the study. A similar approach was used in a MD study conducted by Yasuoka and Matsumoto [80], which involved the simulation of a supersaturated vapour at a high supersaturation, in which the number of clusters of different sizes were directly counted from the trajectory and used to determine the nucleation rate.

In the present case of *n*-nonane clusters we have to use a different strategy because the likelihood of decay is quite small due to the relatively strong interactions between cluster molecules. To generate sufficient decay statistics we would need to perform unfeasibly lengthy MD simulations, which is undesirable and inefficient as only a small fraction of the trajectory contains relevant decay information. To overcome this problem, we employ a statistical approach developed by Ford and Harris for liquid argon clusters [39] to overcome the difficulty in treating molecular clusters with long lifetimes. The evaporation

process involves complex dynamics of the cluster's constituent molecules. Each molecule is subject to interactions with all the other cluster molecules, as well as interactions with the surrounding heat bath. These two types of interaction occur over different timescales, and can be simplified using random force fluctuations over appropriate timescales. Occasionally, a random force fluctuation is sufficiently large to expel the molecule from the cluster, resulting in an evaporation event or in other words cluster decay. The randomly modelled interactions of a cluster molecule with the other cluster molecules, and the heat bath, are used to predict a third, random, yet rare event of cluster decay.

The motion of a molecule is modelled using a Langevin equation for noise driven dissipative motion in a potential well, which was originally stated in Chapter 4. The Langevin Equation (6.1)) is repeated here for convenience,

$$m\dot{v} = f(r) - m\gamma\, v + \tilde{f}(t) \tag{6.1}$$

where $f(r)$ is the mean radial force, $-m\gamma\, v$ is the friction force, γ is the friction coefficient, and $\tilde{f}$ is the stochastic random force. This equation describes the centre of mass motion of molecules. This is a reasonable simplification since the internal molecular motions (bond vibrations, rotations) occur over much shorter timescales than the gross motion of the molecule through the cluster, and can be assumed to be averaged out over the timescale of molecular movements. For simplicity, all the forces on a molecule are resolved to act in 1-dimension along a radial co-ordinate relative to the cluster's centre of mass.

6.1 The Potential of Mean Force

The potential of mean force $\Phi(r)$ is related to the mean radial force through the integral relation along the radius r given by Equation (4.37), which is repeated here for convenience as

$$\Phi(r) = -\int_0^r f(R)dR. \tag{6.2}$$

To obtain the mean radial force toward the cluster centre of mass, the cluster radius is divided into suitable intervals, and the total force experienced by particles in each interval is calculated and divided by the number of particles within that radial interval. This is the mean radial force felt by a cluster particle at a radius r from the centre of mass, at any instant in the simulation.

The mean radial force of a 67-cluster is plotted against the midpoint of each radial interval from the centre of mass in Figure 6.1. The sampling of forces near the centre of mass appears to be quite noisy, which is most likely due to the small relative volume associated with small radii, leading to poor sampling. As the radial distance increases, the mean radial force acting on a cluster molecule becomes more attractive, and appears to have a minimum value at just over 20Å. Beyond this point the force becomes less attractive and levels off toward 30Å. The shape of the curve shows that between the radii 10Å−30Å, a molecule feels a preferential force toward the centre of mass. The peripheral regions of the cluster will have a comparatively low particle density to the rest of the cluster, since there are fewer particles contained around the cluster's surface. Consequently, the sampling of forces around the edge of the cluster may be rather poor, and the mean force for these regions may not be well defined. This limitation will be most apparent in the absence of cluster decay since particles do not explore certain configurations that a decay particle would explore via its trajectory of escape.

The potential of mean force is determined by integrating the mean radial force over all radial positions, from the centre of mass ($r = 0$) to the desired radius. The integration is numerically calculated using the trapezium rule.[1] The potential of mean force of the 67-cluster is plotted against radial position from the centre of mass, in Figure 6.2. The shape of the potential of mean force indicates that the work done in moving a molecule from the edge of the cluster outward is much less than the work done in moving a molecule out from the centre. Close to the cluster centre of mass, the potential of mean force takes a local minimum value of about $-12\,kT$. Moving outward from the centre of mass, the potential of mean force increases rapidly until it reaches a plateau around the cluster's periphery. The plateau can be interpreted as a particle no longer being influenced by the cluster, in which case it has escaped. The radius at which the potential of mean force first levels off is called the escape radius, which can be loosely viewed as the cluster radius, as discussed on page 55 and in Figure Caption 4.2.

A similar analysis is employed for the 40-cluster and 50-cluster, and the mean radial force is plotted against radius from the cluster centre of mass, in Figures 6.3 and 6.4 respectively. Clearly, the mean force plots for 40 and 50-clusters appear to have an undefined force beyond a particular radius in comparison to the 67-cluster force. We recall that the 40-cluster and 50-cluster simulations do not exhibit cluster decay, and the unquantified mean radial force beyond a certain radius may be attributed to the insufficient data available

[1] Area of trapeziums = $\frac{h}{2}(f_1 + f_2), \frac{h}{2}(f_2 + f_3) + \frac{h}{2}(f_3 + f_4) \ldots + \frac{h}{2}(f_{(N-1} + f_N)$, where h is width of the trapezium.

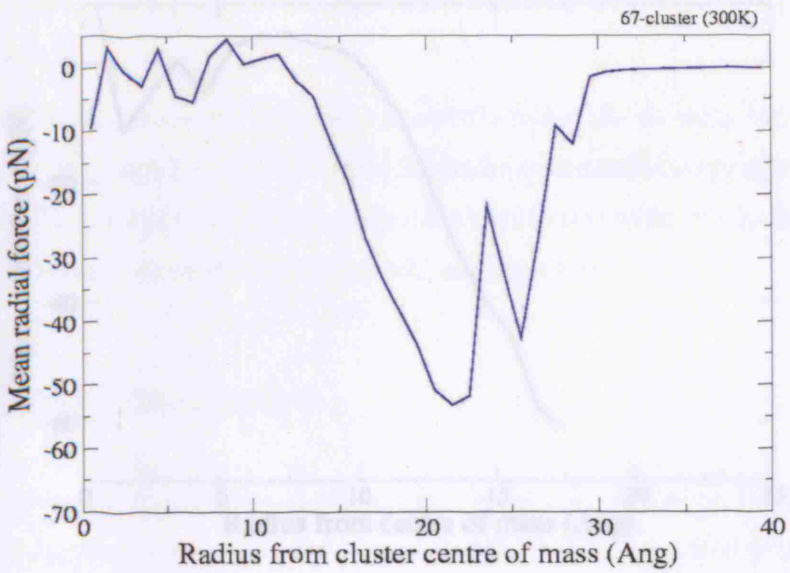

Figure 6.1: The mean radial force for a 67-cluster, simulated at $T = 300$K.

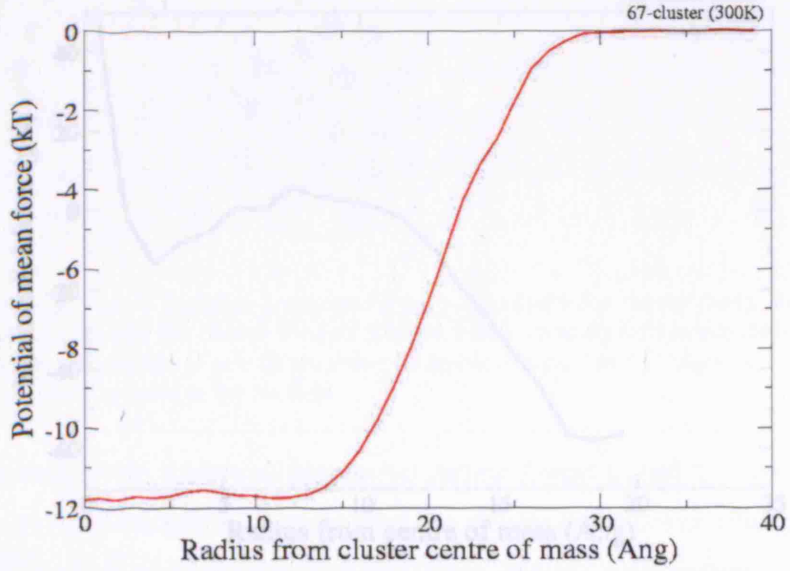

Figure 6.2: The potential of mean force for a 67-cluster simulated at $T = 300$K.

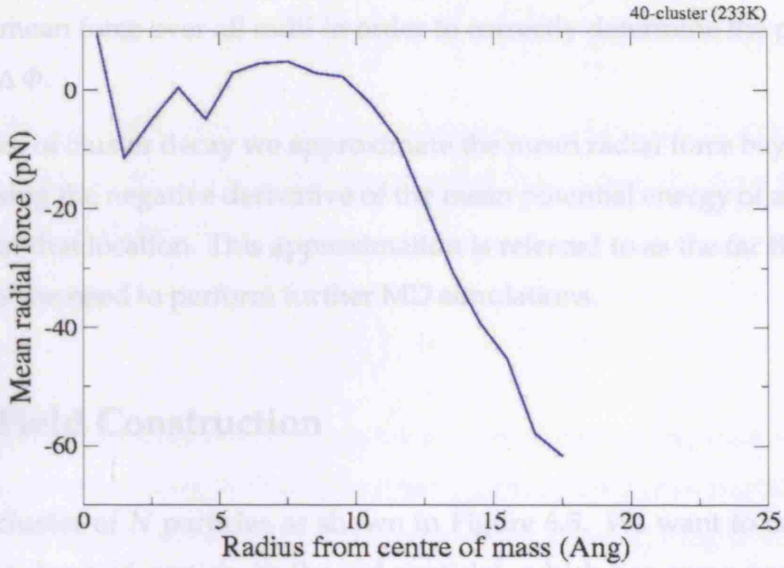

Figure 6.3: The mean radial force of a 40-cluster, (233K) plotted against radius from the cluster centre of mass. As radial distance increases, the mean radial force acting on a cluster molecule becomes more attractive and stops abruptly at around 17.5Å . This is because there are no molecular forces measured beyond this radius due to the absence of cluster decay.

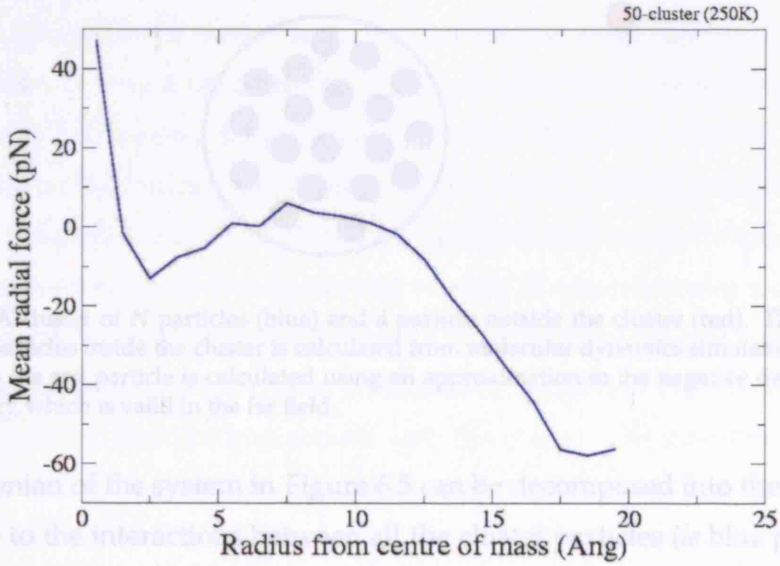

Figure 6.4: The mean radial force of a 50-cluster (250K) plotted against radius from the cluster centre of mass. The mean radial force acting on a cluster molecule stops abruptly at around 19Å , since no molecular forces are measured beyond this radius due to the absence of cluster decay.

around the cluster's periphery. We have to find a means to deduce the mean force for these peripheral regions, since it is important that we obtain a complete description of the potential of mean force over all radii in order to correctly determine the potential of mean force depth $\Delta\Phi$.

In the absence of cluster decay we approximate the mean radial force beyond the cluster's periphery using the negative derivative of the mean potential energy of an imaginary particle placed at that location. This approximation is referred to as the far field construction, and it avoids the need to perform further MD simulations.

6.2 Far Field Construction

Consider a cluster of N particles as shown in Figure 6.5. We want to calculate the force acting on the decayed particle (*ie* the red particle), which has some position r_o. The far field approximation assumes that beyond the cluster's escape radius r_e the mean radial force experienced by a molecule at position r_o is approximately equal to the mean force between the cluster and an imaginary molecule placed at that location. The imaginary molecule does not affect the MD generated cluster configurations, which means the cluster is "blind" to the imaginary molecule. This assumption is valid as $r \to \infty$.

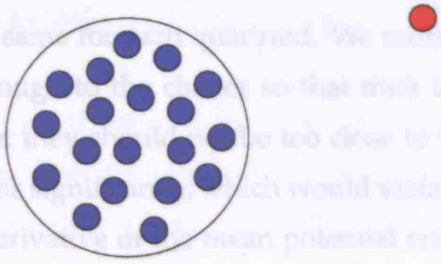

Figure 6.5: A cluster of N particles (blue) and a particle outside the cluster (red). The mean radial force acting on the particles inside the cluster is calculated from molecular dynamics simulations. The mean radial force acting on the red particle is calculated using an approximation to the negative derivative of the mean potential energy, which is valid in the far field.

The Hamiltonian of the system in Figure 6.5 can be decomposed into the cluster Hamiltonian H_c due to the interactions between all the cluster particles (*ie* blue particles) and the Hamiltonian H_{oc} due to interactions of the decay particle (red particle) with all the other cluster particles, which is given by

$$H = H_c + H_{oc}. \tag{6.3}$$

The mean radial force in the far field is approximated by saying

$$\left\langle -\frac{\partial H_{oc}}{\partial r_o} \right\rangle \simeq \left\langle -\frac{\partial H_{oc}}{\partial r_o} \right\rangle_c \tag{6.4}$$

where the subscript "c" refers to averages taken over cluster configurations only. For numerical convenience, we evaluate the mean radial force using the derivative of the mean potential energy, as shown by

$$\left\langle -\frac{\partial H_{oc}}{\partial r_o} \right\rangle_c = -\frac{\partial \langle H_{oc} \rangle_c}{\partial r_o} \tag{6.5}$$

which holds true, provided averages are taken over cluster configurations. To implement the far field construction we evaluate the mean potential energy of an imaginary molecule (*ie* an effective escapee) at radial positions outside the cluster, using only the non-bonded interactions, which are modelled using a Lennard-Jones potential. We integrate over a random set of orientations for a given cluster configuration and different escapee conformations. The centre of mass of the escapee is randomly chosen to lie within a spherical region of volume surrounding the cluster. For convenience, the random escapee's positions are selected within the positive xyz quadrant of the sampling region, which is a reasonable approximation provided that cluster decay is equally likely to occur in all directions relative to its centre of mass. This means we can assume that the average potential energy of an escapee is the same for each quadrant. We must bear in mind that escapees need to be placed close enough to the cluster so that their interactions with the cluster can be evaluated. However, they should not be too close to the cluster as they could affect the cluster configurations significantly, which would violate the approximations made by equating the negative derivative of the mean potential energy to the mean force. The minimum separation between escapees and existing cluster molecules must be at least one Lennard-Jones radius σ. The conformational structure of the escapee is constructed using molecular conformations of the cluster molecules as templates. The potential energy of the escapee is calculated from its interactions with the cluster. The interactions between cluster molecules and the interactions within the escapee itself are excluded, since we are only interested in the effect of the cluster on the escapee. We take the numerical derivative of the mean potential energy of the escapee, plotted against radius, which is shown in Figure 6.6 for the 40-clusters (black line), along with the previously determined MD generated mean radial force, which was calculated inside the cluster (blue line). Similarly, the mean radial force for the 50-cluster is shown in Figure 6.8, which is generated using MD data

(blue line) and the far field approximation (black line).

Clearly, there is a quantitative disparity between the force inside the cluster and the far field approximated force, close to the cluster's escape radius r_e. This could be due to the fact that we use cluster molecule conformations to approximate the escapee's conformation, instead of real evaporated molecule configurations. Obviously a molecule inside the cluster will interact strongly with the other molecules, which invariably affects its conformation, whereas a decay molecule that has escaped from the cluster is not surrounded by the same type of molecules, and is therefore likely to have a very different conformation. In any case, the quantitative difference between the derivative of the mean potential energy and mean force is relatively small, and can be resolved by interpolation between the two curves (shown in red in Figures 6.6 and 6.8). This combines the actual force acting on molecules inside the cluster (determined by MD) with the force predicted to act on a molecule outside the cluster, determined by the far field construction. The total force is numerically integrated from radius 0 to ∞ to give an estimate of the complete potential of mean force for all radii, including in the cluster's peripheral region. The complete potential of mean force for the 40-cluster and 50-cluster is shown in Figures 6.7 and 6.9 respectively. The far field construction allows us to identify the variation of the potential of mean force beyond r_e, which enables us to estimate the depth of the potential well $\Delta\Phi$.

6.3 Calculating the friction coefficient

To calculate the cluster lifetime it remains for us to determine the friction coefficient γ. We can determine the friction coefficient from the reciprocal of the velocity autocorrelation time, which is the time taken for the mean velocity fluctuations to decay by $\frac{1}{e}$.

The velocity autocorrelation function

To do this we calculate the velocity autocorrelation function, defined in Chapter 4 by Equation (4.17), using the time evolved radial velocities of a molecule taken from an MD trajectory at constant energy (NVE). The velocity data from the trajectory is in intervals of 0.05ps, and the MD time step is 0.5fs (*ie* data is taken every 100 snapshots). The product of the radial velocity of a molecule at time t and a later time $(t+\tau)$ is calculated, and averaged over all the molecules in the cluster to improve statistics. This is plotted as a function of time interval in Figure 6.10. The velocity autocorrelation function is fitted approximately

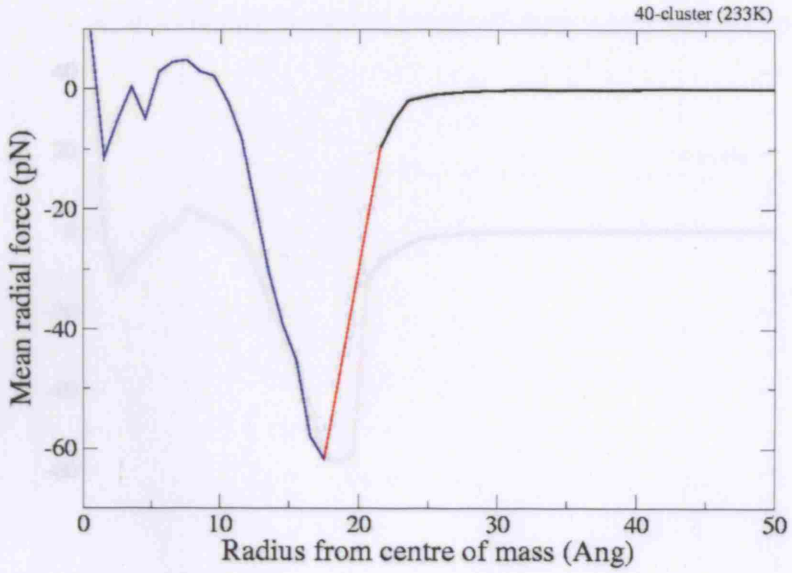

Figure 6.6: The mean radial force felt by a molecule in a 40-cluster plotted against radial position from the cluster's centre of mass. The black line shows force approximated outside the cluster (derivative of the mean potential energy), and the blue line shows the mean force inside the cluster determined from the simulations. The red line shows the interpolation between the two forces. The force inside the cluster was calculated from a 40-cluster simulation at 233K for approximately 5ns.

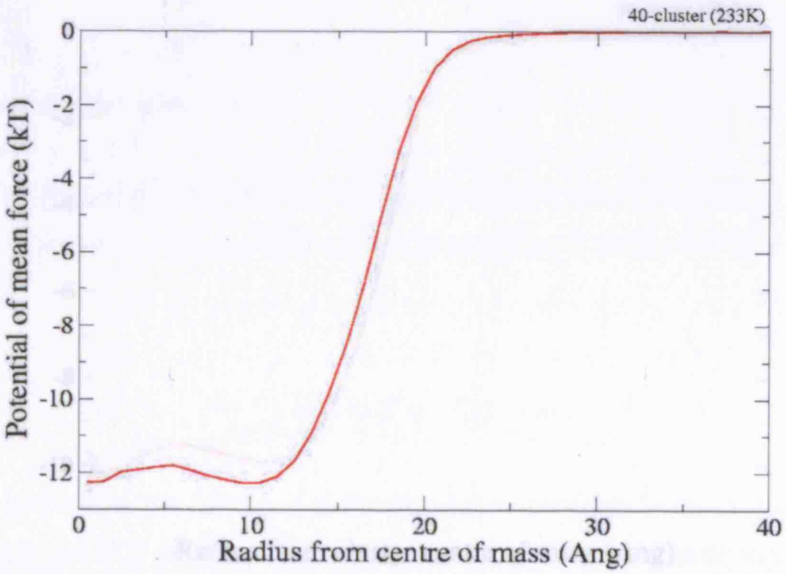

Figure 6.7: The complete potential of mean force for the 40-cluster determined from an integration of the mean radial forces shown in Figure 6.6.

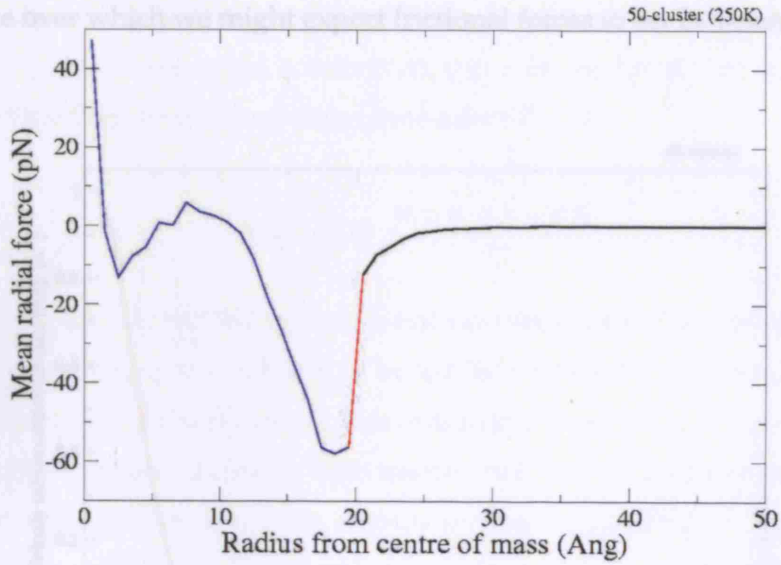

Figure 6.8: The mean radial force for a 50-cluster as a function of radial position from the cluster's centre of mass. The black line shows the derivative of the mean potential energy (far field construction), and the blue line shows the mean force inside the cluster, determined from the simulations. The red line shows the interpolation between the two forces. The data used was from a 50-cluster, simulated at 250K for approximately 5ns.

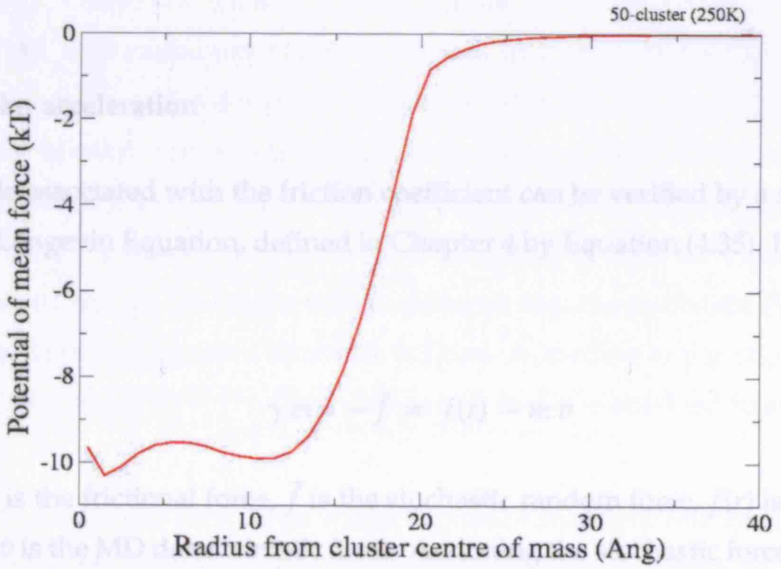

Figure 6.9: The complete potential of mean force for the 50-cluster determined from an integration of the mean radial forces shown in Figure 6.8.

to a decaying exponential, according to Equation (4.32), which yields a velocity autocorrelation time (relaxation time) of approximately 0.16ps. This can be loosely interpreted as the timescale over which we might expect frictional forces to act in n-nonane clusters.

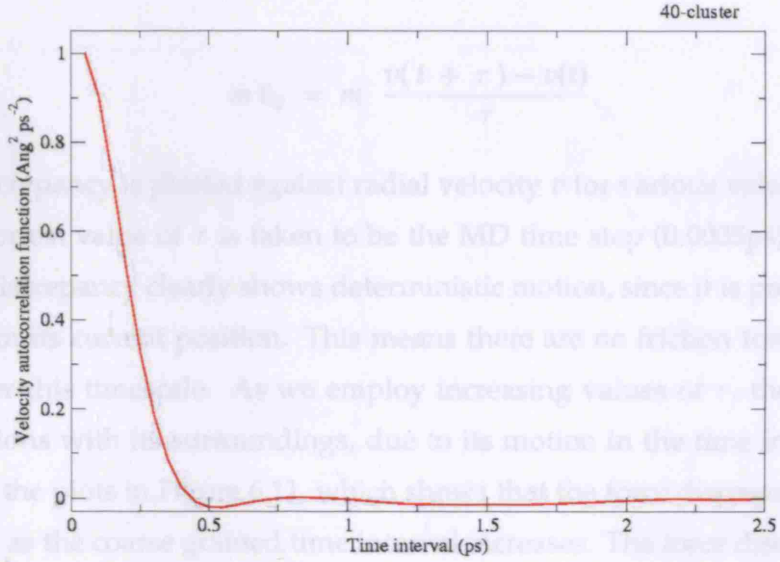

Figure 6.10: The velocity autocorrelation function plotted against time. The timescale associated with the fall off of the correlation function is approximately 0.5ps. The data is fitted very approximately to a decaying exponential which yields a fall off timescale of 0.16ps. This indicates the approximate timescale over which there is a linear correlation between a molecule's velocity and the force it experiences due to collisions with surrounding molecules.

The molecular acceleration

The timescale associated with the friction coefficient can be verified by a numerical evaluation of the Langevin Equation, defined in Chapter 4 by Equation (4.35). It is recast here in the form

$$\gamma\, m\, v - \tilde{f} = f(r) - m\,\dot{v} \tag{6.6}$$

where $\gamma\, m\, v$ is the frictional force, $\tilde{f}$ is the stochastic random force, $f(r)$ is the mean radial force, and $m\dot{v}$ is the MD deterministic force. Assuming the stochastic force is averaged out over some suitable coarse grained timescale, the Langevin Equation attributes the friction force to a "discrepancy force" (*ie* right hand side of Equation (6.6)). We evaluate Equation (6.6) over a suitable coarse grained time interval τ, in an attempt to observe a correlation

between velocity and the discrepancy force. To do this we take data for radial velocity v and mean radial force at position r, over intervals of 0.05ps, from the trajectory of a single molecule (at NVE). This is repeated for each molecule in the cluster to improve the statistics. We evaluate the radial acceleration $\dot{v}$ of a single particle by taking the velocity difference divided by the coarse grained time interval τ, by

$$m\,\dot{v}_\tau \;=\; m\;\frac{v(\,t\,+\,\tau\,)-v(t)}{\tau}. \tag{6.7}$$

The force discrepancy is plotted against radial velocity v for various values of τ, in Figure 6.11. The shortest value of τ is taken to be the MD time step (0.0005ps). The behaviour of the force discrepancy clearly shows deterministic motion, since it is predictable and determined from its current position. This means there are no friction forces acting on the molecule over this timescale. As we employ increasing values of τ, the molecule experiences collisions with its surroundings, due to its motion in the time interval τ. This is illustrated in the plots in Figure 6.11, which shows that the force discrepancy appears less deterministic as the coarse grained time interval increases. The force discrepancy is taken to have the general form

$$y \;=\; -A\,x \;-\; \tilde{f} \tag{6.8}$$

where $y = f(r) - m\dot{v}_\tau$, $x = v$, and $\tilde{f}$ is the stochastic force. Taking the average of the force discrepancy per unit mass over suitable intervals of v (for $\tau = 0.025$ps), yields a linear relation with the intercept through the origin as shown in Figure 6.12. Clearly, there is a strong linear relation between the mean force acting on a molecule and its velocity at time t. The linear relation appears to become more noisy for large negative and positive velocities, which is probably due to the poor sampling of data for these velocities. The intercept passes through the origin, which indicates that the stochastic force contribution vanishes over the coarse grained timescale 0.025ps. According to Equation (6.6), the mean of the data corresponds to $-\gamma\,m\,v$ (per unit mass), and γ is obtained from the gradient of Figure 6.12.

This treatment is repeated for a range of coarse grained time intervals increasing by 0.025ps, which yields similar correlations between force discrepancy and velocity, as shown in Figure 6.13. The gradient of the force velocity plot increases with increasing τ until it reaches a maximum value, and does not change for increasing τ for approximately 0.1ps. The behaviour of the friction coefficient γ can be observed by plotting the gradient against the

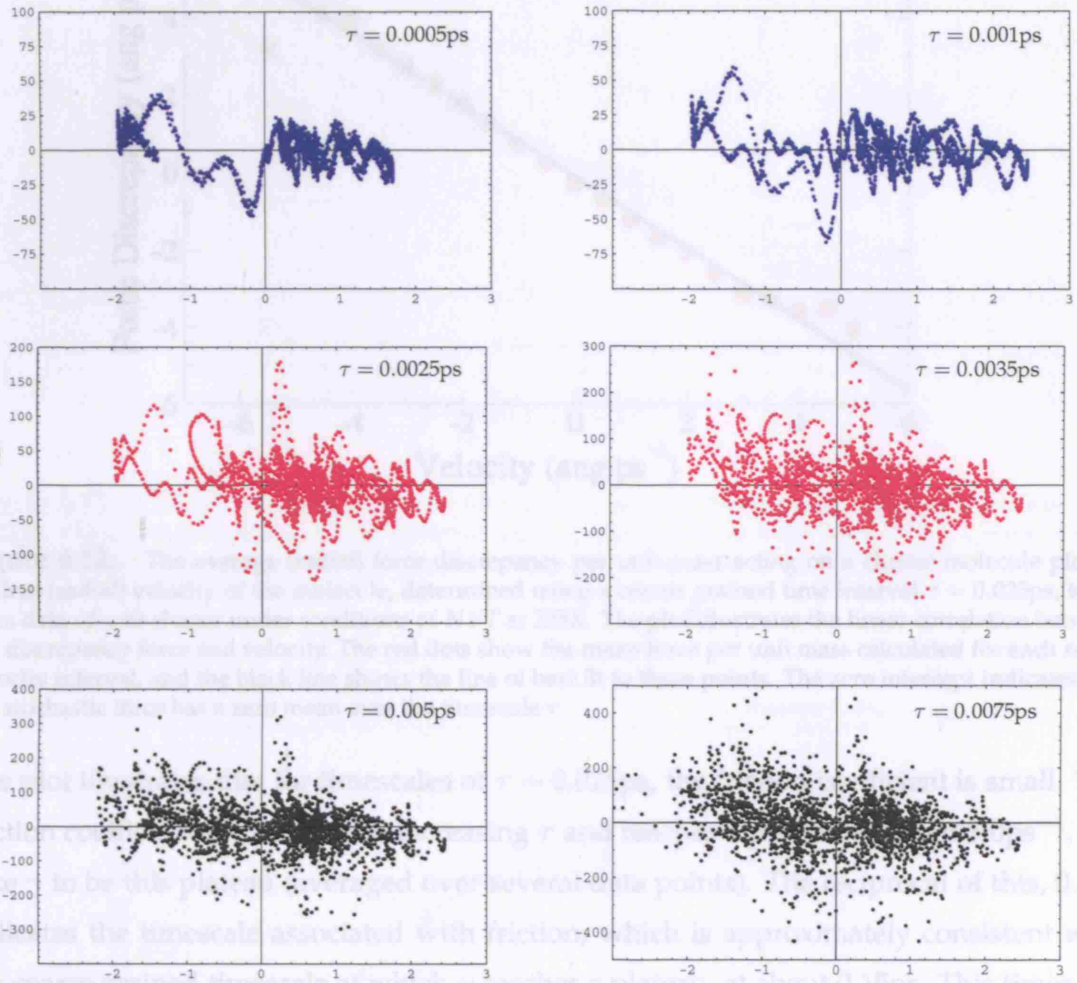

Figure 6.11: A series of plots showing the time evolution of the radial force discrepancy plotted against radial velocity for a molecule in the cluster. The first blue plot is coarse grained over the time interval $\tau = 0.0005$ps, which is the MD time step. The second blue plot is coarse grained over twice that time interval. The pink and black plots are coarse grained over $\tau = 0.005$ps and $\tau = 0.0075$ps respectively. The plots have been generated using data from a 40-cluster simulation maintained at constant energy. A negative correlation with radial velocity gradually becomes apparent with increasing τ.

coarse grained time interval, as shown in Figure 6.14.

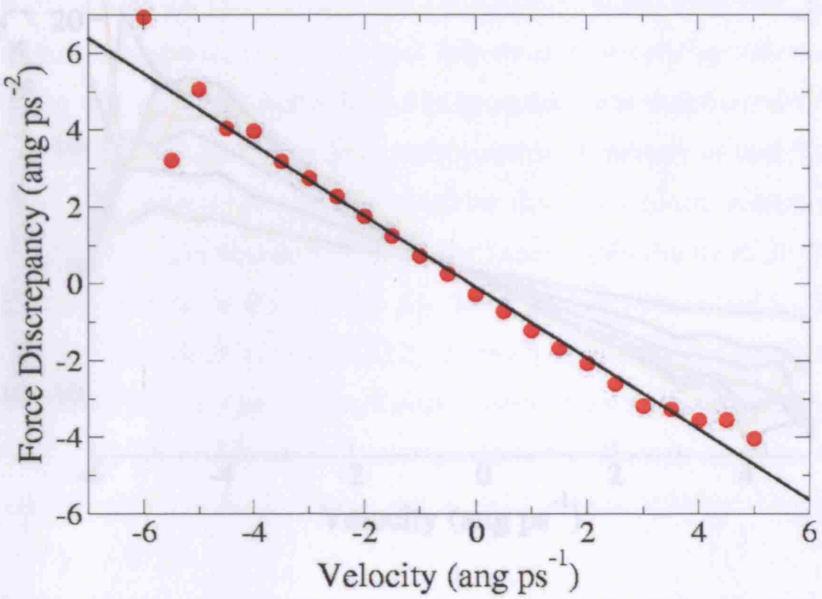

Figure 6.12: The average (radial) force discrepancy per unit mass acting on a cluster molecule plotted against (radial) velocity of the molecule, determined using a coarse grained time interval $\tau = 0.025$ps, taken from data of a 40-cluster under conditions of NVT at 225K. The plot illustrates the linear correlation between the discrepancy force and velocity. The red dots show the mean force per unit mass calculated for each radial velocity interval, and the black line shows the line of best fit to these points. The zero intercept indicates that the stochastic force has a zero mean over the timescale τ.

The plot illustrates that for timescales of $\tau \sim 0.025$ps, the friction coefficient is small. The friction coefficient increases with increasing τ and reaches a plateau at about 3.0ps^{-1}. We take γ to be this plateau (averaged over several data points). The reciprocal of this, $0.\dot{3}$ps indicates the timescale associated with friction, which is approximately consistent with the coarse grained timescale at which γ reaches a plateau, at about 0.15ps. This timescale agrees very well with the velocity autocorrelation time, which was calculated in the previous section to be 0.16ps. For $\tau < 0.025$ps, there are insufficient collisions for the friction force to act. For τ between 0.1ps - 0.2ps there is a good linear correlation between discrepancy force and velocity. This can be regarded as the timescale over which frictional forces act in the system. For $\tau > 0.25$ps the linear correlation between the force discrepancy and velocity starts to break down. This is evident as the friction coefficient in Figure 6.14 starts to decrease beyond 0.025ps, which is due to the molecule experiencing so many collisions that its motion starts to become diffusive. As time continues to increase, we expect the friction coefficient to eventually reduce to zero.

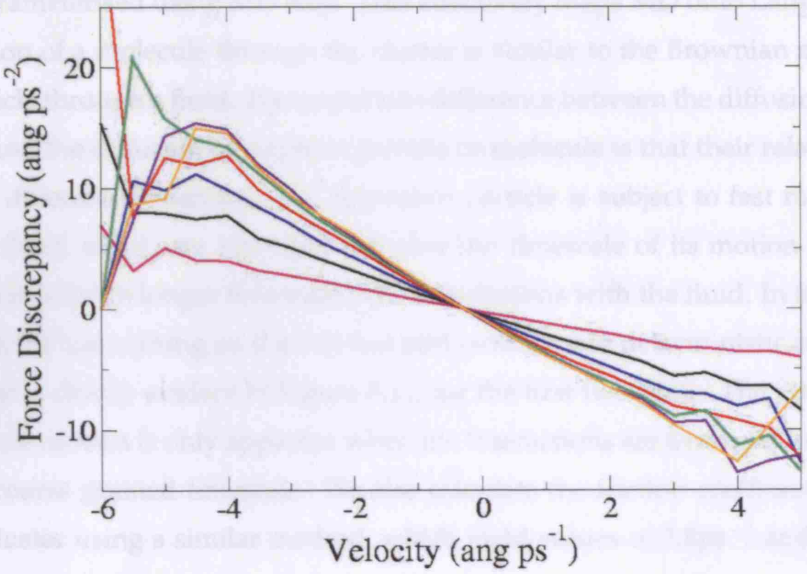

Figure 6.13: The radial components of the force discrepancy for the 40-cluster under conditions of NVT at 225K, plotted against velocity for six different coarse grained time intervals: pink- 0.025ps, black- 0.05ps, blue- 0.075ps, red- 0.1ps, green- 0.125ps, purple- 0.15ps, and orange- 0.2ps.

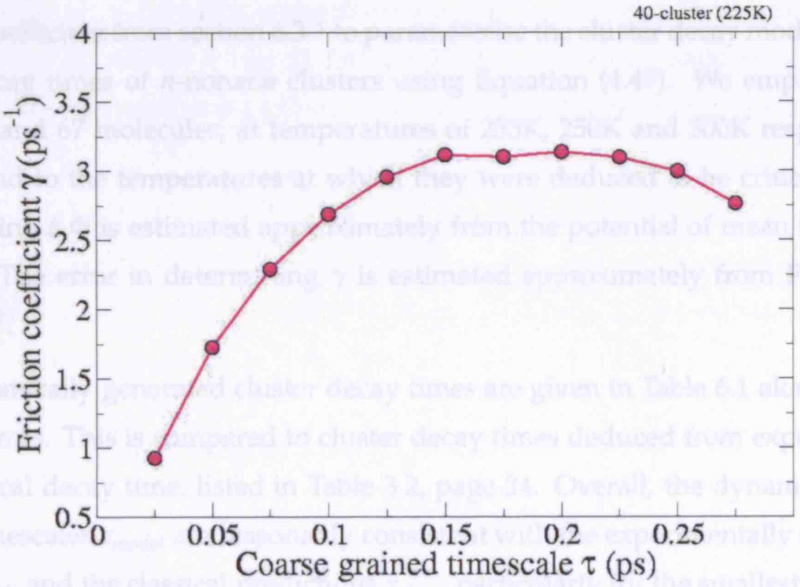

Figure 6.14: The friction coefficient for varying coarse grained timescales τ, calculated from a 40-cluster trajectory under conditions of NVT at 225K. The plot shows that γ reaches a plateau at about 3ps^{-1}. Therefore we expect the friction timescale to be the inverse of this value, and indeed τ does appear approximately consistent with this.

To summarise this section, we have calculated the friction coefficient of n-nonane clusters, using a Langevin equation to model the dynamics of single molecule motion as point particles, parameterised using MD data. This effectively maps MD onto Langevin Dynamics. The motion of a molecule through the cluster is similar to the Brownian motion of a massive particle through a fluid. The important difference between the diffusion of a Brownian particle and the diffusion of a lighter particle or molecule is that their relative motions occur over different timescales. The Brownian particle is subject to fast random collisions with the fluid, which are averaged out over the timescale of its motion since its motion occurs over a much longer timescale than its collisions with the fluid. In the case of a light molecule, the force acting on it is not fast and random, but deterministic and smooth. This behaviour is clearly evident in Figure 6.11, for the first two plots. The random behaviour of molecule motion is only apparent when the interactions are averaged over a sufficiently lengthy coarse grained timescale. We also calculate the friction coefficient of a 50-cluster and 67-cluster using a similar method, which yield values of 2.8ps^{-1} and 2.7ps^{-1} respectively.

6.4 Calculation of Dynamic-Langevin Decay Timescale

We use the potential of mean force depth obtained in sections 6.1 and 6.2, together with the friction coefficient from section 6.3.1 to parameterise the cluster decay model, and calculate mean decay times of n-nonane clusters using Equation (4.49). We employ cluster sizes of 40, 50 and 67 molecules, at temperatures of 233K, 250K and 300K respectively, which correspond to the temperatures at which they were deduced to be critical. The error in determining $\Delta\,\Phi$ is estimated approximately from the potential of mean force plots to be $\pm\,0.2$kT. The error in determining γ is estimated approximately from Figure 6.14 to be $\pm\,0.1\text{ps}^{-1}$.

The dynamically generated cluster decay times are given in Table 6.1 along with the estimated errors. This is compared to cluster decay times deduced from experiments, and to the classical decay time, listed in Table 3.2, page 34. Overall, the dynamically generated decay timescales τ_{model} are reasonably consistent with the experimentally estimated decay times τ_{expt}, and the classical predictions τ_{class}, particularly for the smallest cluster sizes.

There is a strong agreement with the dynamically generated lifetimes and the experimentally estimated lifetimes for the smallest cluster size. In contrast, CNT makes the poorest prediction for the smallest cluster size, which is precisely where we might expect the CNT

i	T (K)	r_e (Å)	$\Delta\Phi\,(kT)$	τ_{model} (ns)	τ_{expt} (ns)	τ_{class} (ns)
40	233	25	12.15	46.0 ± 18.0	44.0	34.0
50	250	26	10.08	8.10 ± 3.00	8.80	9.20
67	300	27	11.70	6.00± 2.00	0.53	0.47

Table 6.1: The error in τ_{model} is determined from estimated errors in r_e of ±1 Åand $\Delta\Phi$ of ±0.2kT.

treatment of molecular clusters to breakdown. To identify whether CNT becomes completely unsuitable for calculating decay times of even smaller molecular clusters, further investigations are required, which might involve simulations of a broader range of cluster sizes. The agreement for the dynamical decay times with experiment is poorest for the largest cluster size. This could be due to the fact that larger cluster sizes need longer simulation run times to obtain sufficient data.

Overall, these results indicate the dynamic model predicts cluster decay times better for smaller sized clusters than larger sized clusters compared to CNT. However, it is important to understand that the model is fundamentally microscopic, whereas the classically derived lifetimes are based on a thermodynamic treatment of clusters in equilibrium using bulk phase properties. Molecular decay models provide a means of predicting the decay timescales of clusters that are long lived, where the direct observation of cluster decay from the MD is currently unfeasible to perform. However, there remains an ongoing need to establish reliable methods that combine theory and computational techniques to correctly deduce the lifetime of small molecular clusters that maintain a certain longevity.

Chapter 7

Stability of Supercooled Embryonic Ice Clusters

The second study in this thesis involves a very different type of system to condensation. It concerns the freezing phase transition from supercooled water into ice I. [1] This study applies the Langevin interpretation of cluster dynamics and decay to ice clusters that form during the water freezing phase transition in order to estimate ice cluster lifetimes.

7.1 Introduction to Supercooled Water

Water is the principle component of all living organisms that plays a major role in many chemical and biological processes such as oxidation and photosynthesis, which are essential to life on earth [81], [82]. One of the most important characteristics of water is its ability to form hydrogen bonds [83]. An example of the importance of hydrogen bonding, is its role in binding DNA strands, which is central to protein synthesis [84]. At atmospheric pressure bulk water freezes at 273K, however, it has the unusual property of expanding when cooled below 277K. Water can be cooled at ambient pressure to well below its freezing temperature to around 240K [85] with a density comparable to ice, before ice begins to form. This remarkable feature is called supercooling. It means that a liquid can exist in a metastable state well below its normal freezing temperature. The concept of supercooling is similar to a condensing vapour becoming supersaturated. In both cases the existing phase becomes metastable and deviates from equilibrium behaviour. This is illustrated for condensation in Figure 1.1, where the metastable vapour, which is supersaturated, is

[1] There are ten known isomorph's of ice, each with a unique structure and properties

shown in red. In principle, the same plot can be used to illustrate the nature of supercooling except the original phase is a liquid and the final phase solid. A well known example of supercooling in nature is the presence of cloud droplets of liquid water, which exist at temperatures well below the freezing point [86], [87]. The presence of supercooled water in the atmosphere plays an important role in the formation of clouds, which has generated much interest into the behaviour of water under supercooled conditions.

Supercooled water is metastable in nature. It is sensitive to spontaneous fluctuations in density and order, which lead to the formation and dissociation of hydrogen bonds between molecules. This is a nucleation process which results in networks of hydrogen bonded molecules, which we refer to as embryonic ice clusters. The process of hydrogen bond formation and dissociation leads to the growth and decay of the ice embryo clusters. Very occasionally, there is a large enough fluctuation or ice cluster that drives the entire system to freeze into ice. In principle, this process is similar to the condensation of a liquid droplet from a supersaturated vapour in the sense they are both driven by nucleation events. However, the difference is that in condensation, cluster growth is controlled by monomer flux from the vapour, whereas in the case of crystallisation, the water molecules are already in contact with the embryo, and growth is a matter of molecular reorientation of hydrogen bonds. The aim of this study is to develop a greater insight into the properties of these small ice cluster embryos, which are the precursors to crystallisation in supercooled water.

Experimentally, it is very challenging to perform reliable measurements on supercooled water below 238K because it requires an exceptionally clean sample, free from trace impurities, which is difficult to achieve experimentally [85], [88], [89]. This makes it difficult to validate theoretical models of supercooled water against experimental measurements. Theoretically, there are two general approaches to water models at low temperatures. The first was proposed by Röentgen in 1892 who treated water as a mixture of a bulky "ice like" component and a less bulky "normal liquid" component [90]. This basic idea has successfully explained some of the anomalous properties of water, and has been extended by many authors [91], [92]. The second treatment of water is the distorted hydrogen bond model, which was first proposed by Bernal and Fowler about 50 years ago [93]. They suggested that water forms a network that is almost completely hydrogen bonded. This basic principle has been extended in a variety of studies [94], [95]. A notable extension to the distorted hydrogen bond model is the percolation model proposed by Stanley [96], [97], which uses molecular connectivity rather than molecular positions to examine the

behaviour of supercooled water. If the mean number of hydrogen bonds is larger than a certain value (which will depend on the hydrogen bond definition), there will be an infinitely large network of bonded molecules, by means of percolation. The mean number of hydrogen bonds per molecule at which percolation occurs is called the percolation threshold.

One of the first molecular dynamics studies of liquid water was performed in 1971 by Rahman and Stillinger [98], using rigid molecules and simple effective pair potentials. Their simulations reproduced many dynamic and structural properties of water. One of the main difficulties in modelling liquid water at the microscopic level is the correct description of the rearrangement of hydrogen bonds, and its effect on structural changes within the liquid dynamics. More recently, Ford investigated nucleation processes in supercooled water. In these studies the properties of relatively large ice clusters were extracted from experimental freezing rates measured in the temperature range 230K-240K, using the nucleation theorems [99]. Similar studies by Vortisch *et al.* [100] extracted the free energy of formation of ice cluster embryos from the homogeneous freezing rates of aerosol droplets. However, the studies made by Ford and Vortisch deal with the continuum dynamics of freezing systems as opposed to the microscopic detail, which is not necessarily the most appropriate tool at the microscopic scale concerned.

Recently, Matsumoto *et al.* [37] have conducted an extensive study of nucleation and growth of ice cluster embryos leading to freezing into ice I, using molecular dynamics simulations. They define ice cluster embryos as long lived hydrogen bonded networks, which coexist with the surrounding unbound supercooled water, which represents the metastable liquid. The most striking feature is that the clusters do not show a strong degree of crystalline ordering, but instead appear amorphous and disordered in nature.

Aim of the study

The aim of this study is to investigate whether the presence of molecular disorder in supercooled water can be explored through the treatment of ice embryo dynamics at the molecular length scale using a theoretical approach similar to that used for liquid clusters of *n*-nonane (discussed in the first part of the thesis). The MD trajectory provided by Matsumoto *et al.* provides an accurate means of investigating the decay of the smaller and more numerous of these structures. The trajectory is used to parameterise an effective model of the dynamics of the ice embryos, which employs Langevin dynamics to represent the non-bonded water environment. Since the surrounding water is not included

explicitly, the model provides an efficient means to study the decay, and perhaps growth processes, of small ice clusters. In addition to this, the mean population of embryos of a variety of sizes can also be extracted from the MD trajectory.

7.2 The Structure and Properties of Water

7.2.1 Hydrogen bonding

To investigate the properties of ice cluster embryos it is essential to understand the nature of hydrogen bonding. It is thought that hydrogen bonding is responsible for many of water's unusual properties, such as its relatively high melting and boiling points, its unusually large heat capacity [101], [102], and more specifically its ability to be supercooled to well below its freezing temperature [85].

Hydrogen bonds are specific intermolecular interactions that form between strongly polar molecules that contain hydrogen atoms. Polar molecules have permanent dipole moments (partial charges) that arise due to the tendency of certain atoms to attract electrons more than others [103]. This property is called electronegativity, and atoms with a strong tendency to attract electrons such as oxygen or nitrogen are said to be electronegative, whereas Group I metals that have a tendency to lose rather than attract electrons, are said to be electropositive. Water is an example of a polar molecule. It has an oxygen atom attached to two hydrogen atoms. The equilibrium bond length of the $O-H$ covalent bond is 0.95718Å , measured from the vibration-rotation spectra of water vapour [81].

The geometric structure of a water molecule is importantly affected by its electronic structure. Oxygen is a Group VII element with six electrons in its unfilled atomic valence orbital, which can be written as $2s^2\ 2px^2\ 2py^1\ 2pz^1$ [104]. The $2py$ and $2pz$ Pi orbitals are unfilled and only have one electron out of a maximum of two. In atomic orbital theory, it is thought that orbitals overlap and mix together, which is called hybridisation [103]. In the case of an oxygen atom this results in four sp^3 hybrid orbitals, which are roughly tetrahedral in shape. In a water molecule, two of the oxygen hybrid orbitals overlap with the hydrogen orbitals, and the two remaining hybrid orbitals have one electron each, which are referred to as a "lone pair". Each lone pair electron is free to pair with an electron from another water molecule's hydrogen, and each hydrogen can bond with another water molecule's oxygen lone pair. This gives water a total number of four hydrogen bonds per molecule: a quantity which is generally known as the molecular co-ordination number.

Hydrogen bonding in ice I

The hexagonal structure of ice I was first suggested by Bragg in 1922 [105]. It was later formalised by Pauling using X-ray scattering studies, which determined the arrangement of the oxygen atoms [106]. Each oxygen atom sits at the centre of a larger tetrahedron, formed by four surrounding oxygen atoms at the corners, which are 2.76Å away from the central oxygen as shown in Figure 7.1.

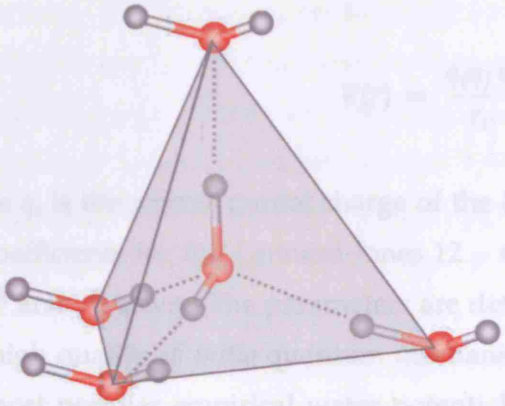

Figure 7.1: The arrangement of the oxygen atoms in ice I is due to the highly localised partial charges and geometry of the hybrid orbitals. This results in a hydrogen bonding axis that is tetrahedral in shape, which leads to an open hexagonal structure.

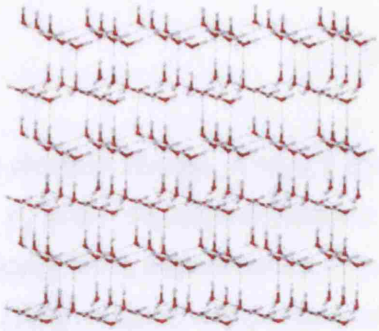

Figure 7.2: The structure of ice I is built up from the water's tetrahedral shape.

Each water molecule is hydrogen bonded to four of its nearest neighbours. The hydrogen bond tetrahedral angle between the central oxygen and any two neighbouring oxygens (O-O-O) is 109.5°. It is easy to see how the hexagonal structure of ice I can be built up from this arrangement, as shown in Figure 7.2.

7.2.2 Empirical water models

There is an important difference between hydrogen bonds and bonding due to permanent dipoles in other types of polar molecules. The difference is that in hydrogen bonding, the hydrogen atom of one molecule has strong preferential attraction to the second molecule's lone pair to such an extent that the hydrogen atom is partially transferred to the second molecule. This results in a strong, highly directional bond, which characterises a hydrogen bond. The average energy of a hydrogen bond in water is approximately 23 $kJmol^{-1}$, which is calculated from the cohesive energy of ice assuming an average of two 2 hydrogen bonds per molecule [101]. This is much stronger than Van der Waals interactions which are about 1.25 $kJmol^{-1}$ but weaker than typical covalent bonds, which are usually about 400 $kJmol^{-1}$

[101].

The charge distribution around a water molecule is often approximated by an electrostatic point charge model [1]. In such models, a point charge is usually assigned to specific locations in the molecule, such as the atom sites or the centre of mass, and the overall charge on the molecule is neutral. A familiar type of empirical molecular water model that uses point interaction sites and a rigid geometry is commonly known as the $TIPS$ potentials [107], [108]. The potential function of the $TIPS$ potential is generally given by

$$V(r) = \frac{q_i q_j e^2}{r_{ij}} + \frac{A}{r_{ij}^{12}} - \frac{B}{r_{ij}^{6}} \tag{7.1}$$

where q_i is the atomic partial charge of the i^{th} atom, e is the electron charge, A and B are the coefficients for the Lennard-Jones $12-6$ potential, and r_{ij} is the separation between the i^{th} and j^{th} atom. The parameters are determined empirically from experimental data and high quality *ab initio* quantum mechanical calculations [109]. A good comparison of the most popular empirical water potentials is made by Jorgensen [109] using classical Monte Carlo simulations. Two of the most widely used water forcefields are the $TIP3P$ and $TIP4P$ potentials. The main difference between these two potentials is the positioning of the oxygen's partial charge. In the $TIP3P$ potential the oxygen charge is positioned on the oxygen's centre of mass, where as in the $TIP4P$ potential it is positioned on the molecules centre of mass (slightly off the oxygen's position).

There are more sophisticated empirical water models which treat the charge distribution of the electrons more sensitively than a point charge on the atom's centre of mass. Such models are often called polarisable water potentials. A notable example of a polarisble water model is the charge-on-spring model [110], which views an atom as being made up of a core and a shell region. The core region is charged, and uses a harmonic constraining potential to tether the core to lie within the region of the shell. This type of model provides a more accurate description of the fluctuating dielectric field, which is important for systems such as ionic solids surrounded by water molecules [111]. In the case of this study, an average mean field treatment of the dipole interactions is a reasonable approximation, since the dipole interaction is averaged out over the surrounding molecular configurations and orientations of the surrounding liquid molecules.

7.3 Embryo Identification and Analysis

In this study we aim to identify ice cluster embryos that form during the water freezing phase transition, and estimate cluster properties such as the mean cluster lifetime. The ice clusters emerge spontaneously due to localised fluctuations in molecular positions and orientations, and break up quickly. The clusters are unstable with respect to their surroundings and are bound for short periods of time by hydrogen bonds and Van der Waals interactions. The hydrogen bonds create a bonding network surrounded by unbound supercooled water molecules. The freezing simulations show that the bonding networks appear inherently disordered, changing size and shape much like a cold liquid cluster, rather than an ordered crystalline solid. This is mainly due to the low temperature of the supercooled water, which prevents the hydrogen bonds from rearranging into a more ordered ice-like configuration. The motion of an ice cluster molecule is modelled subject to a random force due to its interactions with the other cluster molecules and the surrounding water. The random force drives a molecule to "escape" from the cluster in the sense that it violates the cluster definition. However, it will not be able to move very far from the cluster due to the surrounding water molecules.

We utilise a molecular dynamics freezing trajectory generated by Matsumoto *et al.* [37]. The molecular dynamics simulation was conducted at NVT using a bulk liquid water density of 0.96gcm^{-3}, and a temperature of 230K. The interactions between water molecules were modelled using $TIP4P$ potentials. The simulation trajectory provides the time evolved positions of all the molecules during the freezing transition, which are output in intervals of 200ps over the complete simulation, which is just under 500ns. We describe the mobility of molecules in terms of the diffusion coefficient, defined by the mean square displacement. This is used to estimate the friction coefficient. The mean radial force is determined from an evaluation of the derivative of the potential using molecular positions from the trajectory. The mean radial force is numerically integrated to give a potential of mean force, from which we can estimate the potential of mean force depth. This is used together with the friction coefficient to parameterise the cluster decay equation given by Equation (4.49) in Chapter 4 to estimate the mean ice cluster lifetime.

7.3.1 Defining a hydrogen bond

In order to identify ice embryos we must first be able to identify a hydrogen bond. One of the simplest means of defining a bond is to use a geometric criterion, which imposes a min-

imum radial separation between particles in the system. A popular example of a geometric definition is the Stillinger cluster definition [42]. It considers neighbouring molecules that lie within a minimum radius of a given molecule to be bonded. The Stillinger definition is a rather crude approach to a complex problem, as it imposes a stringent constraint that all molecules that lie within a given radius of each other must be hydrogen bonded, regardless of whether the configurations are favourable in terms of energy or longevity. However, it can be argued that neighbours which lie within a minimum radius of each other are likely to have energetically favourable orientations and those that lie outside the bond radius are more likely to have unfavourable energetic configurations. Alternatively, one could use an energetic hydrogen bond definition, which requires pairs of particles have a minimum specified potential energy if they are to be considered bonded. This was the approach used in a study of collective liquid dynamics, whereby pairwise potential energy surfaces were used to identify hydrogen bonded networks [102]. A drawback to this definition is that the pairwise evaluation of the potential energy is computationally demanding. In this respect the Stillinger definition has the advantage of being intuitive and easy to implement.

We employ a radial constraint between the oxygen and hydrogen atoms of different molecules. If any pair of molecules has an oxygen and hydrogen that lie within a minimum radius of each other, the pair of molecules are considered as candidates for hydrogen bonding. In addition to the geometric constraint, we demand that molecule pairs must also maintain a certain longevity. This means a pair of molecules must maintain a minimum separation for a specified duration in order to be considered as hydrogen bonded. This constraint is referred to as the lifetime of the hydrogen bond, although strictly speaking it is not a true lifetime, but rather a minimum lifetime requirement that we have imposed. The longevity constraint provides a simple means of selecting bonds that maintain a certain stability. Furthermore, it avoids the crude assumption suggested by a purely geometric definition that all molecules which lie within a certain radius of each other must be hydrogen bonded.

The choice of bond criterion employed is an important part of defining clusters, as different bond definitions will identify different clusters. For instance, the separation radius must be large enough to include interactions with neighbours, however, it should not be too large so that every molecule is bonded to every other molecule in the system by means of percolation. The separation radius at which this occurs is called the percolation threshold. The equilibrium distance between neighbouring oxygens in ice is about 2.75Å [81], so it is sensible to select a separation radius no greater than this value. The choice of hydrogen bond lifetime will reflect the relative stability of the molecule pairs. Generally speaking,

pairs which survive for a relatively long timescale will be more stable than those that survive for a shorter timescale. A suitable hydrogen bond lifetime will determine clusters which represent truly bound quasi-stable structures, rather than random fluctuations. The freezing study conducted by Matsumoto *et al.* utilises a maximum separation radius of 2.5Å between oxygen and hydrogen atoms, and a hydrogen bond lifetime of 2ns to define a hydrogen bond. This means that molecular separations (between an oxygen and a hydrogen) that are equal to or smaller than this value and maintain this maximum separation for at least 2ns, qualify as hydrogen bonds.

We employ the same bond criterion used by Matsumoto *et al.* to extract a list of bonded pairs of atoms from the freezing trajectory. In addition to this we are only interested in qualifying pairs that maintain a minimum separation for a minimum timescale, which we call the hydrogen bond lifetime τ_h. In a sense, we are coarse graining the MD trajectory over the timescale τ_h to extract a list of time resolved bonded pairs of atoms. The atom pairs list is used to deduce a corresponding list of hydrogen bonded molecules. We recall there are 512 molecules in the system, which means there are 1536 atoms, labelled by atom index number in the order HHO. If an atom number is divisible by 3 then it is an oxygen. This is also the molecule number. If the atom number plus 1 is divisible by 3, then the atom is the second hydrogen. If the atom number plus 2 is divisible by 3, then the atom is the first hydrogen. This calculation identifies the corresponding molecule number for a given atom number. We plot the population of molecule pairs (hydrogen bonds) against simulation time in Figure 7.3. The plot illustrates the evolution of the number of hydrogen bonds during the freezing transition, based on the employed bond definition ($r_h = 2.5$Å , $\tau_h = 2$ns). There is a sharp increase in the population of hydrogen bonds at around 300ns. The number of hydrogen bonds levels off at around 400ns, with approximately 400 bonds. Beyond 400ns, all of the hydrogen bonds will be participating in the final ice lattice. Hydrogen bonds that are determined using a shorter bond lifetime of 1.4ns are also shown in Figure 7.3 for comparison.

7.3.2 Defining a cluster

The molecule pairs list is used to identify which molecules are connected to each other. This is determined using a cluster identification algorithm, which identifies all the molecules that are participating in the same cluster for each time resolved snapshot. The algorithm searches for repeated occurrences of a given molecule number, and then searches for repeated occurrences of those molecules, and so on. This is a hierarchical calculation, which

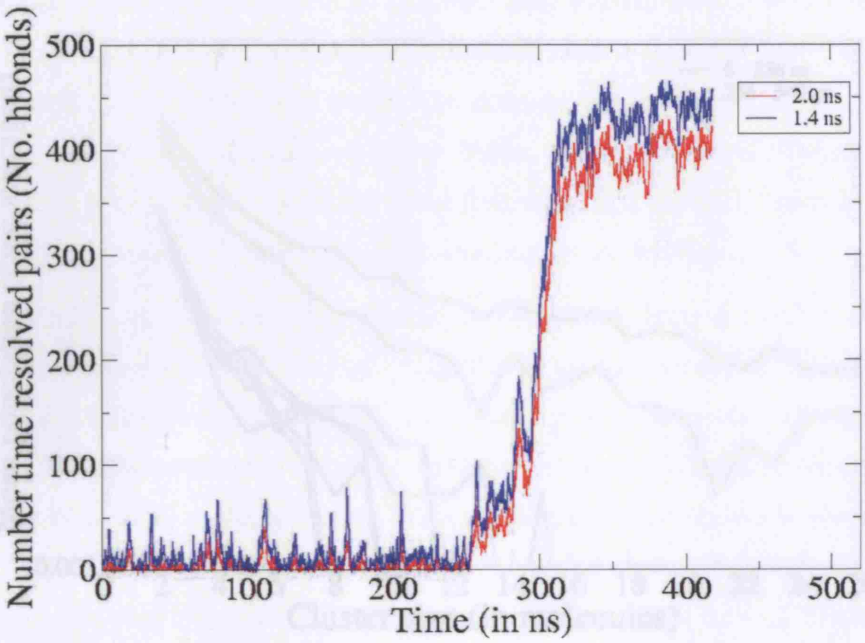

Figure 7.3: The number of bonded pairs of molecules, based on a hydrogen bond definition of radial separation $r_h = 2.5$Å and a longevity of $\tau_h = 2$ns (red line) and for comparison $\tau = 1.4$ns (blue line). The system is maintained at NVT (constant particle number N, volume V and temperature T respectively) at 230K.

is repeated until there are either no more repeated occurrences of molecules in that time resolved snapshot, or the number of molecular connections is so great that the calculation is no longer viable to perform. The details of the calculation are given in Appendix B. The cluster identification algorithm identifies clusters up to approximately 340ns of the trajectory for the employed bond definition of 2.5Å and 2ns.

7.3.3 Population size distribution of ice clusters

The size of an ice cluster embryo is defined by its number of constituent molecules. We explore the evolution in population of different cluster sizes before the predominant ice phase (up to 340ns). To do this we divide the trajectory into 8 sections or "sub-blocks", which are approximately 42.5ns long. We calculate the average number of ice cluster embryos of a given size in each sub-block, which is the total population of each cluster size (in a sub-block) divided by the number of intervals for which we have data. The mean population of ice embryos for each sub-block is plotted against cluster size in molecules, as shown in Figure 7.4. The first 6 sub-blocks (up to 256ns) are shown by the blue lines and the last 2 sub-blocks ($256 - 340$ns) are shown by the red lines.

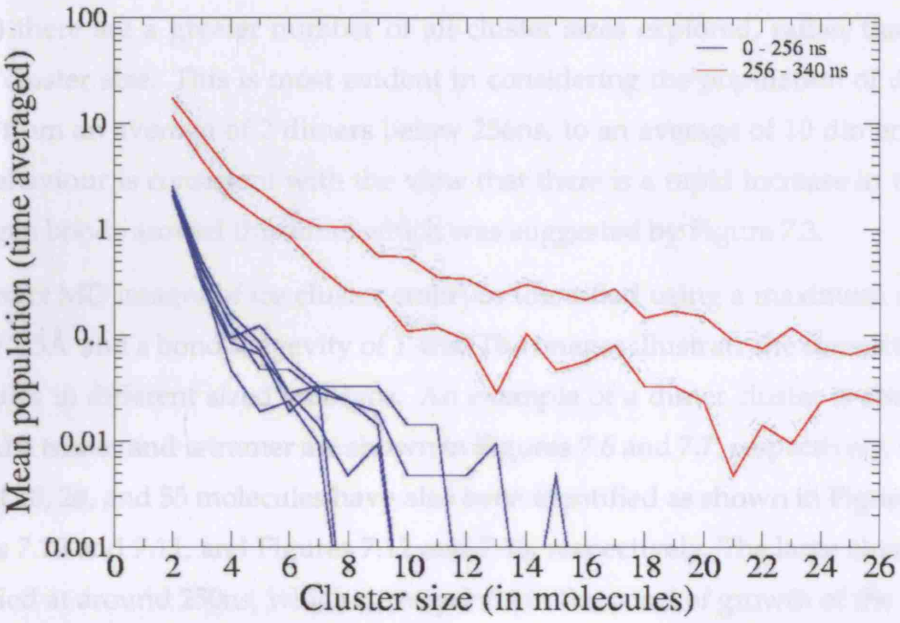

Figure 7.4: A log-linear scale of the mean population of clusters averaged over sub-blocks (coarse grained time intervals of the trajectory up to 340ns) plotted against cluster size in molecules. The clusters are identified using a cut of radius of 2.5Å and longevity of 2ns. The system is maintained at NVT (constant particle number N, volume V and temperature T respectively) at 230K.

The smallest cluster size is a dimer, which contains two water molecules. At the early stages of the simulation (up to 256ns), the mean population of dimers is just above 2. This means that at any instant in a sub-block (below 256ns), there will be on average 2 dimers with a minimum lifetime of 2ns. Another way of interpreting the mean population is to consider that each sub-block is made up of 210 snapshots, since we have data in intervals of 0.2ns. A mean dimer population of 2, corresponds to an average of 2 dimers (that are long lived) in each snapshot of the sub-block. Similarly, a mean trimer population of 0.1 means that there are on average 21 snapshots (out of 210) in a sub-block that contain a tetramer (that is long lived).

Overall, the plot shows at the early stage of the freezing process there are a relatively large number of small sized clusters (*ie* dimers and trimers). This is due to water molecules forming hydrogen bonds momentarily with neighbours, and then breaking up very quickly. There are generally no clusters larger than 15 molecules as the probability of forming large hydrogen bond networks at an early stage is very small. As the freezing transition progresses more large sized clusters emerge, which is evident as the populations indicated by the red lines are higher than the blue lines, they extend further, and are less noisy. Overall,

there are a greater number of clusters of all sizes in the data taken from the latter interval $256 - 340$ns than the first interval $0 - 256$ns. This illustrates that at the onset of growth (256ns) there are a greater number of all cluster sizes explored, rather than the growth of one cluster size. This is most evident in considering the population of dimers, which jumps from an average of 2 dimers below 256ns, to an average of 10 dimers 42.6ns later. This behaviour is consistent with the view that there is a rapid increase in the number of hydrogen bonds around this time, which was suggested by Figure 7.3.

We extract MD images of ice cluster embryos identified using a maximum separation radius of 2.5Å and a bond longevity of 1.4ns. The images illustrate the connectivity between molecules in different sized embryos. An example of a dimer cluster is shown in Figure 7.5, and a trimer and tetramer are shown in Figures 7.6 and 7.7, respectively. Larger cluster sizes of 18, 28, and 55 molecules have also been identified as shown in Figures 7.8 and 7.9, Figures 7.10 and 7.11, and Figures 7.12 and 7.13, respectively. The large cluster sizes were identified at around 250ns, which corresponds to the onset of growth of the ice phase (according to Figure 7.3). The 55-cluster appears to have the beginnings of a distinct ordered structure.

7.3.4 Molecular co-ordination

The structure of hydrogen bonding in the ice embryos is examined in terms of the molecular co-ordination number. This is the number connections (bonds) that each cluster molecule possesses. The co-ordination number reveals how the hydrogen bonds are arranged in the cluster. A cluster molecule may be bonded to up to 4 other molecules, which is evident in the 55-cluster images. The molecular co-ordination number of each cluster molecule is plotted against cluster size in Figure 7.14. This is the number of connections possessed by each cluster molecule, for each cluster size. The number of molecules with a particular co-ordination number (over the 340ns trajectory) is indicated in Figure 7.14. The plot shows that the maximum co-ordination number possessed by cluster molecules is 4. It is also seen that embryos as small as 5-clusters contain molecules that are 4 co-ordinated.

The mean molecular co-ordination number is the average number of connections of each cluster molecule. This is exactly twice the value of the average number of bonds in the cluster per molecule, which is the total number of bonds divided by the number of molecules. The mean molecular co-ordination number is determined for each ice cluster identified, and averaged over the total number of clusters of that size in the trajectory. This is plotted against cluster size in Figure 7.15.

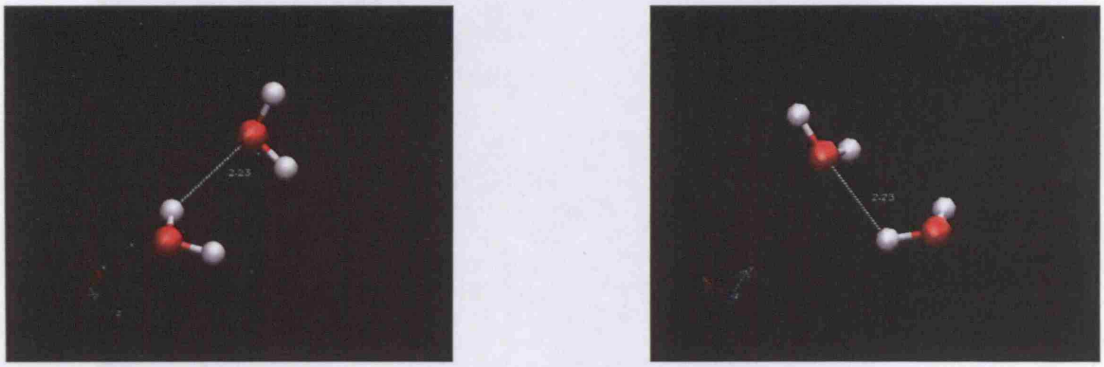

Figure 7.5: An example of an ice dimer shown for two different perspectives, identified from the simulation trajectory where $r_h = 2.5$Å and $\tau_h = 1.4$ns. The system is maintained at NVT (constant particle number N, volume V and temperature T respectively) at 230K.

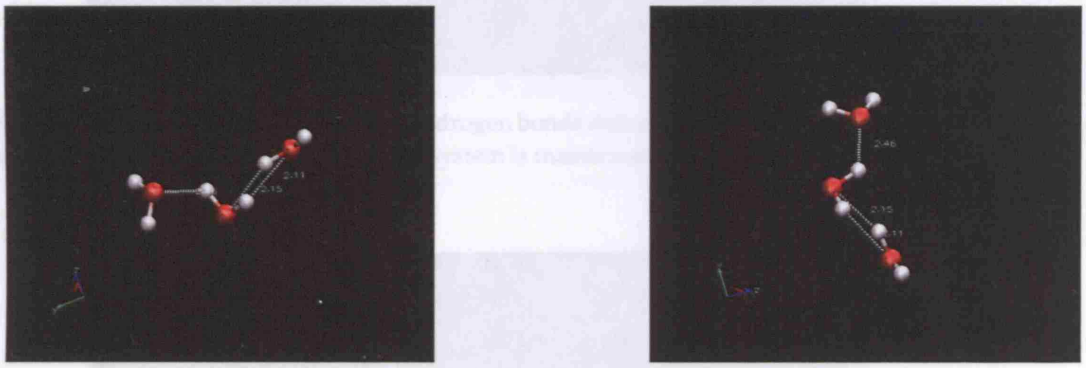

Figure 7.6: An example of an ice 3-cluster with two hydrogen bonds, shown for two different perspectives. The system is maintained at NVT at 230K.

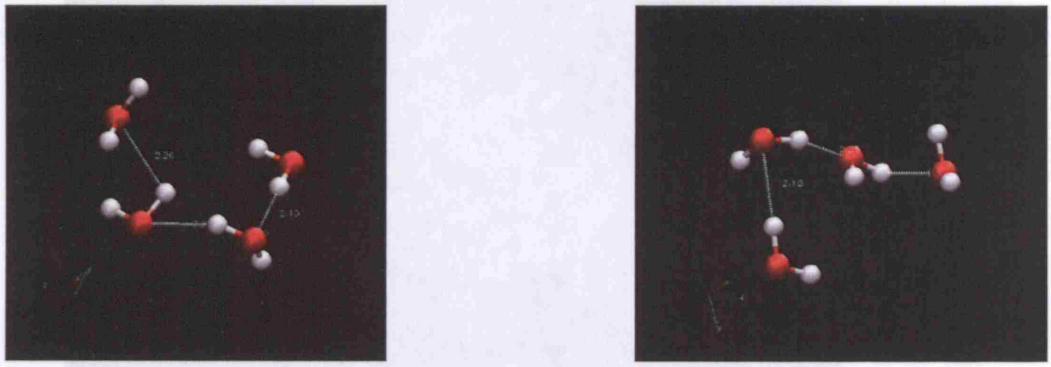

Figure 7.7: An example of an ice 4-cluster with four hydrogen bonds shown for two different perspectives. The system is maintained at NVT at 230K.

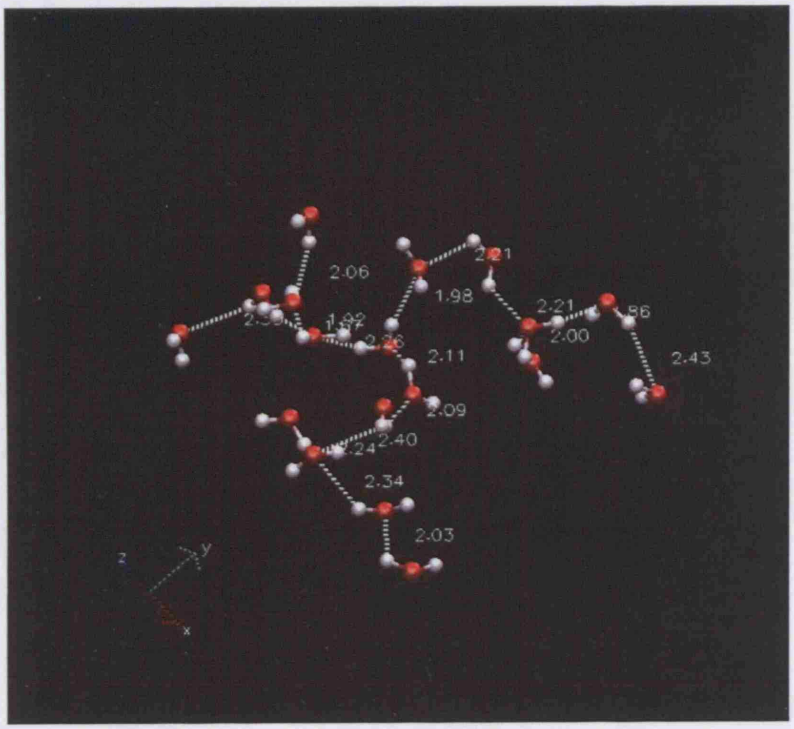

Figure 7.8: An image of an ice 18-cluster with hydrogen bonds defined using a maximum separation radius of 2.5Å , maintained for a minimum of 1.4ns. The system is maintained at NVT at 230K.

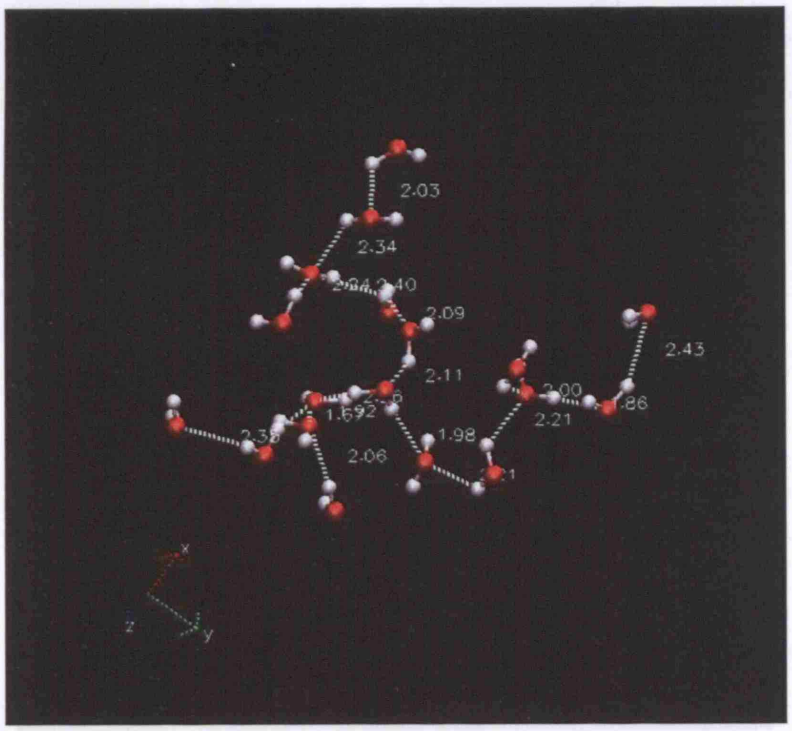

Figure 7.9: An image of the same ice 18-cluster shown in Figure 7.8 illustrated for a different perspective. The system is maintained at NVT at 230K.

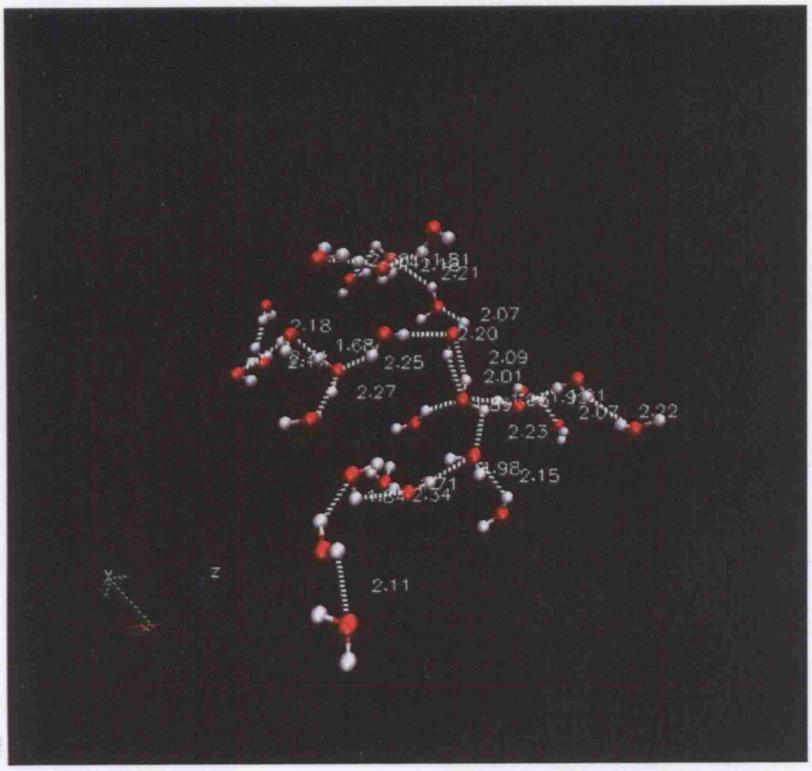

Figure 7.10: An image of an ice 28-cluster with hydrogen bonds defined using a maximum separation radius of 2.5Å , maintained for a minimum of 1.4ns. The system is maintained at NVT at 230K.

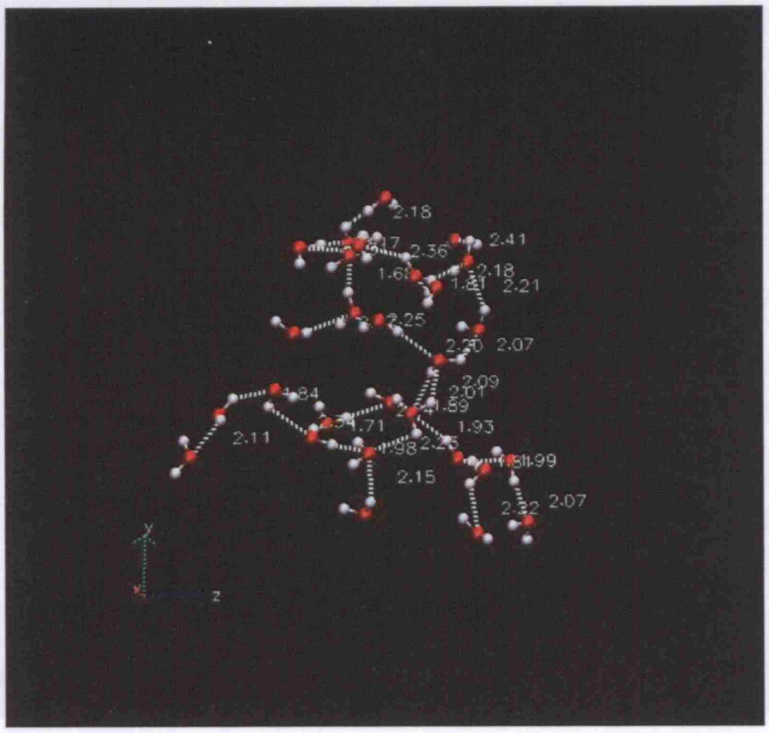

Figure 7.11: An image of the same ice 28-cluster shown in Figure 7.10 illustrated for a different perspective. The system is maintained at NVT at 230K.

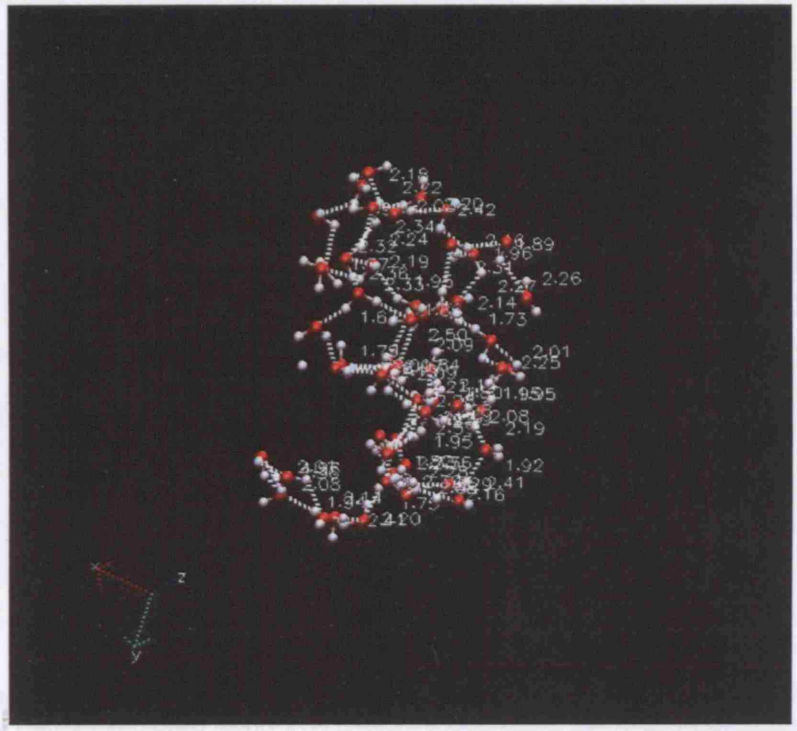

Figure 7.12: An image of an ice 55-cluster with hydrogen bonds defined using a maximum separation radius of 2.5Å , maintained for a minimum of 1.4ns. The system is maintained at NVT at 230K.

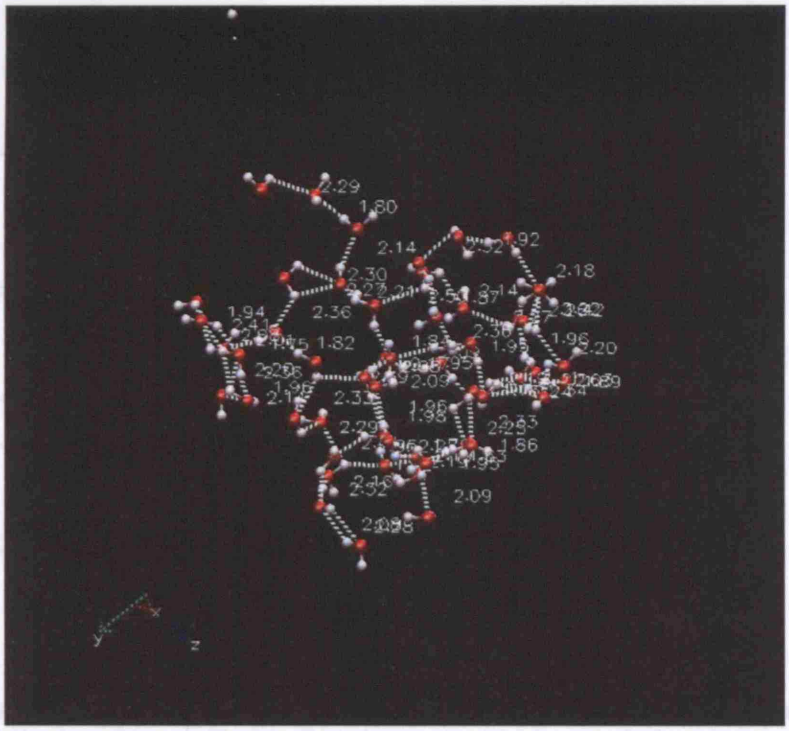

Figure 7.13: An image of the same ice 55-cluster shown in Figure 7.12 illustrated for a different perspective. The system is maintained at NVT at 230K.

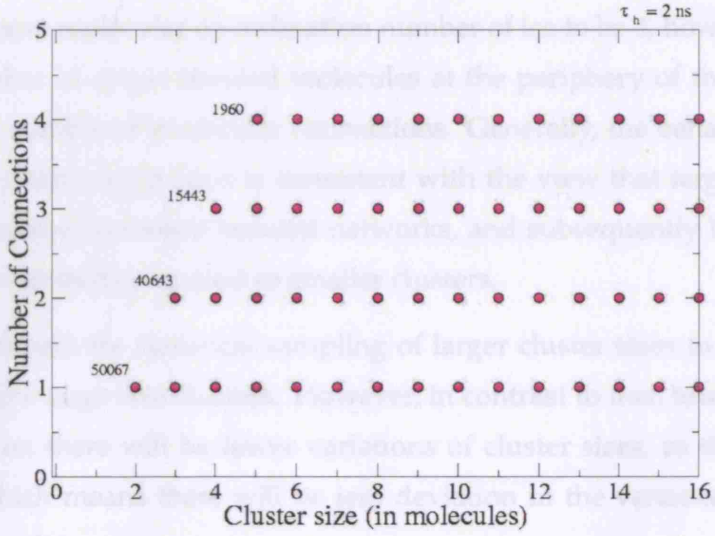

Figure 7.14: Each dot represents the number of connections possessed by a molecule, plotted against cluster size in molecules. The data is plotted before averages are taken, which means there are multiple dots on top of each other. The numbers next to the dots, such as 1960, indicate the total number of molecules (over all cluster sizes and time) that are 4 co-ordinated. Similarly, 15443 are the number of molecules that are 3 co-ordinated. The system is maintained under conditions of NVT at 230K.

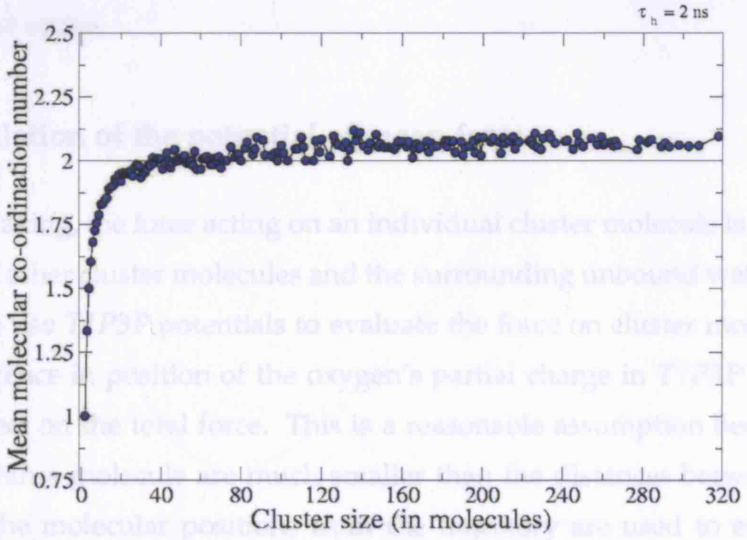

Figure 7.15: The mean molecular co-ordination number of each cluster size, averaged over the total number of clusters of that size in trajectory. The smallest cluster size is a dimer, which contains two molecules has mean co-ordination number of 1. The mean molecular co-ordination number increases with cluster size, and levels off at a value just above 2. The system is maintained under conditions of NVT at 230K.

The dimer cluster has a mean co-ordination number of 1. The mean molecular co-ordination number increases with cluster size, and appears to reach a plateau at a value just above 2. We expect the mean molecular co-ordination number of ice to be 4, however, if there there are a large number of single bonded molecules at the periphery of the cluster, this will lower the mean number of molecular connections. Generally, the behaviour of the mean number of molecular connections is consistent with the view that large size clusters are involved in extensive hydrogen bonded networks, and subsequently have more of their potential bonds satisfied compared to smaller clusters.

In general, we expect the statistical sampling of larger cluster sizes to be relatively poor since there are few large size clusters. However, in contrast to this, toward the end of the freezing transition there will be fewer variations of cluster sizes, as the ice phase starts to dominate, which means there will be less deviation in the variance of the molecular co-ordination number.

7.4 Hydrogen Bond Longevity in Ice Dimers

We aim to determine the mean lifetimes of ice dimers, using an estimation of the potential of mean force depth and the friction coefficient of the bulk liquid. An ice dimer should not be confused with a hydrogen bond pair, which is a component of a larger network rather than a separate entity.

7.4.1 Calculation of the potential of mean force

Generally speaking, the force acting on an individual cluster molecule is due to its interactions with the other cluster molecules and the surrounding unbound water molecules. For simplicity, we use $TIP3P$ potentials to evaluate the force on cluster molecules, assuming that the difference in position of the oxygen's partial charge in $TIP3P$ and $TIP4P$ has a negligible effect on the total force. This is a reasonable assumption because the internal distances within a molecule are much smaller than the distances between neighbouring molecules. The molecular positions from the trajectory are used to evaluate the mean radial force on each cluster molecule. The force is evaluated instantaneously from the positions using *DL_POLY*, which does not require generating any further dynamics.

To determine the potential of mean force depth we calculate the mean radial force acting toward the dimer centre of mass, averaged over the number of dimers, and over all snap-

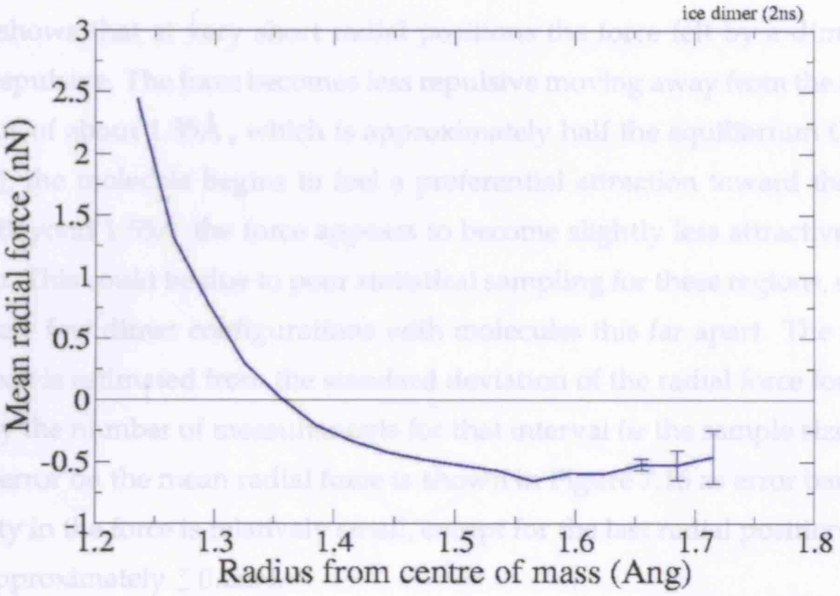

Figure 7.16: The mean radial force for ice dimers classified using a hydrogen bond radius of $r_h = 2.5$Å, and hydrogen bond lifetime of $\tau_h = 2$ns. The error bars are generally too small to be seen on the plot, and are only shown for the last three radial positions. The system is maintained under conditions of NVT at 230K.

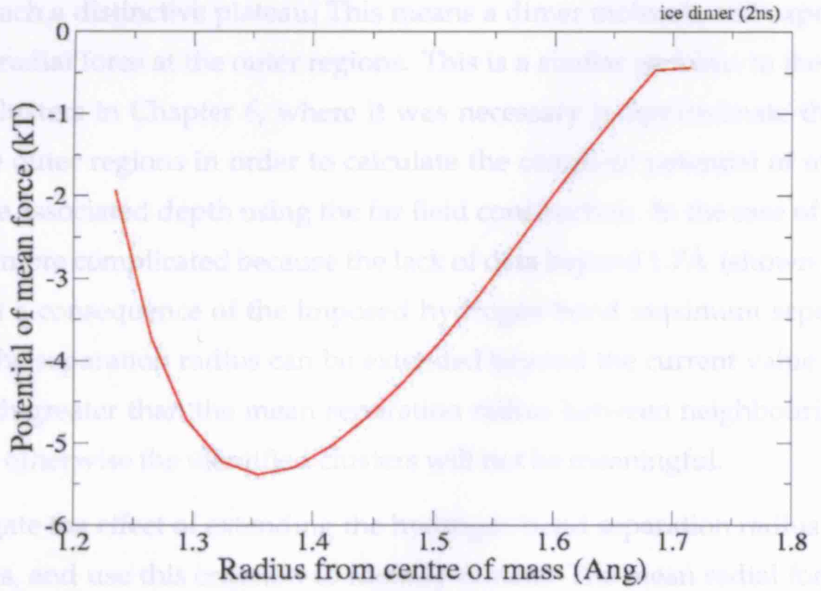

Figure 7.17: The potential of mean force calculated by a numerical integration of the forces for the ice dimers in Figure 7.16. The potential of mean force depth is approximately 5kT. The system is maintained under conditions of NVT at 230K.

shots up to 340ns (before percolation occurs). The mean radial force toward the dimer centre of mass is plotted against radius from the centre of mass in Figure 7.16 (for $\tau_h = 2$ns). The plot shows that at very short radial positions the force felt by a dimer molecule is strongly repulsive. The force becomes less repulsive moving away from the centre of mass. At a radius of about 1.35Å , which is approximately half the equilibrium O-O separation of ice [81], the molecule begins to feel a preferential attraction toward the dimer centre of mass. Beyond 1.55Å the force appears to become slightly less attractive, but does not reach zero. This could be due to poor statistical sampling for these regions, since there will be relatively few dimer configurations with molecules this far apart. The standard error on the mean is estimated from the standard deviation of the radial force for each interval, divided by the number of measurements for that interval (*ie* the sample size for that interval). The error on the mean radial force is shown in Figure 7.16 as error bars. Overall, the uncertainty in the force is relatively small, except for the last radial position, which has an error of approximately $\pm$ 0.2nN.

The mean radial force is numerically integrated from the dimer's centre of mass position ($r = 0$) to the furthest molecule position, which gives the potential of mean force. The potential of mean force is plotted against radial intervals in Figure 7.17. The shape of the potential of mean force illustrates that the dimer molecules have preferential positions toward the centre of the dimer. However, in the outer regions the potential of mean force does not reach a distinctive plateau. This means a dimer molecule still experiences a non-zero mean radial force at the outer regions. This is a similar problem to the non-decaying *n*-nonane clusters in Chapter 6, where it was necessary to approximate the mean radial force in the outer regions in order to calculate the complete potential of mean force and quantify the associated depth using the far field construction. In the case of ice dimers the situation is more complicated because the lack of data beyond 1.7Å (shown in Figures 7.16 and 7.17) is a consequence of the imposed hydrogen bond maximum separation radius. Although the separation radius can be extended beyond the current value of 2.5Å it can not be much greater than the mean separation radius between neighbouring oxygens in ice (2.76Å), otherwise the identified clusters will not be meaningful.

We investigate the effect of extending the hydrogen bond separation radius to 3.0Å keeping $\tau_h = 2$ns, and use this criterion to identify dimers. The mean radial force for a dimer is plotted against radius in Figure 7.18. The mean radial force reaches a minimum at a radius of about 1.55Å . Beyond this radius, the mean radial force becomes less attractive and appears to tend toward zero. The potential of mean force is calculated and plotted against

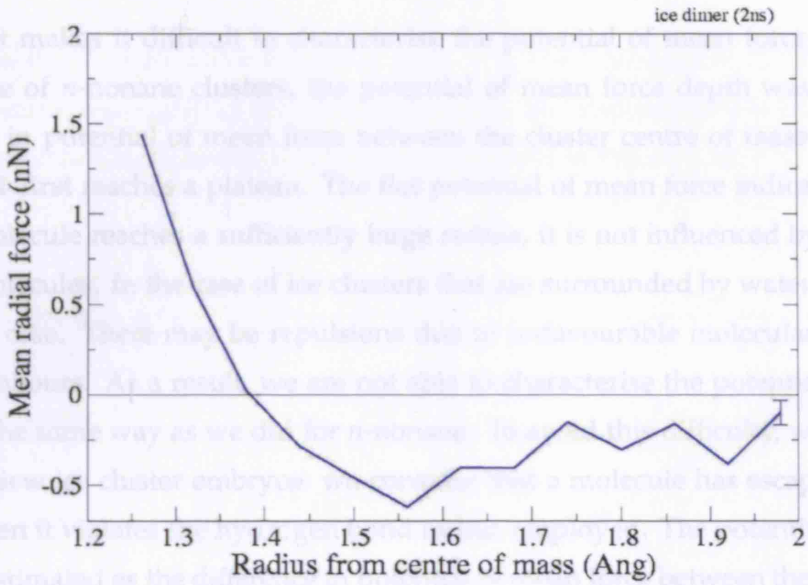

Figure 7.18: The mean radial force toward the ice dimer centre of mass plotted against radius. The hydrogen bond separation radius employed is 3.0Å, and the hydrogen bond lifetime is 2ns. The error bars are generally too small to be seen on the plot, and are only shown for the last radial position. The system is maintained under conditions of NVT at 230K.

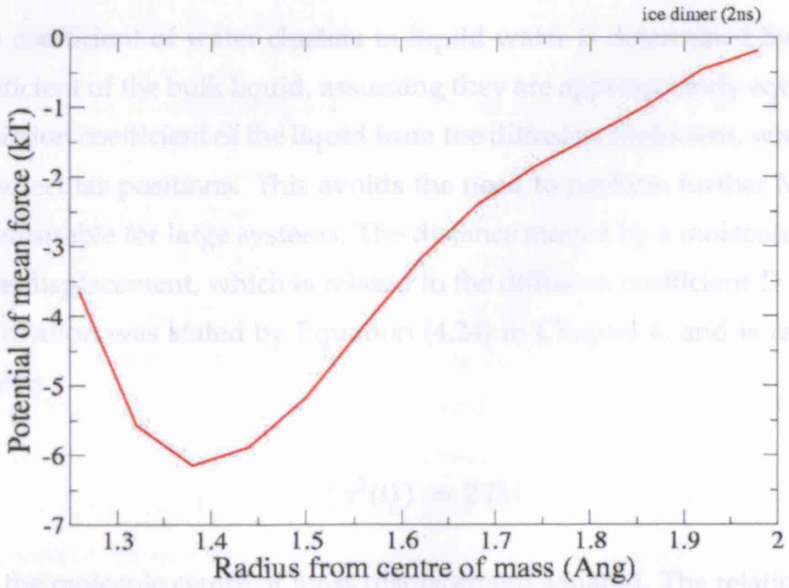

Figure 7.19: The potential of mean force plotted against radius from the ice dimer centre of mass position. The system is maintained under conditions of NVT at 230K.

radius in Figure 7.19. Once again, the dimer molecules do not appear to experience a flat potential of mean force at the large dimer separation.

This result makes it difficult to characterise the potential of mean force for ice dimers. In the case of n-nonane clusters, the potential of mean force depth was defined as the difference in potential of mean force between the cluster centre of mass and the radius at which Φ first reaches a plateau. The flat potential of mean force indicates that when a cluster molecule reaches a sufficiently large radius, it is not influenced by the remaining cluster molecules. In the case of ice clusters that are surrounded by water molecules, this is not the case. There may be repulsions due to unfavourable molecular configurations with neighbours. As a result, we are not able to characterise the potential of mean force depth in the same way as we did for n-nonane. To avoid this difficulty, we must redefine how we view ice cluster embryos: we consider that a molecule has escaped from the ice dimer when it violates the hydrogen bond radius employed. The potential of mean force depth is estimated as the difference in potential of mean force between the dimer centre of mass and the furthest radius for which there is data available (this will be dependent on the employed separation radius). We estimate the potential of mean force depth for an ice dimer defined using the bond criterion $r_h = 2.5\text{Å}$ and $\tau_h = 2\text{ns}$ to be approximately 5kT.

7.4.2 Calculation of the friction coefficient

The friction coefficient of water clusters in liquid water is determined by calculating the friction coefficient of the bulk liquid, assuming they are approximately equivalent. We calculate the friction coefficient of the liquid from the diffusion coefficient, which is calculated using the molecular positions. This avoids the need to perform further MD simulations, which is undesirable for large systems. The distance moved by a molecule determines the mean square displacement, which is related to the diffusion coefficient D in the long time limit. This relation was stated by Equation (4.24) in Chapter 4, and is repeated here for convenience as

$$\langle x^2(t) \rangle = 2\,D\,t \tag{7.2}$$

where x^2 is the molecule centre of mass displacement squared. The relation indicates that the further a molecule travels in a given time interval, the greater the diffusion coefficient. The diffusion coefficient can be expressed in terms of the molecule mobility, which was stated by Equation (4.27) in Chapter 4, and is repeated here as

$$D = \frac{kT}{m}\tau_c \tag{7.3}$$

where τ_c is the velocity autocorrelation time, T is the temperature (230K), and m is the mass of a water molecule (18.015AMU). The molecule displacement squared x^2, from the freezing trajectory, is plotted against simulation time t in Figure 7.20.

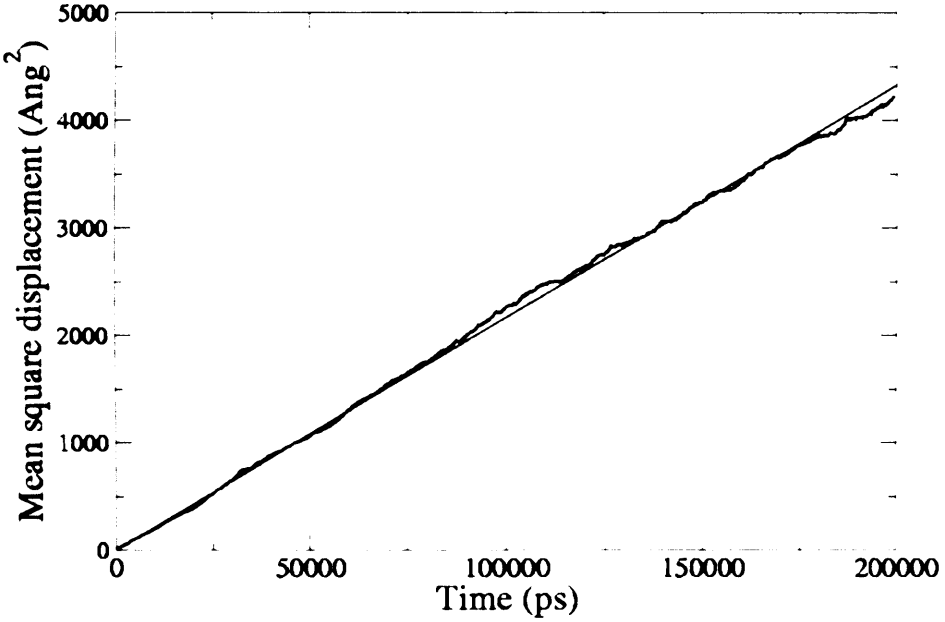

Figure 7.20: The mean square displacement plotted against simulation time in picoseconds shows a linear relation with a gradient given by $2D$. The system under conditions of NVT at 230K.

The gradient of the plot is approximately $0.02\text{Å}^2\text{ps}^{-1} = 2D$, which provides an estimate of the diffusion coefficient D. This is used in Equation (7.3) along with the mass of a water molecule and a temperature of 230K to estimate the velocity autocorrelation timescale. We recall that the velocity autocorrelation time is the inverse of the friction coefficient (as stated by Equation (4.33)). The friction coefficient is thus determined to be 975ps^{-1}, which is relatively large compared to that of n-nonane clusters (3.0ps^{-1}). This indicates that the system is viscous and sticky, rather than fluid like, which is probably due to the strong directional nature of the hydrogen bonding and the considerably low (supercooled) temperature.

7.4.3 Calculation of dimer lifetimes

The friction coefficient of ice clusters (calculated in section 7.4.2) is used together with an estimation of $\Delta\Phi$, from Figure 7.19, with estimated errors of $\pm$0.2kT, to evaluate Equation (4.49), which yields a mean dimer lifetime of 2.4ns (using a hydrogen bond definition of 2.5Åand 2ns). Obviously, different hydrogen bond definitions will produce different dimer lifetimes. If the employed hydrogen bond longevity is too short, then the dimers do not represent the truly bound quasi-stable structures that we are interested in, but random fluctuations, which we want to avoid. We investigate a range of hydrogen bond lifetime definitions from 0.8ns - 2.4ns in intervals of 0.2ns, which identifies a range of time resolved dimer clusters, and corresponding potential of mean force depths. Similarly, we calculate the mean dimer lifetimes using an estimation of the potential of mean force depth and the friction coefficient (from section 7.4.2). The mean dimer lifetimes are plotted against the defined hydrogen bond lifetimes in Figure 7.21, along with the estimated errors (from the estimated error in the potential of mean force depth). A relative comparison of the mean dimer lifetime with the defined hydrogen bond lifetime (τ_{model}/τ_h) is plotted against defined hydrogen bond lifetime as shown in Figure 7.22.

To deduce the most suitable hydrogen bond lifetime, we seek a consistency between the calculated mean dimer lifetime and the defined hydrogen bond lifetime. For short hydrogen bond lifetimes of around 0.8ns the mean dimer lifetime is about 6ns as shown by Figure 7.21. As the defined hydrogen bond lifetime increases, the dimer lifetime decreases. Toward the larger hydrogen bond lifetimes above 2.2ns, the calculated mean dimer lifetimes appear to be less than the hydrogen bond lifetimes, which is an inconsistency, suggesting that the defined hydrogen bond lifetime is too stringent. The most sensible choice of hydrogen bond lifetime appears to be 2ns, which supports the value employed by Matsumoto *et al.*. We shall proceed with this hydrogen bond lifetime definition together with a maximum separation radius of 2.5Å , employed to extract larger cluster sizes, which are analysed in the next section.

7.5 The Potential of Mean Force for Larger Clusters

We calculate the mean radial force and potential of mean force for a 5-cluster and 8-cluster, as shown in Figures 7.23, 7.24, 7.25 and 7.26 respectively. The potential of mean force plots of ice clusters are characteristically very different to the potential of mean force plots for liquid *n*-nonane clusters. The ice cluster embryos exhibit a linear rise in potential of mean

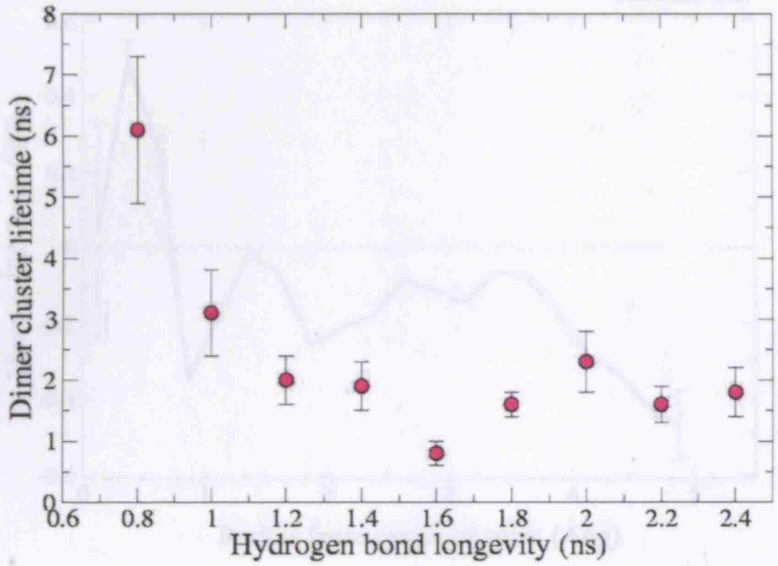

Figure 7.21: The mean lifetime of the ice dimer plotted against hydrogen bond lifetime. The system is maintained under conditions of NVT at 230K.

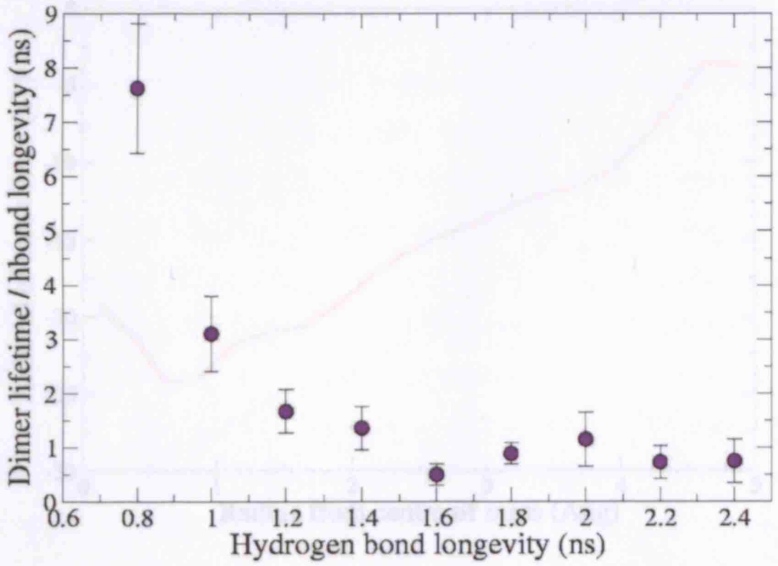

Figure 7.22: The mean lifetime of the ice dimer divided by hydrogen bond lifetime, plotted against hydrogen bond lifetime. The system is maintained under conditions of NVT at 230K.

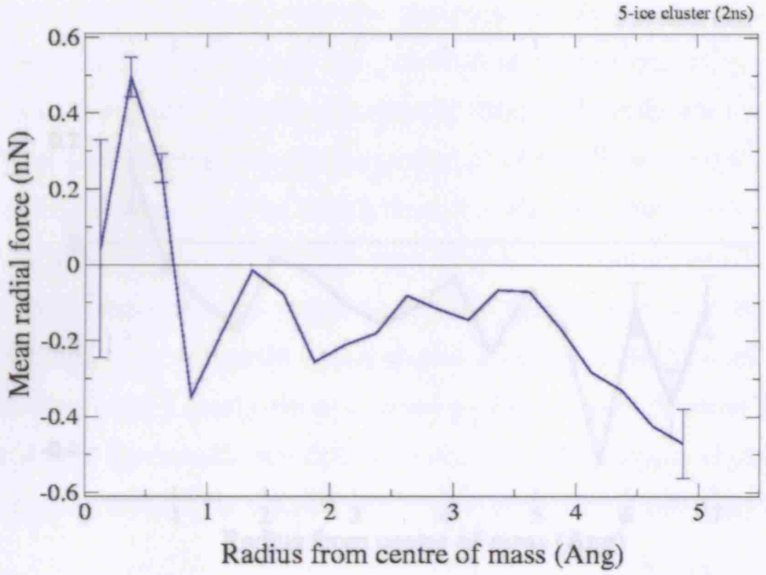

Figure 7.23: The mean radial force for an ice 5-cluster plotted against radius from the centre of mass. The system is maintained under conditions of NVT at 230K.

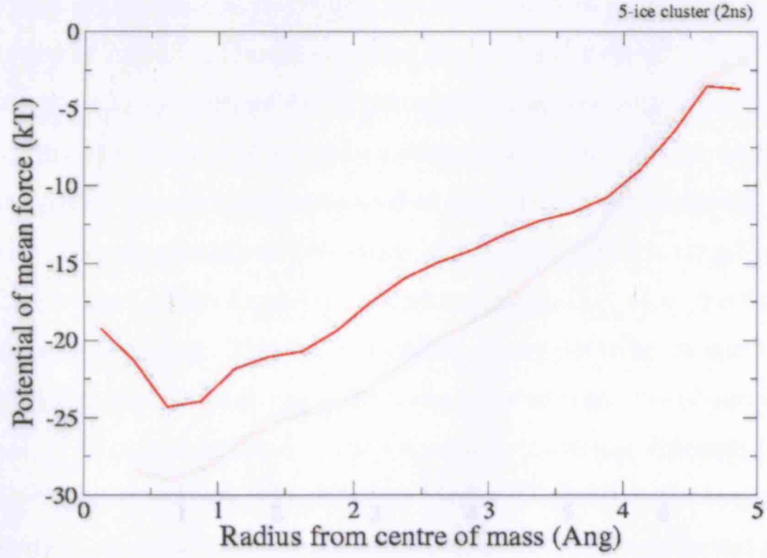

Figure 7.24: The potential of mean force for an ice 5-cluster. The potential of mean force is calculated from the mean forces in Figure 7.23, through a numerical integration using the trapezium rule. The system is maintained under conditions of NVT at 230K.

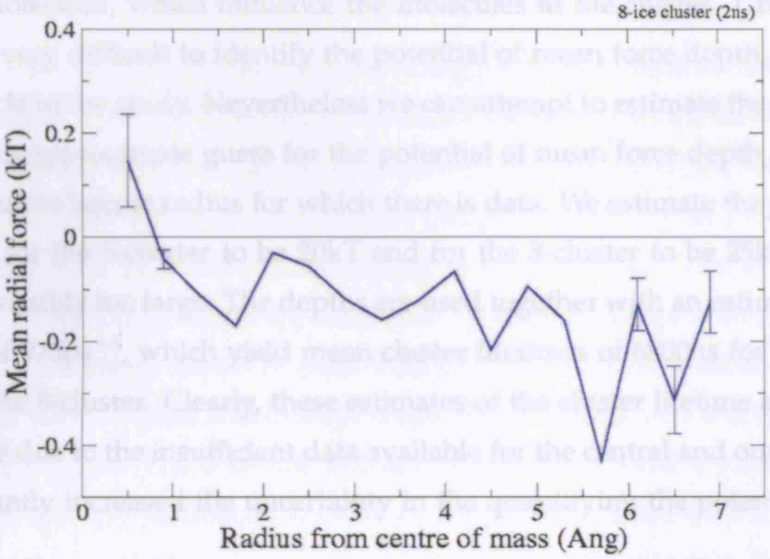

Figure 7.25: The mean radial force for an ice 8-cluster plotted against radius from the centre of mass. The system is maintained under conditions of NVT at 230K.

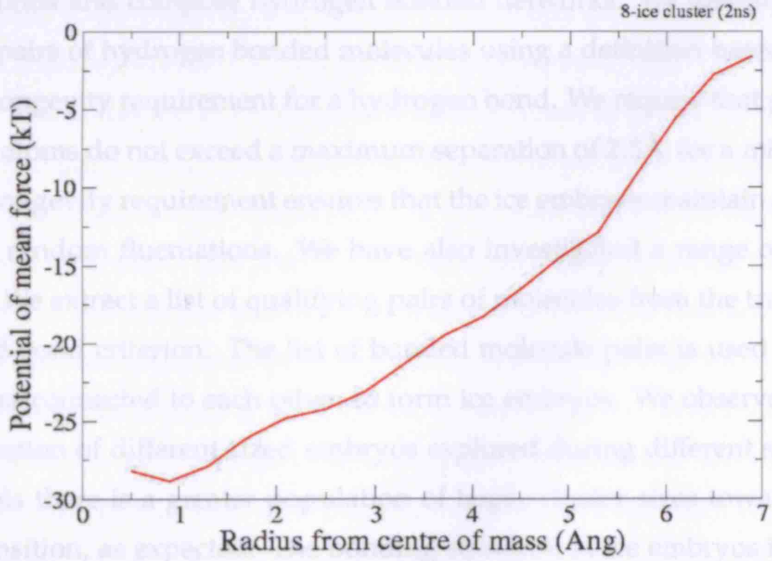

Figure 7.26: The potential of mean force for an ice 8-cluster. The potential of mean force is calculated from the mean forces in Figure 7.25, through a numerical integration using the trapezium rule. The system is maintained under conditions of NVT at 230K.

force with increasing radius, which ends abruptly toward the outer regions of the cluster. We are not able to easily approximate the force for the outer regions, due to the surrounding water molecules, which influence the molecules in the cluster. Under such circumstances it is very difficult to identify the potential of mean force depth, which presents a major obstacle in the study. Nevertheless we can attempt to estimate the mean cluster lifetime using an approximate guess for the potential of mean force depth, defined from the centre of mass to largest radius for which there is data. We estimate the potential of mean force depth for the 5-cluster to be 20kT and for the 8-cluster to be 25kT, although these values are possibly too large. The depths are used together with an estimate of the friction coefficient of 975ps^{-1}, which yield mean cluster lifetimes of 6800ns for the 5-cluster, and 8700μs for the 8-cluster. Clearly, these estimates of the cluster lifetime are too great. This error may be due to the insufficient data available for the central and outer regions, which has significantly increased the uncertainty in the quantifying the potential of mean force depth.

7.6 Summary of Ice Embryo Study

In this study we investigated the structure and dynamics of supercooled ice cluster embryos, which emerge during the freezing phase transition. The ice embryos are bound by hydrogen bonds and compose hydrogen bonded networks. We identify ice embryos by identifying pairs of hydrogen bonded molecules using a definition based on a radial constraint and longevity requirement for a hydrogen bond. We require that pairs of hydrogen and oxygen atoms do not exceed a maximum separation of 2.5Å for a minimum timescale of 2ns. The longevity requirement ensures that the ice embryos maintain a certain stability, and are not random fluctuations. We have also investigated a range of hydrogen bond longevities. We extract a list of qualifying pairs of molecules from the trajectory that meet the specified bond criterion. The list of bonded molecule pairs is used to deduce which molecules are connected to each other, to form ice embryos. We observe the evolution in mean population of different sized embryos explored during different stages of freezing, which reveals there is a greater population of larger cluster sizes toward the end of the freezing transition, as expected. The bonding structure in ice embryos is investigated by a calculation of the mean molecular co-ordination number for different cluster sizes. This reveals that larger ice embryos have a mean molecular co-ordination number just above 2, and participate in a greater number of bonds than smaller ice embryos such as dimers, which have a mean molecular co-ordination number of 1. This is consistent with the view

that larger clusters participate in larger bonding networks and have more of their potential hydrogen bonds satisfied. Nevertheless, the larger clusters have a co-ordination number well below the value of 4, expected of hexagonal ice, due to their amorphous nature.

We model the motion of a dimer molecule using a Langevin representation of its dynamics. This treatment is used to estimate the mean lifetime of an ice dimer. The lifetime is viewed in terms of the the probability of a molecule's escape from a constraining potential of mean force. The process of a molecule's escape is driven by its interactions with the other cluster molecules and the surrounding water molecules. The timescale of friction between the cluster molecules is approximated by calculating the friction coefficient of the liquid water molecules. To avoid performing further MD simulations we calculate the diffusion coefficient, which requires the molecular positions, and this is used to estimate the friction coefficient. The friction coefficient of the supercooled water is calculated to be 975ps^{-1}, which is approximately 3 orders of magnitude greater than for *n*-nonane. This indicates that the system is much more sticky and viscous rather than fluid like, probably due to the strongly directional hydrogen bonds, and the considerably low temperature of the system.

The potential of mean force is determined from the mean radial force acting toward the dimer centre of mass. The mean radial force of a dimer is evaluated from the derivative of the potential using the molecular positions from the MD trajectory. The mean radial force is deduced to be highly repulsive close to the dimer centre of mass, corresponding to repulsive molecular interactions, and becomes less repulsive and more attractive further out from the dimer. The mean radial force reaches a minimum value, and then stops rather abruptly due to the imposed cut off radius. The hydrogen bond radius was explored out to 3.0Å , which yields a mean radial force for the outer regions that is less attractive but does not quite reach zero. This is could be due to the highly localised partial charges and specific orientational valence geometry of water which means that most configurational orientations between molecules are likely to be unfavourable, which may cause repulsions at the dimers peripheral regions. The problem of sampling the correct force at the outer regions of the dimer is similar to the problem encountered with the non-decaying *n*-nonane clusters. However, in the case of ice clusters there is a problem with extending the maximum separation radius beyond a certain threshold as it means every molecule is connected to every other molecule, which we want to avoid, as the bond definition is too stringent. The fact that the mean force does not reach zero at large dimer separations means that molecules do not then sample a flat potential of mean force. This leads us to redefine our

view of molecular escape from a cluster. Instead of viewing "escape" as occurring when a molecule samples an unchanging potential of mean force, we characterise escape to occur when the molecule violates the hydrogen bond radius. The potential of mean force depth is estimated as the difference in potential of mean force from the centre of mass to the furthest radius occupied by a molecule. The potential of mean force depth for a dimer defined using a hydrogen bond separation radius of 2.5Å and longevity of 2ns, is determined to be approximately 5kT.

We have explored a range of hydrogen bond lifetime definitions from 0.8ns-2.4ns. The mean dimer lifetimes are calculated using Equation (4.49). The results show that for hydrogen bond lifetimes above 2ns, the calculated dimer lifetimes are under 2ns, which is inconsistent in the sense that the mean lifetime of the dimer exceeds the minimum lifetime of the hydrogen bond. This inconsistency indicates that the bond definition may be too stringent. For longevities shorter than this, at 0.8ns the mean dimer lifetime is about 6ns. Although this is an agreeable result, we seek to select the most suitably consistent lifetime in comparison to the minimum hydrogen longevity. A minimum hydrogen bond longevity of 2ns yields a mean dimer lifetime of about 2.3ns, which appears to be the most sensible choice. Furthermore, a hydrogen bond longevity of 2ns is consistent with the value employed in the study by Matsumoto *et al.* [37].

We apply this minimum hydrogen bond longevity together with a maximum separation radius of 2.5Å to identify larger ice clusters. We investigate the potential of mean force for a 5-cluster and a 8-cluster. The results show there is a linear rise in the potential of mean force with increasing radius from the centre of mass, which stops abruptly due to the imposed separation radius. The behaviour of the potential of mean force very different to the behaviour of *n*-nonane clusters, which makes further analysis via this approach difficult to proceed with. Nevertheless, we have attempted to estimate the mean ice cluster lifetimes for a 5-cluster a 8-cluster, calculated using Equation (4.49), which yield values of 6000ns and 8700μs respectively. These mean lifetimes are clearly incorrect, as they are far too large and exceed the time taken form the ice phase in the simulation.

Chapter 8

Concluding Remarks

This thesis focuses attention on predicting the lifetime of organic condensed phase liquid clusters. The cluster lifetime is viewed as the mean time taken for particles to leave the cluster, which is referred to as cluster decay. The cluster decay process views the motion of a single particle in the cluster as being driven by its interactions with the surrounding cluster particles. Any given cluster particle feels a mean force due to the average interactions it experiences with its surroundings, and a stochastic force due to the random collisions from its surroundings. The motion of a cluster particle is modelled using a Langevin equation, which treats the force acting on a cluster particle in 1-dimension, which assumes a certain symmetry of the cluster. The cluster particle forces are dynamically generated, and are used to parametrise the Langevin equation. This is achieved by performing MD simulations conducted at constant temperature using the Andersen stochastic thermostat. The use of a stochastic thermostat mimics the experimental conditions at which clusters sizes of 40-67 *n*-nonane molecule were deduced to be critical. The MD simulations are computationally demanding calculations, even for small cluster sizes and thus simulations of larger cluster sizes are not practical.

The mean interactions of a molecule within the cluster are used to determine the potential of mean force, and the associated potential well depth $\Delta\Phi$. In the absence of cluster decay, the mean force on a molecule at the cluster's periphery is not properly sampled. Consequently, the potential of mean force for this region is not completely established and the potential well depth cannot be correctly quantified. In order to address this shortcoming, the mean force for these regions is approximated by the radial derivative of the mean potential energy of an imaginary molecule placed at that location, provided it does not affect the cluster's configuration. This avoids the need to perform further MD simulations under

circumstances of insufficient MD data for the cluster's peripheral regions and beyond (*ie* in absence of cluster decay).

The friction force is characterised by the friction coefficient γ. It is extracted by using an analysis that involves mapping MD onto the coarse grained timescale of Langevin dynamics. The difference between the force on a molecule evaluated over a coarse timescale, and the MD force on a molecule averaged over all molecular configurations, is referred to as the mean discrepancy force. We find that this force has a linear correlation with the molecule's velocity, and the gradient is related to the friction coefficient. The Langevin derived parameters $\Delta\Phi$ and γ are used together in an Arrhenius type of equation for cluster decay, which yields estimates for the decay timescale of the simulated *n*-nonane clusters.

Overall, the stochastic cluster decay model is an essential tool for systems with long decay timescales, for which decay events may not be observed during a typical MD trajectory. It appears that the dynamic decay model taken to represent the cluster behaviour, together with the Langevin interpretation of the dynamics, provides a successful description of the real cluster behaviour, particularly for the smallest cluster sizes. These findings are in good agreement with the decay times estimated from experimental data, and those suggested by classical nucleation theory. Further simulations of varying cluster sizes would help better characterise the decay model so that it can be applied to a complete distribution of cluster sizes.

The latter study focuses on predicting the lifetime of amorphous ice clusters. The clusters form during the freezing phase transition of supercooled water into ice. This is a very different system to condensed phase liquid clusters, nevertheless, we aim to extend the treatment of cluster decay in liquid clusters so that it can be applied to amorphous ice clusters. The process of cluster decay in amorphous ice clusters is viewed as a single particle escape, driven by a mean and stochastic force, due to the average interactions and random collisions an ice cluster molecule experiences with its surroundings. The mean force felt by an ice cluster molecule is not properly quantified at the periphery of the cluster. This is due to the fact that the ice clusters are surrounded by "unbound" supercooled water, which means that a cluster molecule does not necessarily sample an unchanging potential of mean force at the cluster's periphery, as expected. This makes it difficult to quantify the potential of mean force depth. Consequently, any subsequent calculations of the cluster lifetime are strongly influenced by how we choose to define a cluster.

The application of the Langevin model in the treatment of ice clusters has raised some important questions concerning the driving force of the water freezing phase transition. On

a molecular level, it is likely that the probability of particle escape is largely characterised by the molecule orientation rather than position. The centre of mass positions of cluster molecules do not undergo significant displacements, due to the very low temperature of the system. In this sense, the Langevin interpretation of ice cluster dynamics represents a limited description of the entropic differences between the cluster and its surroundings, for supercooled water. In condensation, the liquid phase has a lower entropy than the vapour phase due to the smaller volume of phase space available to it. The difference in entropy is a component of the driving force of the condensation phase transition. In the case of freezing, the situation is rather different. Although the solid phase has a lower entropy than the liquid phase, the relative volumes they occupy are similar. The difference in entropy is brought about by the larger number of bond orientations available in a liquid than in the solid. This suggests there are different entropic contributions that are important for condensation than for freezing. Essentially, the nucleation of liquid droplets from a supersaturated vapour is controlled by monomer flux from the vapour, whereas the growth of ice embryos from a supercooled liquid is a matter of molecular reorientation of hydrogen bonds.

Perhaps a more suitable approach to this problem would be to employ a confining potential of mean force that is orientation dependent, which would include entropy of order as an important factor. However, this is a development which would complicate the relatively simple picture of cluster decay drawn here, but it would be a potentially interesting future advancement for this study.

Bibliography

[1] H. R. Pruppacher and J. D. Klett. *Microphysics of clouds and precipitation*. Kluwer Academic Publishers, 1997.

[2] S. Twomey. *Atmospheric Aerosols*. Elsevier scientific publishing company, 1977.

[3] Inc Engineering Jonas and Consultancy. *Company Website: www.steamcycle.com*, 2006.

[4] F. Bakhtar, M. Ebrahimi, and B. O. Bamkole. On the performance of a cascade of turbine rotor tip section blading in nucleating steam part2: wake traverses. *Proc. Instn. Mech. Engrs.*, 209:169–177, 1997.

[5] C. R. T. Wilson. Condensation of water vapour in the presence of dust-free air and other particles? *Philos. Trans. R. Soc. London A*, 189:265, 1897.

[6] B. Cowan. *Topics in Statistical Mechanics*. Imperial College Press, 2004.

[7] H. Arstila. (thesis) gas-liquid nucleation in non-ideal molecular systems. *Report series in Aerosol science (Finnish association for aerosol research)*, 1997.

[8] A. Hyvärinen. *(Thesis) Experiments on homogeneous nucleation and physiochemical properties related to atmospheric new particle formation*. Finnish Association for Aerosol Research, 2006.

[9] D. W. Oxtoby. Homogeneous nucleation: theory and experiment. *J. Phys: Condens Matter 4.*, 4:7627–7650, 1992.

[10] A. Langsdorf. The diffusion cloud chamber. *Indus. Eng. Chem*, 44(6):1298–1300, 1936.

[11] H. C. Hung, M. J. Krasnopoler, and J. L. Katz. Condensation of a supersaturated vapour. viii. the homogeneous nucleation of *n*-nonane. *J. Chem. Phys.*, 90:1856, 1989.

[12] P. E. Wagner and R.Strey. Measurements of homogeneous nucleation rates for *n*-nonane vapor using a two-piston expansion chamber. *J. Chem. Phys.*, 80:5266, 1984.

[13] R. Strey, P. E. Wagner, and Y.Viisanen. The problem of measuring homogeneous nucleation rates and the molecular contents of nuclei: progress in the form of nucleation pulse measurements. *J. Phys. Chem*, 98:7748, 1994.

[14] K. Hämeri, M. Kulmala, E. Krissinel, and G. Kodenyov. Homogeneous nucleation in a laminar flow diffusion chamber: the operation principles and possibilities for quantitative rate measurements. *J. Chem. Phys*, 105(17):7683, 1996.

[15] B. E. Wyslouzil, J. H. Seinfield, R. C. Flagan, and K. Okuyama. Binary nucleation in acid-water systems i methane sulfonic acid-water. *J. Chem. Phys*, 94(10):6827, 1991.

[16] B. E. Wyslouzil, J. H. Seinfield, R. C. Flagan, and K. Okuyama. Binary nucleation in acid-water systems ii sulfuric acid-water and comparison with methane sulfonic acid-water. *J. Chem. Phys*, 94(10):6842, 1991.

[17] M. Volmer and A. Weber. Elementary principles in statistical mechanics. *Z. Phys. Chem*, 119:277, 1926.

[18] R. Becker and W. Döring. Kinetische Behandlung der Keinbildung in übersättigten Dämpfen. *Ann. Phyz. (Leipzig)*, 24:719, 1935.

[19] J. W. Gibbs. *The Scientific Papers of J. Willard. Gibbs*. Dover, New York, 1961.

[20] F. F. Abraham. *Homogeneous Nucleation Theory. The Pretransition Theory of Vapour Condensation*. Academic Press, New York and London, 1974.

[21] R. C. Tolman. *The Principles of Statistical Mechanics*. Oxford University Press, 1938.

[22] I. J. Ford. Thermodynamic properties of critical clusters from measurements of vapour-liquid homogeneous nucleation rates. *J. Chem. Phys.*, 105:8324, 1996.

[23] Hanna Vehkamäki. *Classical Nucleation Theory in Multicomponent Systems*. Springer, 2006.

[24] I. J. Ford. Statistical mechanics of nucleation: a review. *Proc. Instn. Mech. Engrs. (J. Mech. Engr. Sci)*, 218 (Part C):883–899, 2004.

[25] P. E. Wagner and R. Strey. Homogeneous nucleation rates of water vapor measured in a two-piston expansion chamber. *J. Phys. Chem.*, 85:2694, 1981.

[26] Y. Viisanen, R. Strey, and H. Reiss. Homogeneous nucleation rates for water. *J. Chem. Phys.*, 99(6):4680–4692, 1993.

[27] R. C. Miller, R. J. Anderson, J. L. Kassner, and D. E. Hagen. Homogeneous nucleation rate measurements for water over a wide range of temperature and nucleation rate. *J. Chem. Phys.*, 78(6):3204, 1983.

[28] M. M. Rudek, J. A. Fisk, V. M. Chakarov, and J. L. Katz. Condensation of supersaturated vapor. xii. the homogeneous nucleation of the *n*-alkanes. *J. Chem. Phys.*, 105(11):4707–4713, 1996.

[29] J. Lothe and G. M. Pound. Reconsiderations of nucleation theory. *J. Chem. Phys.*, 36:2080, 1962.

[30] J. Lothe and G. M. Pound. Concentration of clusters in nucleation and the classical phase integral. *J. Chem. Phys.*, 48:1849, 1968.

[31] A. C. Zettlemoyer. *Nucleation Phenomena (The replacement free energy in nucleation theory, H.Reiss)*. Elsevier, 1977.

[32] H. Reiss. Treatment of drop like clusters by means of the classical phase integral in nucleation theory. *J. Stat. Phys.*, 2:83, 1970.

[33] A. Dillman and G. E. A. Meier. A refined droplet approach to the problem of homogeneous nucleation from the vapour phase. *J. Chem. Phys.*, 94:3872, 1990.

[34] M. E. Fisher. Theory of equilibrium critical phenomenon. *Rep. Prog. Phys*, 30:615 (703), 1967.

[35] D. W. Oxtoby and R. Evans. Non classical nucleation theory for the gas-liquid transition. *J. Chem. Phys.*, 89:7521, 1988.

[36] D. I. Zhukhouvitiskii. Molecular dynamics study of cluster evolution in supersaturated vapour. *J. Chem. Phys*, 103(21):9401–9407, 1995.

[37] M. Matsumoto, S. Saito, and I. Ohmine. Molecular dynamics simulations of nucleation and growth processes leading to water freezing. *Nature*, 416:409–413, 2002.

[38] S. A. Harris and I. J. Ford. A dynamical definition of quasi-bound molecular clusters. *J. Chem. Phys.*, 118:9216, 2003.

[39] I. J. Ford and S. A. Harris. Molecular cluster decay viewed as escape from a potential of mean force. *J. Chem. Phys.*, 120(9):4428, 2004.

[40] B. Senger, P. Schaaf, D. S. Corti, R. Bowles, J.-C Voegel, and H. Reiss. A molecular theory of the homogeneous nucleation rate. *i.* formulation and fundamental issues. *J. Chem. Phys.*, 110(13):6421–6437, 1999.

[41] H. Reiss, J. L. Katz, and E. R. Cohen. Translational-rotational paradox in the theory of nucleation. *J. Chem. Phys.*, 48:5553, 1968.

[42] F. H. Stillinger. Rigorous basis of the frenkel-band theory of association equilibrium. *J. Chem. Phys.*, 38(7):1486, 1962.

[43] T. L. Hill. Molecular clusters in imperfect gases. *J. Chem. Phys.*, 23(4):617–622, 1955.

[44] G. W. Adams, J. L. Schmitt, and R. A. Zalabsky. The homogeneous nucleation of nonane. *J. Chem. Phys.*, 81:5074, 1984.

[45] P. E. Wagner and R.Strey. The homogeneous nucleation of *n*-nonane. *J. Chem. Phys.*, 81:5074, 1984.

[46] D. Kashchiev. On the relation between nucleation work, nucleus size, and nucleation rate. *J. Chem. Phys*, 76(10):5098, 1982.

[47] D. W. Oxtoby. A general relation between the nucleation work and the size of the nucleus in multicomponent nucleation. *Phys. Rev. E*, 56:5615, 1994.

[48] I. J. Ford. Nucleation theorems, the statistical mechanics of molecular clusters, and a revision of classical nucleation theory. *Phys. Rev. E*, 56:5615, 1997.

[49] H. Feshbach. Small systems: when does thermodynamics apply? *Physics Today*, 40(11):9–11, 1987.

[50] C. Kittel. Temperature fluctuation: an oxymoron. *Physics Today*, 41(5):93, 1988.

[51] B. B. Mandelbrot. Temperature fluctuation: a well defined and unavoidable notation. *Physics Today*, 42(1):71–73, 1989.

[52] K. Huang. *Statistical Mechanics*. John Wiley and Sons, 1963.

[53] B. Cowan. *Topics in Statistical Mechanics*. Imperial College Press, 2004.

[54] J. Lindhard. *Complementarity between energy and temperature in The lesson of quantum theory*. New York, 1986.

[55] J. Uffink and J. Lith van Dis. Thermodynamic uncertainty relations. *Foundations of Physics*, 29(5):655, 1999.

[56] A. R. Leach. *Molecular Modelling: principles and applications, 2nd edition.* Prentice Hall, 2001.

[57] J. O. Hirschfelder, C. F. Curtiss, and R. B. Bird. *Molecular Theory of Gases Solids and Liquids.* Wiley, New York, 1964.

[58] W. Smith and T. Forrester. Dl_poly. *J. Molec. Graphics*, 14(139), 1996.

[59] X. Daura, A. E. Mark, and W. F. van Gunsteren. Parameterization of aliphatic ch_n united atoms of gromos96 force field. *J. Chem. Phys.*, 19:535, 1997.

[60] M. Shinya and A. Fournier. Stochastic motion- motion under the influence of wind. *Comp. Graphics. Forum.*, 11(3):119, 1992.

[61] A. A. Farhadi and D. Vvedensky. Risk, randomness, crashes and quants. *Contemporary physics*, 44(3):237–257, 2003.

[62] A. Einstein. Investigations on the theory of the brownian movement. *Ann. Physik.*, 17, 19:549,371, 1905, 1906.

[63] A. Einstein. *Investigations on the the theory of the Brownian movement.* Dover, 1956.

[64] B. Cowan. *Topics in Statistical Mechanics.* Imperial College Press, 2004.

[65] K. Huang. *Statistical Mechanics.* John Wiley and Sons, 1963.

[66] H. Risken. *The Fokker-Plank Equation, methods of solution and application.* Springer-Verlag, 1988.

[67] B. Nowakowski and E. Ruckenstein. A kinetic approach to the theory of nucleation in gases. *J. Chem. Phys.*, 94:1397–1402, 1991.

[68] B. Nowakowski and E. Ruckenstein. Homogeneous nucleation in gases: a three dimensional fokker-plank equation for evaporation from clusters. *J. Chem. Phys.*, 94:8487–8492, 1991.

[69] H. Tang and I. J. Ford. Microscopic simulations of molecular cluster decay: Does the carrier gas affect evaporation? *J. Chem. Phys.*, 125(1):0021, 2006.

[70] H. Vehkamäki and I. J. Ford. Critical cluster size and droplet nucleation rate from growth and decay simulations of lennard-jones clusters. *J. Chem. Phys.*, 112(9):4193–4202, 2000.

[71] W. F. van Gunsteren, S. R. Billeter, A. A Eising, P. H. Hunenberger, P. Kruger, A.E Mark, W. R. P. Scott, and I. G. Tirioni. Biomolecular simulation: The gromos96 manual and user guide. 1996.

[72] L. D. Schuler, X. Daura, and W. F. van Gunsteren. An improved gromos96 force field for aliphatic hydrocarbons in the condensed phase. *J. Chem. Phys.*, 22:1205, 2001.

[73] H. J. C. Berendsen, J. P. M. Postma, W. F. van Gunsteren, A. Di Nola, and J. R. Haak. Molecular dynamics with coupling to an external heat bath. *J. Chem. Phys.*, 81:3684, 1984.

[74] M. L. Boas. *Mathematical Methods in Physical Sciences*. John Wiley and Sons, 1983.

[75] S. Harris. Private communication.

[76] H. C. Andersen. Molecular dynamics simulations at constant pressure and temperature. *J. Chem. Phys.*, 72:2384, 1979.

[77] D. Frenkel and B. Smit. *Understanding Molecular Simulation from algorithms to applications, 2nd edition*. Academic Press, 2002.

[78] E. Weisstien. *Math world*. Wolfram, 1999.

[79] C Kittel. *Introduction to solid state physics*. John Wiley and Sons, 1996.

[80] K. Yasuoka and M. Matsumoto. Molecular dynamics of homogeneous nucleation in the vapour phase. i. lennard-jones fluid. *J. Chem. Phys.*, 109(19)):8451–8462, 1998.

[81] D. Eisenberg and W. Kauzmann. *Structure and Properties of Water*. University College London, 1969.

[82] P. G. Debenedetti. *Metastable Liquids: Concepts and Principles*. Princeton University Press, 1996.

[83] W. M. Latimer and W. H. Rodebush. Polarity and ionisation from the standpoint of the lewis theory of valance. *J. Am. Chem. Soc*, 42:1419–1433, 1920.

[84] S. A. Harris. The physics of dna stretching. *Contemporary physics*, 45, 2004.

[85] C. A. Angell. Supercooled water. *Water: A Comprehensive Treatise*, 7:1–76, 1982.

[86] K. Sassen, K. N. Liou, S. Kinner, and M. Griffin. Highly supercooled cirrus cloud water confirmation and climatic implications. *Science*, 227:411–413, 1985.

[87] D. Rosenfield and W. L. Woodley. Deep convective clouds with sustained supercooled liquid water down to -37.5^o. *Nature*, 405:440–442, 2000.

[88] O. Mishima and H. E. Stanley. The relationship between liquid, supercooled and glassy water. *nature.*, 396:329–335, 1998.

[89] H. A. Chang, T. Koop, L. T. Molina, and M. J. Molina. Phase transitions in emulsified hno_3/h_2o and $hno_3/h2so_4/h_2o$ solutions. *J. Phys. Chem*, 103:2673–2679, 1999.

[90] W. C. Roentgen. *Ann. Phys.*, 45:91, 1892.

[91] H. S. Frank and Wen-Yang Wen. Ion-solvent interaction. structural aspects of ion-solvent interaction in aqueous solutions: a suggested picture of water structure. *Discuss. Faraday. Soc*, 24:133, 1957.

[92] H. S. Frank. The structure of ordinary water. *Science*, 169, 1970.

[93] J. D. Bernal and R. H. Fowler. A theory of water and ionic solution, with particular reference to hydrogen and hydroxyl ions. *J. Chem. Phys*, 1, 1933.

[94] J. A. Pople. The molecular orbital theory of chemical valency v. the structure of water and similar molecules. *Proc. R. Soc. A.*, 202:323, 1950.

[95] M. G. Sceats and S. A. Rice. Amorphous solid water and it's relationship to liquid water: a random network model for water. *Water: A Comprehensive Treatise*, 7:83–211, 1982.

[96] H. E. Stanley. A polychromatic correlated-site percolation problem with possible relevance to the unusual behaviour of supercooled h2o and d2o. *J. Phys. A: Math*, 12(12):L329–L337, 1979.

[97] H. E. Stanley and J. Teixeria. Interpretation of the usual behaviour of h2o and d2o at low temperatures: tests of a percolation model. *J. Chem. Phys.*, 73(7):3404–3422, 1980.

[98] A. Rahman and F. H. Stillinger. Molecular dynamics study of liquid water. *J. Chem. Phys.*, 55(7):3336–3359, 1971.

[99] I. J. Ford. Properties of ice clusters from an analysis of freezing nucleation. *J. Phys. Chem. B*, 105:11649–11655, 2001.

[100] H. Vortisch, B. Kramer, I. Weidinger, L. Woste, T. Leisner, M. Schwell, H. Baumgartel, and E. Ruhl. Homogeneous freezing nucleation rates and crystallisation dynamics of single levitated sulfuric acid solution droplets. *J. Phys. Chem*, 2:1407–1413, 2000.

[101] F. H. Stillinger. Water revisited. *Science*, 209:451, 1980.

[102] I. Ohmine. Liquid water dynamics: collective motions, fluctuations, and relaxations. *J. Phys. Chem.*, 99:6767–6776, 1995.

[103] A. P. Sutton. *Electronic structure of materials*. Oxford Science Publications, 1994.

[104] P. W. Atkins. *Molecular Quantum mechanics*. University College London, 1983.

[105] Sir W. H. Bragg. The crystal structure of ice. *Proc. Phys. Soc. London*, 34:98–103, 1922.

[106] L. Pauling. The structure and entropy of ice and of other crystals with some randomness of atomic arrangement. *Am. Chem. Soc.*, 57:2680–2684, 1935.

[107] W. L. Jorgensen. Transferable intermolecular potential functions of water, alcohols, and ethers. application to liquid water. *J. Am. Chem. Soc*, 103:335, 1981.

[108] W. L. Jorgensen. Revised tips for simulations of liquid water and other aqueous solutions. *J. Chem. Phys*, 77:4156, 1982.

[109] W. L. Jorgensen, J. Chandrasekhar, J. D. Madura, R. W. Impey, and M. L. Klein. Comparison of simple potential functions for simulating liquid water. *J. Chem. Phys*, 79:926, 1983.

[110] H. Yu and W. van Gunsteren. Charge-on-spring polarizable water models revisited: From water clusters to liquid water to ice. *J. Chem. Phys*, 121(19):9549, 2004.

[111] N. H. de Leuuw and S. C. Parker. Molecular-dynamics simulation of mg0 surfaces in liquid water using a shell-model potential for water. *Phy. Rev. B.*, 58(20):13901, 1998.

Appendix A

Computational Specifications

The MD calculations were run on a Dell Precision Work Station Intel Pentium 4, with a 2.853 GHz processor and 500 MB of RAM. The simulations were conducted under conditions of constant temperature, implemented using the Andersen stochastic thermostat. The time taken to run the simulations varied from a few hours to several weeks, depending on the sizes of the systems considered. For instance, the time taken to simulate a cluster of 67 molecules for about 5ns, took approximately 35 days, without any other major processes being run simultaneously. The smaller cluster systems containing 50, 40 and 5 molecules took approximately 28 days, 14 days, and less than 1 day respectively.

Appendix B

Cluster Identification Algorithm

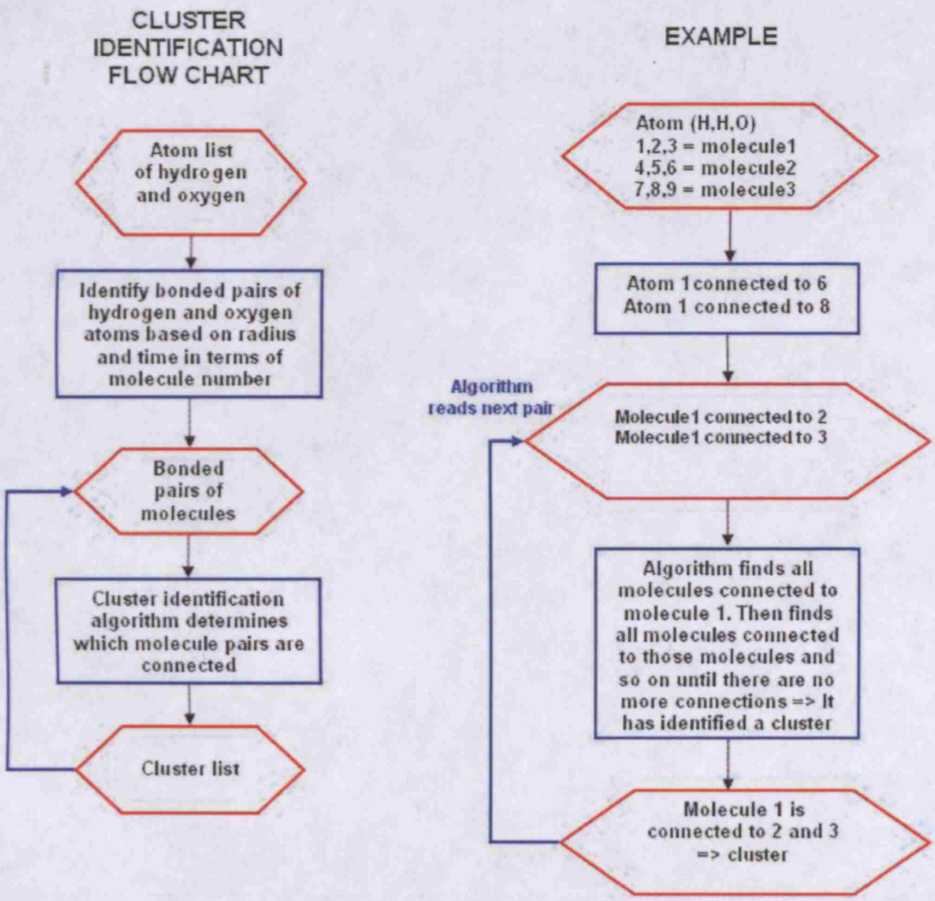

Figure B.1: Flow chart illustrating the identification of clusters from a list of hydrogen bonded pairs of atoms. The cluster identification algorithm is a topology based program. It uses a list of bonded pairs of molecule numbers to deduce which molecules are participating in the same cluster. The algorithm is repeated for each snapshot.